JOURNAL OF PETROLOGY | VOLUME 54 | NUMBER 11 | PAGES 2193–2234 | 2013 | doi:10.1093/petrology/egt044

Andean Adakite-like high-Mg Andesites on the Northern Margin of the Chilean–Pampean Flat-slab (27–28·5°S) Associated with Frontal Arc Migration and Fore-arc Subduction Erosion

ADAM R. GOSS[1], SUZANNE MAHLBURG KAY[2]* AND CONSTANTINO MPODOZIS[3]

[1]EXXONMOBIL CORPORATION, UPSTREAM RESEARCH COMPANY (URC), 3120 BUFFALO SPEEDWAY, HOUSTON, TX 77098, USA

[2]CORNELL UNIVERSITY, DEPARTMENT OF EARTH AND ATMOSPHERIC SCIENCE, SNEE HALL, ITHACA, NY 14853, USA

[3]ANTOFAGASTA MINERALS, APOQUINDO 4001, PISO 18, SANTIAGO, CHILE

RECEIVED JULY 23, 2012; ACCEPTED JULY 2, 2013
ADVANCE ACCESS PUBLICATION AUGUST 21, 2013

Glassy, plagioclase phenocryst-free, ~7–3 Ma, andesitic lavas erupted at the southern end of the Andean Central Volcanic Zone (CVZ) at 27–28·5°S are argued to contain a component from continental crust that was incorporated into the sub-arc mantle in a major pulse of fore-arc subduction erosion that removed ~50 km of fore-arc. The 7–3 Ma amphibole-bearing Pircas Negras (54–64% SiO_2) and ~7·7 Ma pyroxene-bearing Dos Hermanos lavas erupted as the frontal arc was displaced some 50 km eastward over a developing bend in the Wadati–Benioff zone at the northern margin of the Chilean–Pampean flat-slab region. Their chemistry differs from that of older Miocene and younger CVZ arc lavas in the region in having more pronounced high field strength element (La/Ta = 40–100; Ba/Ta = 800–2400) and heavy rare earth element (Sm/Yb ~ 4–9) depletions and an extreme adakitic-like character (~600–1400 ppm Sr; Sr/Yb ~ 400–1350). They also differ from older Miocene lavas in having higher $^{87}Sr/^{86}Sr$ and lower $^{143}Nd/^{143}Nd$ at the same wt % SiO_2, while still showing trends with increasing wt % SiO_2 that are best attributed to contamination in the ~65–70 km thick crust. Overall, the trace element and isotopic features of the Pircas Negras lavas are consistent with modeling that attributes differences from older and younger lavas to enrichment of the arc mantle wedge by partial melts of tectonically eroded fore-arc crust, with the modeled eroded component being an outcrop and geophysically constrained mixture of 80–90% Jurassic mafic magmatic rocks and 10–20% silicic Paleozoic crust. An adakitic-type partial melt of this eroded crust generated at >2 GPa, reacted with mantle peridotite, can explain the high Mg# values (50–61) and Cr (100–350 ppm) and Ni (40–70 ppm) contents in some 5–3 Ma Pircas Negras lavas. Pre-eruption temperatures over 1060°C, calculated from mineral thermometry and the MELTS program, permit these magmas to subsequently melt and react with overlying eclogitic crust. Magma storage in this thick crust then led to amphibole crystallization and suppression of plagioclase fractionation. Quartz and feldspar xenocrysts were acquired from locally pooled mid-crustal magmas and the silicic upper crustal basement during final rapid ascent to the surface. Given a constant arc–trench gap of 300 km over the last 10 Myr, ~198 $km^3\,Myr^{-1}\,km^{-1}$ of fore-arc crust needs to be removed by subduction erosion at 8–3 Ma to account for the material balance of the fore-arc crust.

KEY WORDS: *adakite; active continental margin; fore-arc subduction erosion; Andean arc; flat-slab subduction; geochemistry*

INTRODUCTION

The presence of arc geochemical signatures in compositional estimates of average continental crust

*Corresponding author. Telephone: +1 607 2554701. E-mail: smk16@cornell.edu

(e.g. Rudnick & Fountain, 1995) suggests an important role for arc magmas in generating continental crust in the same place that sediments subduct and fore-arc subduction erosion occurs (e.g. von Huene & Scholl, 1991; Stern, 2011). A still unresolved question is the fate of subducted fore-arc eroded crust in these regions. Fore-arc subduction erosion processes are considered to be particularly significant along the Andean margin (e.g. von Huene & Scholl, 1991), which is the region where the process was initially suggested by Rutland (1971) to explain the stepwise eastern displacements of the Jurassic to present arc magmatic fronts. Among the most important Neogene arc front displacements are those on the margins of the Chilean–Pampean flat-slab region that runs between latitude 28° and 33°S (Fig. 1). It was in this area that Stern (1991) argued that chemical trends in young arc volcanic rocks could be explained as well by mantle source contamination owing to subduction of sediments and fore-arc crust as by MASH (melting, assimilation, storage and homogenization) processes in the crust, which were specifically elaborated by Hildreth & Moorbath (1988) along the Southern Volcanic Zone arc (SVZ) south of 33°S (Fig. 1). Kay *et al.* (2005) used transient steep rare earth element (REE) patterns and changing isotopic ratios in <25 Ma volcanic rocks at 33–34°S to explicitly argue for a combination of MASH and pulses of enhanced fore-arc subduction erosion to explain chemical trends in magmas erupted as the arc front was displaced ~35 km to the east at ~19–16 Ma, and another ~50 km to the east at ~8–3 Ma. As the crust under the arc and fore-arc is compositionally similar in this region, the proportions contributed by each process are difficult to constrain. Kay & Mpodozis (2002) and Goss & Kay (2009) argued for subducted fore-arc components also playing a role in shaping the chemistry of andesitic volcanic rocks with high Mg# values and adakitic-like depleted heavy REE (HREE) patterns and high Sr concentrations, which erupted north of the flat-slab at 28–26·5°S as the arc front was displaced ~40–50 km eastward at ~8–3 Ma (Figs 1 and 2). As in the northern SVZ to the south, a complicating factor is that mantle-generated magmas need to pass through an ~65–70 km thick crust (e.g. McGlashan *et al.*, 2008). As a consequence, the discussion on the contribution of fore-arc subducted eroded components in Andean arc magma sources continues, with some researchers maintaining that contamination in the underlying crust can adequately explain almost all of the trends in Andean arc magmas (e.g. Mamani *et al.*, 2010).

In this study, we present new K/Ar ages, mineral compositions, whole-rock major and trace element data, and Sr, Nd, Pb and O isotopic data for ~9–2 Ma basaltic andesitic to dacitic lavas that erupted between 27 and 28·5°S in the general period during which the arc front shifted ~50 km eastward and the subducting slab shallowed to the south forming the modern flat-slab. The origins of these lavas are considered in view of their tectonic setting, published experimental data and new petrological and isotopic data and modeling. These lavas include a suite of distinctive glassy high-Mg hornblende-bearing andesites known as the Pircas Negras lavas (Kay *et al.*, 1991), which are characterized by steep REE patterns, extreme high field strength element (HFSE) depletion, and high Sr, Ni, and Cr contents. We conclude that these andesites contain melts of fore-arc subduction-eroded crust that reacted with the sub-arc mantle wedge to form magmas that were subsequently contaminated in the thick crust as they rose to the surface. This model is complementary to proposals relating pulses of high-Mg adakitic volcanism at times of arc displacement on thin continental (Kay *et al.*, 2005; Goss & Kay, 2006) or oceanic (Kay, 2006) crust to accelerated incorporation of fore-arc eroded crust into the mantle source. The model is also compatible with a role for fore-arc crust in the genesis of Cretaceous to Miocene Andean lavas erupted at times of arc migration that researchers such as Haschke *et al.* (2002) have attributed to cycles of crustal thickening and thinning, and Mamani *et al.* (2010) to differentiation at different crustal levels.

GEOLOGICAL AND TECTONIC SETTING

The ~9–2 Ma volcanic rocks examined here erupted between 27 and 28·5°S along the western margin of the Puna Plateau in the transition zone between the modern Chilean–Pampean flat-slab and the Central Volcanic Zone arc (CVZ) (Figs 1 and 2). To the north, the Nazca plate is subducting at an angle of ~30° below the Puna, whereas to the south, a near-horizontal segment lies at a depth of 100 km (Cahill & Isacks, 1992; Mulcahy, 2012; Fig. 1). These lavas erupted over the part of the Wadati–Benioff zone where the depth contours bend to the east under the Incapillo volcanic complex (Goss *et al.*, 2009, 2011), which is the southernmost center with post-Pliocene activity until reaching Volcán Tupungato in the northernmost SVZ near 33°S (Fig. 1). Relative to the slab contours published by Mulcahy (2012), current Wadati–Benioff zone depths are ~100–115 km under these flows and the 26–6 Ma Maricunga Belt arc to the west, ~115 km below the Incapillo complex and ~125 km under the southern CVZ. On the basis of depth phase precursors (McGlashan *et al.*, 2008) and receiver functions (Bianchi *et al.*, 2013), crustal thicknesses under the region are ~65–75 km.

The basement in the region is considered to include Grenville age crust (~1·1 Ga) with Late Proterozoic gneisses and deformed granites and early Paleozoic magmatic and sedimentary rocks exposed east of the Incapillo caldera (Fig. 1). Devonian to Permian sedimentary and volcanic units, including the rhyolites and granites of the late

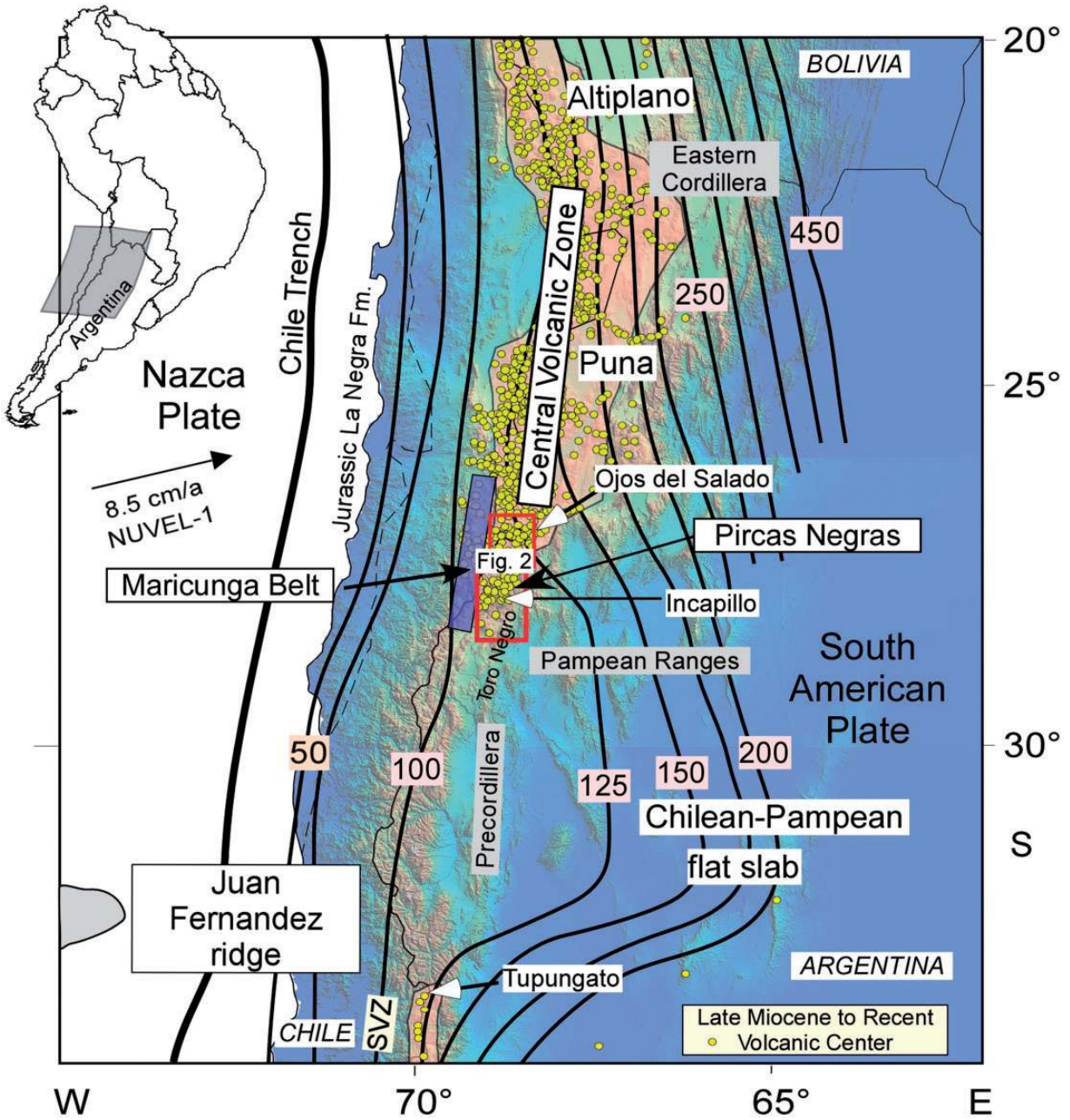

Fig. 1. Shuttle Radar Topography Mission (SRTM) digital elevation image showing the main morphotectonic features of the Central Andes. The Nazca plate convergence direction is the integrated NUVEL-1 rate from DeMets *et al.* (1990). Bold continuous lines show contours of the subducting Nazca plate with depths in kilometers to the Wadati–Benioff zone as modified by Mulcahy *et al.* (2010) and Mulcahy (2012) from Cahill & Isacks (1992). Small circles show late Miocene to Recent volcanic centers of the Andean Central Volcanic Zone (CVZ) and Southern Volcanic Zone (SVZ). Shaded rectangle shows the position of the early to late Miocene Maricunga Belt volcanic arc (Kay *et al.*, 1994, 2013; Mpodozis *et al.*, 1995). White tipped arrows point to the Ojos del Salado volcanic and Incapillo caldera complex regions in the CVZ and the Tupungato volcanic center in the SVZ. The box shows the general region of the Dos Hermanos and Pircas Negras adakitic andesites and the location of the Thematic Mapper (TM) images in Fig. 2.

Paleozoic Choiyoi group, are widespread to the west (e.g. Mpodozis & Kay, 1992; Mpodozis *et al.*, 1997; Rubiolo *et al.*, 2002; Martina *et al.*, 2009; Figs 2 and 3). Mafic complements to these Choiyoi granitic and rhyolitic units and the younger arc region magmatic rocks in the region probably form parts of the deep crust.

Arc volcanism associated with the modern Andean cycle in this region began with the late Oligocene breakup of

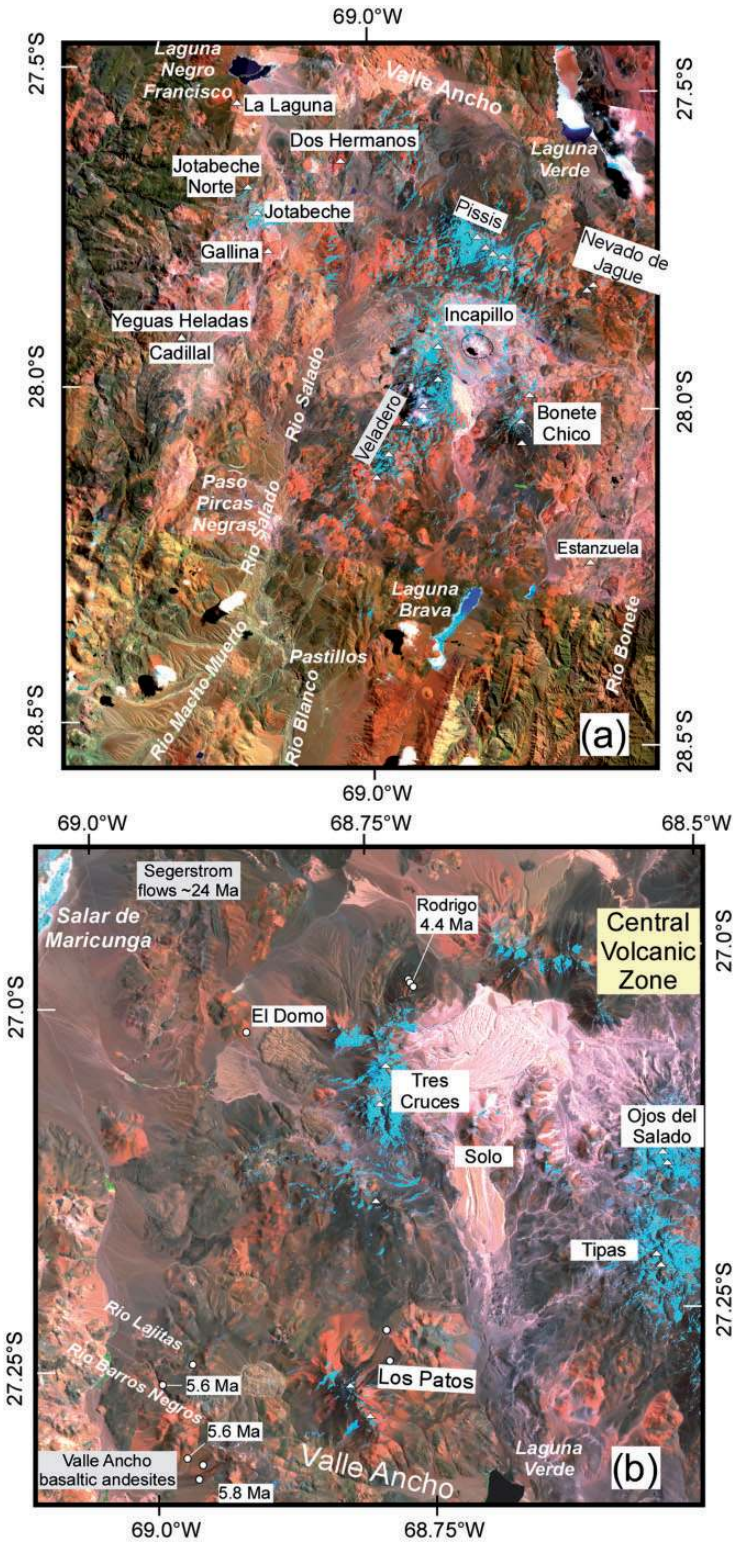

Fig. 2. Thematic Mapper (TM) images showing regional context of the volcanic rocks discussed in the text. Geographical names are in italics, volcanic center names are in black on white labels and triangles are peaks. (a) shows the area of ~9–7 Ma pre-migration, 7–3 Ma syn-migration and 3–2 Ma volcanic center maps in Fig. 3a–c; (b) shows the localities of the 24 Ma Segerstrom lavas, 7–5 Ma Valle Ancho mafic lavas and the Pircas Negras-like 4·4 Ma Rodrigo andesitic flows that are not shown in Fig. 3, and the southern CVZ volcanic centers. White circles in (b) are sample localities, and K/Ar ages in the region from Table 2. The difference in scale of (a) and (b) should be noted. Further details have been given by Kay *et al.* (1994, 2008, 2013) Mpodozis *et al.* (1995, 1996, 1997) and Mpodozis & Kay (2009).

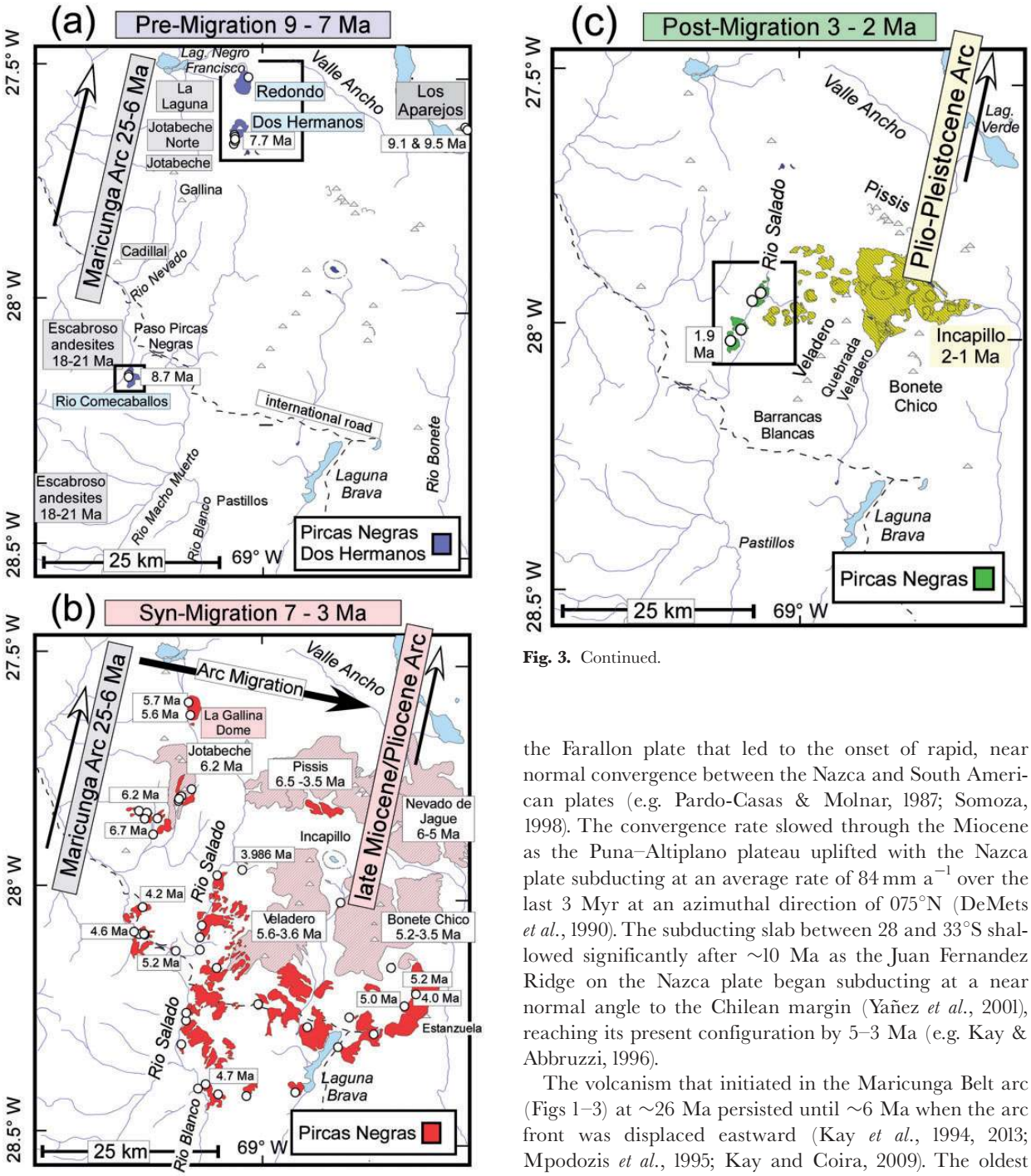

Fig. 3. Maps of the region of the TM image in Fig. 2a showing (a) 9–7 Ma pre-migration, (b) 7–3 Ma syn-migration, and (c) 3–2 Ma post-migration volcanic centers. The ~9–2 Ma Dos Hermanos and Pircas Negras volcanic group centers featured in this study are as indicated in the legend. Other latest Miocene to Pliocene dacitic to rhyodacitic centers are shown by grey shaded areas, with 7–3 Ma centers in (b) and Plio-Pleistocene arc centers in (c). K/Ar ages are as in Fig. 2 and the text; dots are sample localities and triangles are peaks. Base map is from Argentine and Chilean geological maps (SERNAGEOMIN, 2003) with additional mapping by the authors. Dashed line is an international highway.

Fig. 3. Continued.

the Farallon plate that led to the onset of rapid, near normal convergence between the Nazca and South American plates (e.g. Pardo-Casas & Molnar, 1987; Somoza, 1998). The convergence rate slowed through the Miocene as the Puna–Altiplano plateau uplifted with the Nazca plate subducting at an average rate of 84 mm a^{-1} over the last 3 Myr at an azimuthal direction of 075°N (DeMets *et al.*, 1990). The subducting slab between 28 and 33°S shallowed significantly after ~10 Ma as the Juan Fernandez Ridge on the Nazca plate began subducting at a near normal angle to the Chilean margin (Yañez *et al.*, 2001), reaching its present configuration by 5–3 Ma (e.g. Kay & Abbruzzi, 1996).

The volcanism that initiated in the Maricunga Belt arc (Figs 1–3) at ~26 Ma persisted until ~6 Ma when the arc front was displaced eastward (Kay *et al.*, 1994, 2013; Mpodozis *et al.*, 1995; Kay and Coira, 2009). The oldest units are 26–22 Ma dacitic ignimbrites (Tilito Formation) and 21–18 Ma mafic lavas (Escabroso Formation) that probably erupted through an ~40–45 km thick crust over a moderately dipping slab (Fig. 3a; see Kay & Mpodozis, 2002). Their eruption was followed by a pulse of contractional deformation during a near regional magmatic lull at ~18–17 Ma. Volcanism resumed at large, mostly andesitic, stratovolcanic complexes such as the 16–14 Ma Jotabeche Norte and La Laguna and the 15–13 Ma

Cadillal–Yeguas Heladas centers (Fig. 2a; Kay *et al.*, 1991, 1994; McKee *et al.*, 1994; Mpodozis *et al.*, 1995) and continued with emplacement of 13–10 Ma Au–Cu-bearing porphyries (Vila & Sillitoe, 1991; Mpodozis *et al.*, 1995). The final period of volcanism was concentrated in the ~11–7 Ma Copiapó dacitic complex and terminated with the emplacement of ~8–6 Ma rhyodacitic ignimbrites that erupted from the Jotabeche caldera. Crustal thicknesses under the Maricunga Belt are considered to have exceeded 60 km by ~10 Ma (e.g. Kay *et al.*, 1994).

As shown in Fig. 3a–c, the Dos Hermanos and Pircas Negras basaltic andesitic to andesitic lavas began erupting east of the Maricunga Belt after ~9 Ma as the volume of frontal arc volcanism decreased, and the ~50 km eastward displacement of the frontal arc recorded by the Bonete Chico (5·2–3·5 Ma), Pissis (6·5–3·0 Ma) and Veladero (5·6–3·6 Ma) dacitic complexes began (Kay & Mpodozis, 2002; Goss *et al.*, 2009; Fig. 3b). Arc migration ended with the establishment of the CVZ arc in which the centers north of the Valle Ancho have been erupting basaltic andesitic to dacitic lavas for the last 2–3 Myr (Mpodozis *et al.*, 1996; Kay *et al.*, 2008, 2013). South of the Valle Ancho, the southern CVZ Incapillo complex last erupted at 0·5 Ma (Figs 1, 2 and 3c; Goss *et al.*, 2009).

Ages and distribution of the 9–2 Ma Dos Hermanos and Pircas Negras Lavas

The region between the Maricunga Belt and CVZ arc from 27 to 28·5°S where the Dos Hermanos and Pircas Negras and other volcanic rocks featured here crop out is shown in the Thematic Mapper (TM) satellite images in Fig. 2. The distribution of the 9–2 Ma volcanic rocks in the region of Fig. 2a, which erupted as the Maricunga Belt arc terminated and the CVZ stabilized, are shown on maps of 9–7 Ma pre-migration, 7–3 Ma syn-migration and 3–2 Ma post-migration volcanic rocks in Fig. 3a–c. The localities and ages of other volcanic rocks featured in this study are indicated on the TM image in Fig. 2b. The locations, rock types and the mineralogy of all of the samples are given in Table 1. The ages shown on the maps are largely K/Ar ages, for which the analytical data are reported in Table 2.

The map in Fig. 3a shows the 9–7 Ma pre-arc migration volcanic rocks that erupted in the back-arc as activity at the Maricunga Belt front was ebbing (McKee *et al.*, 1994; Mpodozis *et al.*, 1995). The oldest rocks of this group are the isolated Los Aparejos basaltic andesitic flows in the eastern Valle Ancho in Argentina that have K/Ar ages of $9{\cdot}5 \pm 0{\cdot}5$ and $9{\cdot}1 \pm 0{\cdot}6$ Ma (Mpodozis *et al.*, 1997). Others are the Dos Hermanos mafic andesites just south of the Valle Ancho, one of which has a K/Ar age of $7{\cdot}7 \pm 0{\cdot}4$ Ma; the ~8 Ma Redondo lavas at the base of Dos Hermanos volcano; and an isolated Pircas Negras-like flow along the Rio Comecaballos with a K/Ar age of $8{\cdot}7 \pm 0{\cdot}4$ Ma.

The map in Fig. 3b shows the 7–3 Ma syn-migration volcanic rocks, which include the most voluminous flows that erupted between the mostly extinct Maricunga Belt arc and the modern CVZ. This group includes the broad suite of generally glassy, plagioclase-phenocryst-free lavas, which form most of the Pircas Negras group (Kay *et al.*, 1991; Mpodozis *et al.*, 1995). The westernmost and oldest of these include andesitic flows located to the east of the ~15 Ma Cadillal center, of which one has a K/Ar age of $6{\cdot}7 \pm 0{\cdot}9$ Ma, and flows between the Jotabeche caldera and Laguna Negro Francisco, where one has a K/Ar age of $5{\cdot}6 \pm 2{\cdot}5$ Ma. Other flows in this region are the dark, glassy, amphibole-bearing lavas near and south of the Paso Pircas Negras region, two of which have K/Ar ages of $5{\cdot}2 \pm 0{\cdot}9$ and $4{\cdot}2 \pm 0{\cdot}5$ Ma. Dacitic flows with Pircas Negras-like characteristics, one of which has a K/Ar age of $6{\cdot}2 \pm 0{\cdot}9$ Ma, also occur along faults in the Rio La Gallina valley, where one has a K/Ar age of $6{\cdot}2 \pm 0{\cdot}9$ Ma. The most voluminous of the Pircas Negras flows occur in a north–south belt to the east in Argentina, which extends for ~80 km in a topographic depression occupied by the Rio Salado (Fig. 2b). Flows in the valley can be over 10 m thick and probably come from the Sierra de Veladero region; one has a $^{40}Ar/^{39}Ar$ age of $3{\cdot}968 \pm 0{\cdot}192$ Ma (Goss *et al.*, 2009). Other flows occur near the junction of the Rio Blanco with the Rio Salado, where one has a K/Ar age of $4{\cdot}7 \pm 0{\cdot}5$ Ma. The easternmost flows are found on the flanks of the 5·2–3·2 Ma Cerro Bonete Chico dacitic volcanic center, where two have K/Ar ages of $5{\cdot}2 \pm 0{\cdot}6$ and $4{\cdot}0 \pm 0{\cdot}2$ Ma. Other isolated and undated Pircas Negras-like flows occur around Laguna Brava.

Less voluminous Pircas Negras flows to the north (Fig. 2b) include a $5{\cdot}6 \pm 0{\cdot}3$ Ma dacitic flow between the Rio Lajitas and Barros Negros, andesitic and dacitic lavas on the flanks of Volcán Los Patos, a basaltic andesite flow west of Nevado Tres Cruces and glassy andesitic flows at the $4{\cdot}4 \pm 0{\cdot}6$ Ma Rodrigo center (Mpodozis *et al.*, 1996). The basaltic andesite flows in the Valle Ancho with K/Ar ages of $5{\cdot}6 \pm 0{\cdot}3$ to $5{\cdot}8 \pm 0{\cdot}7$ Ma are mineralogically and chemically distinct from the Pircas Negras flows (e.g. Kay *et al.*, 1994). The map in Fig. 3c shows the less voluminous post-migration Pircas Negras flows (Fig. 2c), which are concentrated along the northern extent of the Rio Salado valley. One of these flows yielded a K/Ar age of $1{\cdot}9 \pm 0{\cdot}2$ Ma.

MINERALOGICAL, CHEMICAL AND ISOTOPIC CHARACTERISTICS

Analytical methods

New major element mineral and whole-rock major element, trace element and Sr, Nd, Pb and O isotopic data presented in Tables 3–5 and Supplementary Data Electronic

Table 1: Pircas Negras region basaltic and andesitic samples

Sample	Unit/location	Principal mineralogy	wt % SiO_2	La/Yb	Sm/Yb	La/Ta	Lat. (°S)	Long. (°W)	Altitude (m)	Data source
Early Miocene Escabroso Formation andesites (~21–18 Ma)										
CO291	Río de la Sal	plag, cpx	60·56	15·8	3·4	40·3	28·804	69·631	4505	Appendix 8
CO292	Río de la Sal	plag, cpx	58·33	10·0	2·1	38·6	28·771	69·638	4945	Appendix 8
CO293	Río de la Sal	plag, cpx, ol	60·57	22·4	4·8	42·6	28·776	69·634	4864	Appendix 8
CO294	Río de la Sal	plag, cpx	61·02	16·3	3·0	46·9	28·787	69·630	4772	Appendix 8
CO295	Río de la Sal	plag, cpx	55·94	9·0	2·2	42·3	28·868	69·641	4162	Appendix 8
CO296	Río de la Sal	plag, cpx	60·55	10·7	2·4	43·5	28·869	69·647	4264	Appendix 8
CO297	Río de la Sal	plag, cpx	60·27	13·8	3·0	38·9	28·887	69·646	3997	Appendix 8
CO300	Río de la Sal	plag, cpx, ol	54·53	9·0	1·2	39·5	28·867	69·570	4278	Appendix 8
CO335	West Pircas Negras	plag, cpx	59·41	10·9	2·4	39·1	27·963	69·341	3460	Appendix 8
CO446	West Pircas Negras	plag, cpx	56·82	11·7	2·6	35·6	27·938	69·359	3350	Appendix 8
CO264	Macho Muerto	plag, cpx	59·32	12·0	2·5	31·9	28·537	69·513	4384	Appendix 8
Pre-migration volcanic group (~9–7 Ma)										
CO428	Dos Hermanos	cpx, glassy	58·95	60·5	8·8	101·1	27·626	69·080	4563	Goss & Kay, 2009
CC81	Dos Hermanos	cpx, glassy	57·34	57·3	8·1	91·5	27·615	69·065	4991	Table 4
CC82	Dos Hermanos	cpx, glassy	56·08	57·4	8·0	95·1	27·620	69·073	4840	Goss & Kay, 2009
CC83	Dos Hermanos	cpx, glassy	58·24	61·2	8·6	94·3	27·623	69·073	4837	Goss & Kay, 2009
CC94	Redonda	amp, cpx	63·41	64·4	8·6	64·7	27·491	69·039	4488	Table 4
PN406	Comecaballos	amp	64·15	57·6	8·3	99·5	28·117	69·326	4170	Kay *et al.*, 1991
CO72	Los Aparejos	ol	52·74	21·5	3·8	55·3	27·660	68·336	4455	Table 4
CO24	Los Aparejos	cpx, ol, plag	53·25	17·0	3·3	55·4	27·629	68·339	4547	Table 4
Syn-migration Pircas Negras volcanic group (~7–3 Ma)										
CC17	La Gallina	amp, cpx	58·39	41·8	5·9	63·4	27·733	69·196	5014	Table 4
CC11	La Gallina	amp, cpx	59·05	33·5	5·1	54·6	27·599	69·174	4400	Appendix 7
CC15	Cerro Casale	amp, cpx	59·96	–	–	–	27·825	69·288	4129	Appendix 7
CO415	Cerro Casale	amp, cpx	60·94	48·3	8·0	76·1	27·819	69·285	4157	Table 4
CO416	Cerro Casale	amp, cpx, xeno	58·91	36·4	7·7	49·4	27·864	69·269	3579	Table 4
CO427	Río Gallina	amp, cpx, xeno	59·25	33·9	5·9	63·5	27·773	69·165	4695	Goss & Kay, 2009
PN556	Cerro Casale	amp, cpx	61·06	49·1	7·9	72·8	27·815	69·298	4139	Kay *et al.*, 1991
AC619A	Río Gallina	amp, cpx	61·44	–	–	–	27·825	69·256	3920	Appendix 7
AC623A	Río Gallina	amp, cpx	60·56	–	–	–	27·788	69·203	4233	Appendix 7
AC624A	Río Gallina	amp, cpx	60·15	–	–	–	27·789	69·206	4332	Appendix 7
AC625A	Río Gallina	amp, cpx	61·08	–	–	–	27·792	69·206	4321	Appendix 7
AC626P	Río Gallina	amp, cpx	60·22	–	–	–	27·795	69·209	4252	Table 4
CO412	Pircas Negras	amp, cpx, ol, opx	57·38	26·4	4·6	58·3	28·069	69·300	4179	Table 4
CO413	Pircas Negras	amp, cpx, ol	58·94	30·0	5·2	60·2	28·063	69·307	4042	Table 4
CO414	Pircas Negras	amp, cpx	61·97	38·5	6·2	67·4	28·010	69·297	3976	Table 4
PN408	Pircas Negras	amp, cpx, ol	57·54	25·5	4·2	61·6	28·069	69·289	4145	Kay *et al.*, 1991
PN409	Pircas Negras	amp, cpx, ol	57·36	27·6	4·7	56·3	28·069	69·289	4133	Kay *et al.*, 1991
CO163	Río Salado	amp, cpx	62·76	47·5	7·8	72·9	28·043	69·162	4275	Goss & Kay, 2009
CO170	Lower Río Salado	amp, cpx	57·40	23·4	5·0	47·4	28·388	69·128	3799	Goss & Kay, 2009
CO172	Lower Río Salado	amp, cpx	56·78	18·6	4·3	39·2	28·304	69·209	3629	Appendix 7
CO173	Lower Río Salado	amp, cpx	58·89	21·0	4·4	45·4	28·235	69·188	3905	Table 4
CO175	Río Peñas Negras	amp, cpx	60·57	50·9	7·9	59·9	28·113	69·208	4069	Table 4
CO176	Río Salado	amp, cpx, plag	63·40	31·4	4·7	68·9	28·101	69·156	4033	Table 4

(continued)

Table 1: Continued

Sample	Unit/location	Principal mineralogy	wt % SiO_2	La/Yb	Sm/Yb	La/Ta	Lat. (°S)	Long. (°W)	Altitude (m)	Data source
Syn-migration Pircas Negras volcanic group (~7–3 Ma)										
CO309	Pastillos	amp, cpx	61·71	47·2	8·1	56·8	28·101	69·215	4176	Goss & Kay, 2009
CO310	Río Salado	amp, cpx	59·10	44·0	7·9	53·8	28·114	69·184	4119	Goss & Kay, 2009
CO327	Río Salado	amp, cpx	61·68	40·7	7·0	65·1	28·430	69·309	3890	Goss & Kay, 2009
CO329	Río Salado	amp, cpx	59·00	30·6	5·2	61·6	28·398	69·160	3705	Goss & Kay, 2009
CO331	Pastillos	amp, cpx	61·48	40·0	6·6	62·8	28·409	69·104	4004	Goss & Kay, 2009
CO332	Pastillos	amp, cpx	59·33	34·8	5·9	63·9	28·416	69·043	3989	Goss & Kay, 2009
CO504	Río Salado	amp, cpx, xeno	60·20	38·4	6·7	60·6	27·952	69·119	4450	Goss & Kay, 2009
CO507	Incapillo region	amp, cpx, plag	63·04	41·5	6·3	70·1	27·939	69·051	4747	Table 4
CO159	Laguna Brava	amp, cpx, ol	62·21	33·1	5·5	53·3	28·268	68·874	4449	Table 4
CO160	Laguna Brava	amp, cpx, ol	59·21	22·1	3·4	42·8	28·309	68·804	4283	Table 4
CO161	Laguna Brava	amp, plag	63·80	43·0	6·6	70·5	28·274	68·746	4131	Table 4
CO333	Laguna Brava	amp, cpx, ol	61·95	40·9	6·4	62·2	28·405	68·927	4436	Table 4
CO502	Laguna Brava	amp, cpx	63·26	46·8	7·3	66·9	28·220	69·021	4360	Table 4
CO144	Bonete Chico	amp, cpx	58·20	37·0	6·7	49·9	28·219	68·654	4286	Goss & Kay, 2009
CO145	Bonete Chico	amp, cpx	62·74	49·4	8·4	68·2	28·196	68·634	4112	Goss & Kay, 2009
CO146	Bonete Chico	amp, cpx	57·45	21·5	4·3	47·5	28·136	68·697	4751	Goss & Kay, 2009
CO324	Bonete Chico	ol, cpx, plag, amp, opx	59·11	29·5	5·1	35·6	27·995	68·808	5127	Goss & Kay, 2009
CC252	Los Patos	amp, cpx	63·56	30·3	5·1	42·4	27·251	68·792	4537	Table 4
CC254	Los Patos	amp, cpx	57·11	26·2	4·6	52·6	27·278	68·784	4899	Table 4
CC270	Río Barros Negros	amp, cpx	63·88	56·8	8·4	68·2	27·296	68·959	4418	Table 4
CC271	Río Lajitas	amp, cpx	64·77	56·3	7·6	75·3	27·284	69·938	4709	Table 4
CC104	Valle Ancho	amp, cpx	–	–	–	–	27·339	68·987	4235	Age only
CC279	El Domo	amp, cpx, xeno	59·73	44·4	6·4	60·6	27·045	68·895	4410	Table 4
CC101	Valle Ancho	cpx, ol	55·47	16·2	3·7	44·0	27·359	68·924	4697	Table 4
CC102	Valle Ancho	cpx, ol	55·48	18·2	4·1	42·6	27·353	68·927	4678	Appendix 7
CC262	Valle Ancho	cpx, ol	54·96	18·1	4·2	38·6	27·347	68·954	4535	Table 4
CC296a	Rodrigo	cpx, opx	62·90	48·7	7·1	82·2	26·989	68·766	4753	Table 4
CC296b	Rodrigo	cpx, opx	~62·9	46·5	7·4	70·0	26·989	68·766	4753	Appendix 7
CC297	Rodrigo	cpx, opx	60·91	47·6	6·5	87·2	26·989	68·766	4753	Table 4
Post-migration Pircas Negras volcanic group (<3 Ma)										
CO179	Río Salado	amp, plag	63·33	54·8	8·3	76·6	27·904	69·093	4634	Goss & Kay, 2009
CO177	Río Salado	amp, cpx	61·90	57·5	9·1	81·1	28·001	69·168	4506	Table 4
CO312	Río Salado	amp, cpx	60·89	50·9	8·1	77·9	27·993	69·148	4555	Table 4
CO313	Río Salado	amp, cpx	62·23	50·5	7·8	80·2	27·908	69·094	4623	Table 4

Amp, amphibole; plag, plagioclase; cpx, clinopyroxene; opx, orthopyroxene; ol, olivine; xeno, xenolith.

Appendices 1–8 (available for downloading at http://www.petrology.oxfordjournals.org) for the ~9–2 Ma volcanic rocks discussed here as well as comparative 21–18 Ma Maricunga Belt volcanic rocks complement datasets of Kay *et al.* (1991, 1994, 1999), Mpodozis *et al.* (1995), Tittler (1995) and Goss & Kay (2009). A complete description of the major and trace element analytical methods has been given in Appendix 1 of Goss & Kay (2009). Major element analyses of minerals and glasses made from whole-rock powders in an Ar atmosphere were performed on a JEOL electron microprobe at the Cornell Center for Materials Research using standards from the Smithsonian Institute (e.g. Jarosewich *et al.*, 1980) as described in Table 3 and Supplementary Data Electronic Appendices 1–8. Other whole-rock major element analyses were performed at the Chilean Geological Survey (SERNAGEOMIN) as described by Kay *et al.* (1999). Trace element compositions were determined by instrumental neutron activation

Table 2: Whole-rock K/Ar ages for Pircas Negras region samples

Sample	Location	wt % K	^{40}Ar	% Ar atm.	Age (Ma)	±
Eastern Valle Ancho						
CO24	Los Aparejos	1·321	0·047	62	9·1	0·6
CO72	Los Aparejos	1·315	0·488	59	9·5	0·5
Dos Hermanos						
CC84	Dos Hermanos	2·067	0·618	54	7·7	0·4
Jotabeche, Gallina, Comecaballos						
AC407	Comecaballos	2·410	0·814	56	8·7	0·4
CC15	Cerro Maranceles	1·983	0·520	85	6·7	0·9
AC624	Pircas Negras–Gallina	1·711	0·416	84	6·2	0·9
CC67	Pircas Negras–Gallina	2·169	0·457	75	5·4	0·5
CC11	Pircas Negras	1·780	0·388	96	5·6	2·5
Paso Pircas Negras						
CO413	Pircas Negras	1·956	0·350	78	4·6	0·4
CO414	Pircas Negras	2·187	0·356	81	4·2	0·5
AC409*	Pircas Negras	1·699	0·345	87	5·2	0·9
Southern Rio Salado–Rio Macho Muerto						
CO144†	Pircas Negras	1·737	0·331	93	5·0	1·6
CO145	Pircas Negras	2·450	0·379	49	4·0	0·2
CO146	Pircas Negras	1·722	0·349	83	5·2	0·6
Northern Rio Salado						
CO170	Pircas Negras	1·633	0·300	74	4·7	0·5
CO179	Pircas Negras	2·350	0·178	82	1·9	0·2
Los Patos, Valle Ancho, Tres Cruces						
CC270	Pircas Negras Barros Negros	2·360	0·512	41	5·6	0·3
CC104	western Valle Ancho	2·097	0·432	67	5·3	0·4
CC101	Valle Ancho cone	1·300	0·295	84	5·8	0·7
CC262	Valle Ancho flow	1·336	0·294	56	5·6	0·3
CC296	Rodrigo	2·495	0·430	87	4·4	0·6

*From Kay *et al.* (1991).
†Average of two analyses.
Ages measured at the SERNAGEOMIN geochronology laboratory in Santiago, Chile.

analysis (INAA) and inductively coupled plasma mass spectrometry (ICP-MS) at Cornell University with supplementary analyses on samples analyzed by INAA and atomic absorption at the SERNAGEOMIN in Chile. $^{87}Sr/^{86}Sr$, $^{143}Nd/^{144}Nd$ and some Pb isotopic analyses were performed by thermal ionization mass spectrometry on a VG Sector 54 system in the Keck Isotope Laboratory at Cornell University. Additional Pb isotopic data were obtained on a Nu-Plasma multi-collector ICP-MS system at the University of Florida. Multiple run values for standards are 0·7102957 for $^{87}Sr/^{86}Sr$ on NBS987 and 0·5121436 ($n = 28$) and 0·5118496 ($n = 13$) for $^{143}Nd/^{144}Nd$ on Ames and La Jolla respectively. Pb isotopic data are relative to NBS standard values of $^{206}Pb/^{204}Pb = 16·937$, $^{207}Pb/^{204}Pb = 15·491$ and $^{208}Pb/^{204}Pb = 36·695$. Oxygen isotope compositions of olivine and quartz grains were analyzed in the ArF laser fluorination laboratory at the Universität Göttingen in collaboration with Gerhard Wörner, as described by Kay *et al.* (2011). Analyses were corrected to UWG-2 garnet standard ($\delta^{18}O = 5·7$) with the secondary Doerndrop quartz standard yielding mean values of $\delta^{18}O = 12·32 \pm 0·47‰$ ($n = 3$) and $\delta^{18}O = 12·65 \pm 0·45‰$ ($n = 3$). In-run machine error is estimated at ±0·2‰ with an analytical precision of 0·2–0·5‰.

Petrography and mineral chemistry

The Pircas Negras, Dos Hermanos, and Valle Ancho lava flows are all characterized by a lack of plagioclase phenocrysts, but differ in their mafic phenocryst content. In detail, the Pircas Negras andesites are dark glassy lavas

Table 3: Representative amphibole, olivine, clinopyroxene and orthopyroxene analyses from selected Pircas Negras region samples

	Amphibole								Olivine				
Type:	core	rim	core	rim	core	rim	core	core	core	rim	core	rim	core
Sample:	CO309	CO309	CO427	CO427	CO324	CO324	CO412	CO412	CC101	CC101	CO324	CO324	CO412
SiO_2	40·98	42·29	43·24	43·59	43·64	42·61	42·86	42·89	39·21	37·55	39·31	38·18	39·16
TiO_2	2·92	2·74	2·09	2·26	2·24	3·04	1·90	2·08	0·02	0·03	0·01	0·02	0·05
Al_2O_3	13·36	12·04	11·59	11·15	12·68	12·17	12·65	12·48	0·05	0·02	0·00	0·05	0·05
FeO	13·08	10·96	7·75	8·32	9·18	10·17	7·85	8·77	16·19	26·86	16·20	23·66	17·34
MnO	0·13	0·10	0·09	0·09	0·12	0·06	0·13	0·14	0·23	0·45	0·24	0·44	0·36
MgO	12·60	14·85	16·52	16·80	15·97	15·73	16·71	16·58	44·05	35·19	44·64	38·05	42·78
CaO	11·15	11·41	11·04	11·21	11·18	12·12	11·72	11·48	0·11	0·18	0·11	0·11	0·18
Na_2O	2·70	2·60	2·58	2·49	2·40	2·56	2·48	2·46	–	–	–	–	–
K_2O	0·78	0·78	0·71	0·65	0·71	0·59	0·68	0·77	–	–	–	–	–
Cr_2O_3	0·01	0·03	0·72	0·18	0·17	0·09	0·95	0·22	–	–	–	–	–
Total	97·72	97·80	96·34	96·76	98·29	99·13	97·94	97·87	99·88	100·27	100·50	100·50	99·92
Fo-content									82·9	70·0	83·1	74·1	81·5

	Clinopyroxene									
	Dos Hermanos				Valle Ancho					
Type:	core	rim	core	rim	core	rim	cumulate	core	quartz rim	quartz rim
Sample:	CC81	CC81	CO428	CO428	CC101	CC101	CO309	CO309	CO309	CO427
SiO_2	50·76	50·98	50·11	50·34	51·70	47·52	52·47	50·95	53·30	52·89
TiO_2	0·90	0·73	0·76	0·74	0·53	1·71	0·40	0·67	0·19	0·25
Al_2O_3	4·27	3·08	4·51	3·24	2·14	5·65	2·47	4·59	0·24	0·88
FeO	6·80	6·09	6·75	6·82	6·57	9·98	7·16	7·58	8·51	8·02
MnO	0·10	0·12	0·13	0·17	0·15	0·23	0·13	0·11	0·26	0·25
MgO	14·97	15·41	14·54	15·50	16·56	13·52	16·13	14·78	14·80	15·34
CaO	21·64	22·49	22·30	22·69	20·98	20·00	20·32	20·76	22·04	21·10
Na_2O	0·60	0·43	0·67	0·43	0·22	0·40	0·59	0·78	0·35	0·38
Cr_2O_3	0·31	0·40	0·58	0·07	0·24	0·10	0·28	0·26	0·01	0·00
Total	100·37	99·73	100·35	100·00	99·08	99·12	99·95	100·47	99·69	99·11
En	51·8	52·1	53·9	55·9	52·1	50·5	50·9	51·9	43·3	45·6
Fs	8·1	6·0	5·9	3·9	8·3	13·7	9·6	9·5	12·1	11·6
Wo	40·1	41·8	40·2	40·1	39·6	35·8	39·5	38·6	44·7	42·8

	Clinopyroxene Syn-migration Pircas Negras					Orthopyroxene Syn-migration Pircas Negras				
Type:	core	rim	cum	core	core	core	rim	core	rim	olivine rim
Sample:	CO412	CO412	CO412	CO324	CO324	CO412	CO412	CO324	CO324	CO324
SiO_2	52·36	51·94	52·99	50·97	51·39	54·11	53·71	52·88	52·87	53·85
TiO_2	0·43	0·74	0·18	0·50	0·41	0·19	0·22	0·17	0·18	0·41
Al_2O_3	3·29	1·13	0·92	3·28	3·15	3·06	2·89	1·18	1·19	1·10
FeO	5·82	8·65	8·67	10·85	10·40	10·63	10·65	21·16	21·24	17·00
MnO	0·17	0·35	0·19	0·32	0·26	0·23	0·20	0·55	0·53	0·49

(continued)

Table 3: Continued

	Clinopyroxene					Orthopyroxene				
	Syn-migration Pircas Negras					Syn-migration Pircas Negras				
Type:	core	rim	cum	core	core	core	rim	core	rim	olivine rim
Sample:	CO412	CO412	CO412	CO324	CO324	CO412	CO412	CO324	CO324	CO324
MgO	16·66	15·90	15·55	13·17	13·66	30·22	29·27	23·00	22·90	26·19
CaO	21·15	20·47	21·15	20·03	20·14	1·12	1·64	1·35	1·29	1·58
Na_2O	0·50	0·46	0·54	0·85	0·85	0·04	0·04	0·05	0·02	0·03
Cr_2O_3	0·23	0·00	0·02	0·05	0·14	0·70	0·53	0·01	0·03	0·04
Total	100·60	99·63	100·20	100·00	100·41	100·29	99·14	100·38	100·26	100·70
En	54·2	50·5	48·1	45·1	46·5	2·2	3·3	2·8	2·6	3·2
Fs	6·8	10·1	10·4	15·4	14·2	83·5	81·5	65·5	65·1	72·9
Wo	39·0	39·4	41·5	39·5	39·3	14·2	15·2	31·7	32·3	24·0

with ~10–30% phenocrysts, the majority of which are acicular oxy-amphibole (Fig. 4a–c). Scattered clinopyroxene phenocrysts and olivine clots also occur (Fig. 4c and d), and rare resorbed orthopyroxene phenocrysts are present in a few samples. Plagioclase microlites, rhombic Fe–Ti oxide phases and translucent glass are found in the cryptocrystalline groundmass. Magnetite is present as small (<0·1 mm) equant rhombs or as inclusions in silicate phases, and ilmenite as single grains or in contact with magnetite (Fig. 5). Accessory phases are apatite, zircon and chromite. Plagioclase xenocrysts and highly fractured resorbed quartz xenocrysts rimmed by coronas of radiating acicular clinopyroxene microlaths are also present (Fig. 4b). Lithic clasts composed of highly resorbed albite and quartz grains occur in Pircas Negras syn-migration andesite CO415 (61% SiO_2). The Dos Hermanos andesites differ in having clinopyroxene as their only phenocryst (Fig. 4d), whereas the Valle Ancho basaltic andesites contain both olivine and clinopyroxene phenocrysts.

Amphibole is the dominant phenocryst (85–100%) in the Pircas Negras andesites, where it typically occurs as euhedral grains (0·1–4 mm) with thick opaque reaction rims (Fig. 4a). Glomeroporphyritic cumulate clots are present in a few samples. Most analyzed grains (Table 3; Supplementary Data Electronic Appendix 1) have pargasitic magnesiohastingite compositions with $(Ca + Na) \geq 1{\cdot}00$ and $Na < 0{\cdot}50$ (classification of Leake *et al.*, 1997). A few have tschermakitic compositions with $Na + K < 0{\cdot}5$. Overall, Mg# values vary from 0·62 to 0·80.

Clinopyroxene grains occur in about 60% of the Pircas Negras andesites and all of the Dos Hermanos and Valle Ancho lavas. Compositions of analyzed grains are listed in Table 3 and Supplementary Data Electronic Appendix 2. Where clinopyroxene is present in the Pircas Negras andesites it forms less than 5% of the phenocrysts (Fig. 5c) and can also occur as subhedral to anhedral (<1 mm) grains in crystal clots surrounded by euhedral hornblende laths. Most compositions in the analyzed syn-migration andesites are in the range $En_{44–55}Fs_{5–16}Wo_{38–42}$ (Fig. 6a and b). The slightly more En-rich (55–57) phenocryst cores in andesite CO412 occur with rim and clot compositions ($En_{47–49}Fs_{10–12}Wo_{40–42}$) similar to the core, rim and clot compositions in andesites CO309 and CO412. Overall, the most Wo-rich (43–45) compositions are in rims and clots in andesite CO309, and the most Fs-rich (~16) in phenocrysts in andesite CO324. The <1 mm tabular normally zoned clinopyroxene phenocrysts within the cryptocrystalline glassy matrix of the Dos Hermanos andesites (Fig. 4d) have compositions that overlap those of the more En-rich Pircas Negras clinopyroxene grains ($En_{48–56}Fs_{5–11}Wo_{37–42}$; Fig. 6c). The clinopyroxene phenocrysts (Fig. 6c; CC101) in the Valle Ancho lavas have core compositions overlapping those in the Dos Hermanos and Pircas Negras andesites with rims that reach $Fs_{10–15}$ and $Wo_{39–36}$.

Rare orthopyroxene occurs in some syn-migration Pircas Negras andesites as <1 mm subhedral phenocrysts and as aggregate rims on subhedral olivine grains. Compositions are $En_{82–84}$ and $En_{65–66}$ respectively in phenocrysts in andesites CO412, and CO324, and En_{91} and En_{73} in aggregate rims in andesite CO324 (Table 3; Supplementary Data Electronic Appendix 3; Fig. 6a). The presence or absence of orthopyroxene, like olivine, does not correlate with bulk-rock wt % SiO_2.

Olivine occurs as aggregates of ~10–20 anhedral olivine grains in some Pircas Negras andesites (Fig. 4c) and as phenocrysts in the Valle Ancho basaltic andesites. The compositions of the analyzed grains are reported in Table 3 and Supplementary Data Electronic Appendix 4. The cumulate grains in Pircas Negras andesite CO324 have $Fo_{79–83}$ cores and $Fo_{74–79}$ rims (Fig. 6a). Olivine

Table 4: Representative and new major and trace element analyses for Pircas Negras region samples (~27–28° S latitude)

	Pre-migration					Basaltic andesites		Syn-migration Pircas Negras		
	Los Aparejos		Dos Hermanos		Redonda	Valle Ancho		Jotabeche–Rio La Gallina		
Sample:	CO72	CO24*	CO428*	CC81*	CC94	CC101	CC262	CC17†	CO415	CO416*
SiO_2	52·64	53·25	58·95	57·34	63·41	55·47	54·96	58·39	60·94	58·91
TiO_2	1·09	1·04	1·15	1·05	0·88	1·21	1·28	0·93	0·93	1·15
Al_2O_3	15·23	15·33	16·80	17·66	17·08	16·46	16·59	17·81	16·47	17·51
Fe_2O_3	3·69	3·38	3·40	–	3·67	–	–	–	2·58	–
FeO	3·93	4·76	1·63	–	0·66	–	–	–	1·57	–
FeO_{total}	7·25	7·80	4·69	5·52	3·96	7·31	7·44	5·60	3·89	5·14
MnO	0·13	0·13	0·09	0·09	0·05	0·13	0·12	0·09	0·06	0·09
MgO	8·64	8·37	3·18	3·03	1·92	5·70	5·10	3·51	2·66	2·77
CaO	8·47	8·02	6·50	6·37	4·03	7·55	7·96	6·00	6·69	6·86
Na_2O	3·49	3·36	4·50	4·62	4·58	3·39	3·75	4·42	4·50	4·80
K_2O	1·77	1·68	2·86	2·61	3·05	1·58	1·60	2·34	2·83	2·18
P_2O_5	0·28	0·24	0·40	0·45	0·28	0·29	0·28	0·40	0·31	0·57
Total	98·99	99·22	99·12	98·74	99·24	99·09	99·08	99·49	99·28	99·98
Mg#	68·0	65·7	54·7	49·5	46·3	58·2	55·0	46·3	54·9	49·0
La	32·0	28·5	62·8	57·6	41·6	23·9	24·2	42·2	43·1	30·4
Ce	65·3	63·0	104·8	116·7	79·9	52·5	54·8	84·5	87·3	61·2
Pr	–	7·88	14·87	13·63	9·46	6·47	6·77	–	–	8·30
Nd	31·9	31·2	56·1	51·1	34·0	26·3	27·7	37·8	46·1	32·9
Sm	5·58	5·73	8·64	7·86	5·47	5·44	5·68	5·99	7·15	6·11
Eu	1·50	1·61	2·31	2·24	1·47	1·73	1·81	1·63	1·64	1·81
Gd	–	4·5	5·1	4·5	3·4	4·7	4·7	–	–	4·4
Tb	0·56	0·67	0·62	0·61	0·38	0·62	0·61	0·56	0·46	0·50
Dy	–	3·7	2·9	2·9	1·7	3·3	3·2	–	–	2·3
Ho	–	0·74	0·50	0·51	0·26	0·59	0·55	–	–	0·36
Er	–	1·91	1·18	1·19	0·77	1·64	1·51	–	–	0·98
Tm	–	0·298	0·170	0·174	0·100	0·216	0·197	–	–	0·124
Yb	1·5	1·7	1·0	1·0	0·7	1·4	1·3	1·0	0·9	0·8
Lu	0·223	0·250	0·134	0·140	0·095	0·205	0·185	0·137	0·112	0·114
Y	18·0	19·9	13·7	14·4	9·5	18·3	16·8	11·0	9·0	11·9
Rb	32	31	64	66	79	35	35	55	49	55
Sr	897	767	1402	1278	793	612	672	740	1016	850
Ba	744	624	1231	1156	1034	555	588	854	1312	810
Pb	9·0	8·3	13·0	14·6	13·8	7·1	6·6	7·0	9·0	8·9
Cs	0·4	0·9	1·0	2·0	1·6	1·3	0·9	1·5	0·7	1·9
U	0·90	0·85	1·26	1·41	1·29	0·77	0·77	1·23	1·18	1·11
Th	3·5	4·1	10·1	8·7	8·2	3·0	2·9	6·4	5·3	3·8
Zr	133	185	256	219	223	190	192	231	239	231
Hf	3·7	4·0	5·3	5·8	5·6	4·7	4·8	5·3	5·6	5·5
Nb	8·0	10·2	12·7	12·9	9·9	9·9	10·3	12·0	9·0	12·0
Ta	0·58	0·56	0·66	0·72	0·58	0·60	0·60	0·67	0·57	0·73
Sc	23·7	22·2	9·3	9·5	7·2	23·0	18·5	12·5	10·0	8·4
Cr	632	575	55	57	17	196	188	46	72	46
Ni	228	175	26	20	9	46	49	26	24	23
Co	40	37	17	16	9	26	25	19	15	12
Cu	51	45	–	22	22	13	30	24	92	–
Zn	86	90	–	88	89	81	96	92	107	–
V	191	169	121	115	92	211	203	121	25	102

(continued)

Table 4: Continued

	Syn-migration Pircas Negras									
	Paso Pircas Negras			Rio Salado				Laguna Brava		
Sample:	CO412*	CO413	CO414	CO173	CO175	CO176	CO507*	CO159	CO160	CO161
SiO_2	57·38	58·94	61·97	58·89	60·57	63·40	63·04	62·21	59·21	63·80
TiO_2	1·01	0·96	0·85	0·91	0·93	0·68	0·91	0·98	0·78	0·95
Al_2O_3	18·02	17·32	16·82	16·36	16·67	16·11	16·54	16·23	15·83	16·08
Fe_2O_3	2·15	2·27	1·52	2·76	3·14	2·85	–	2·57	2·89	1·98
FeO	3·38	4·63	2·47	3·47	2·14	1·91	–	2·82	2·67	2·87
FeO_{total}	5·31	6·67	3·84	5·95	4·96	4·48	4·67	5·13	5·28	4·65
MnO	0·10	0·09	0·08	0·10	0·08	0·08	0·08	0·08	0·09	0·06
MgO	4·71	3·67	2·69	4·11	2·55	2·34	2·35	2·37	4·33	2·03
CaO	6·48	6·10	5·19	6·34	5·74	4·77	5·08	4·83	6·03	3·97
Na_2O	4·02	4·05	4·22	4·07	4·68	4·17	4·10	4·26	3·78	4·24
K_2O	2·32	2·66	2·93	2·09	2·30	2·88	2·89	2·67	2·32	2·90
P_2O_5	0·27	0·26	0·24	0·26	0·37	0·17	0·35	0·25	0·24	0·29
Total	99·63	100·73	98·82	99·08	98·86	99·09	100·00	99·01	97·90	98·98
Mg#	61·2	49·50	55·5	55·2	47·8	48·2	47·3	45·2	59·4	43·7
La	36·7	43·0	42·2	25·7	41·8	38·7	46·8	41·8	32·5	47·4
Ce	70·1	88·3	89·5	56·1	86·4	70·9	89·7	91·6	69·5	99·3
Pr	9·25	–	–	–	–	–	10·90	–	–	–
Nd	35·7	47·2	42·0	28·7	37·7	32·7	41·1	36·6	32·3	43·3
Sm	6·46	7·46	6·78	5·41	6·48	5·78	7·07	6·98	4·93	7·28
Eu	1·87	1·78	1·64	1·47	1·68	1·21	1·85	1·59	1·42	1·70
Gd	4·9	–	–	–	–	–	4·7	–	–	–
Tb	0·60	0·65	0·56	0·60	0·52	0·54	0·58	0·67	0·91	0·57
Dy	3·1	–	–	–	–	–	2·8	–	–	–
Ho	0·55	–	–	–	–	–	0·47	–	–	–
Er	1·54	–	–	–	–	–	1·32	–	–	–
Tm	0·202	–	–	–	–	–	0·173	–	–	–
Yb	1·3	1·4	1·1	1·2	0·8	1·2	1·1	1·3	1·5	1·1
Lu	0·196	0·193	0·149	0·169	0·110	0·164	0·163	0·179	0·214	0·152
Y	17·2	14·0	11·0	15·0	11·0	14·0	15·3	17·0	17·0	14·0
Rb	47	52	57	54	56	95	81	80	77	74
Sr	912	995	705	626	897	737	901	665	699	732
Ba	791	1139	1156	700	1002	925	952	852	727	1025
Pb	8·0	9·0	10·0	8·0	8·0	13·0	11·3	11·0	9·0	12·0
Cs	1·1	1·7	1·7	2·5	1·7	1·9	2·0	2·1	4·0	1·8
U	1·05	1·44	1·57	0·86	1·50	2·29	1·44	1·87	2·68	1·47
Th	5·1	7·0	7·3	3·3	5·2	9·2	9·2	7·8	6·0	7·5
Zr	229	247	259	201	249	215	253		222	291
Hf	5·3	5·8	6·1	4·9	5·8	5·0	5·9	7·1	5·2	6·9
Nb	11·2	9·0	9·0	10·0	12·0	9·0	12·1	12·0	10·0	11·0
Ta	0·64	0·72	0·63	0·57	0·70	0·56	0·67	0·79	0·76	0·67
Sc	15·9	14·0	9·0	16·1	8·2	10·7	9·4	9·1	14·3	7·7
Cr	141	100	57	160	61	29	30	38	207	42
Ni	82	18	25	46	24	10	14	13	63	20
Co	20	18	13	21	14	12	11	12	18	12
Cu	95	95	95	32	30	17	–	16	31	20
Zn	127	127	94	85	89	70	–	90	80	92
V	142	29	24	148	107	117	101	107	124	100

(continued)

Table 4: Continued

	Syn-migration Pircas Negras								Post-migration Pircas Negras	
	Laguna Brava		Los Patos–Valle Ancho				Rodrigo		Upper Rio Salado	
Sample:	CO333*	CO502	CC252	CC254	CC271	CC279	CC296a*	CC297	CO177	CO312*
SiO_2	63·80	63·26	63·56	57·11	64·77	59·73	62·90	60·91	61·90	60·89
TiO_2	0·95	0·92	0·88	1·11	0·73	0·78	0·74	0·79	0·89	1·00
Al_2O_3	16·08	16·43	15·64	16·42	16·19	15·51	15·97	16·32	16·82	16·45
Fe_2O_3	1·98	–	–	–	–	–	–	–	2·20	–
FeO	2·87	–	–	–	–	–	–	–	2·37	–
FeO_{total}	4·65	4·29	4·66	6·54	3·97	4·71	4·11	4·23	4·35	4·91
MnO	0·06	0·04	0·08	0·12	0·05	0·09	0·08	0·07	0·06	0·08
MgO	2·03	2·24	2·25	4·20	2·32	3·34	2·16	2·45	1·92	2·43
CaO	3·97	4·87	5·05	7·46	3·96	6·76	4·71	5·14	4·73	5·87
Na_2O	4·24	4·64	4·03	4·01	4·28	3·96	4·28	4·23	4·67	5·06
K_2O	2·90	2·93	2·71	1·98	3·37	2·45	3·10	3·08	2·90	2·90
P_2O_5	0·29	0·35	0·26	0·32	0·22	0·26	0·25	0·24	0·30	0·35
Total	98·98	99·97	99·12	99·27	99·86	97·59	98·30	97·46	98·55	99·93
Mg#	43·7	48·3	46·3	53·4	51·0	55·8	48·4	50·8	44·0	46·9
La	36·2	42·2	38·2	35·1	42·6	46·9	36·8	39·5	46·1	40·5
Ce	83·7	94·2	78·4	67·6	87·2	89·7	80·8	72·6	92·8	91·2
Pr	9·87	–	–	–	–	–	9·65	–	–	11·06
Nd	37·1	44·3	35·2	34·2	35·4	39·3	35·7	32·6	43·2	41·8
Sm	6·26	6·60	6·42	6·12	5·73	6·71	5·89	5·42	7·27	6·95
Eu	1·61	1·82	1·36	1·61	1·33	1·47	1·50	1·24	1·42	1·78
Gd	3·8	–	–	–	–	–	3·5			4·1
Tb	0·52	0·57	0·50	0·65	0·32	0·54	0·47	0·45	0·47	0·54
Dy	2·5	–	–	–	–	–	2·3	–	–	2·5
Ho	0·44	–	–	–	–	–	0·39	–	–	0·43
Er	1·07	–	–	–	–	–	0·94	–	–	1·00
Tm	0·159	–	–	–	–	–	0·136	–	–	0·145
Yb	0·9	0·9	1·3	1·3	0·8	1·1	0·8	0·8	0·8	0·8
Lu	0·134	0·108	0·151	0·181	0·094	0·132	0·110	0·100	0·109	0·116
Y	13·1	–	–	–	8·0	–	11·4	–	11·0	11·6
Rb	87	–	104	46	116	80	93	74	65	68
Sr	831	773	540	778	458	875	821	657	824	863
Ba	998	1081	757	759	1029	737	958	901	1033	984
Pb	15·5		12·0	6·0	13·0	9·0	11·2	7·0	10·0	11·5
Cs	3·3	1·9	3·5	0·7	3·3	4·7	1·3	1·3	1·0	1·2
U	1·64	1·24	3·58	1·03	2·44	3·51	1·37	1·49	1·32	1·13
Th	8·0	6·2	15·0	5·4	14·0	11·0	11·0	8·6	7·2	7·8
Zr	305	–	197	172	218	154	286	213	289	350
Hf	6·2	6·7	5·9	5·1	5·6	5·2	5·8	5·5	6·8	7·3
Nb	11·5	–	9·4	9·9	7·0	9·1	9·2	6·9	10·0	10·9
Ta	0·68	0·63	0·90	0·67	0·57	0·77	0·53	0·45	0·57	0·60
Sc	7·8	7·3	–	17·7	7·9	12·3	8·4	7·6	6·5	7·0
Cr	39	38	39	100	31	97	70	53	25	29
Ni	16	16	17	32	11	37	20	16	9	23
Co	11	11	13	22	12	17	12	11	10	11
Cu		–	17	29	19	26	19	18	16	–
Zn		–	93	94	65	83	93	78	85	–
V	88	–	108	157	97	113	98	59	89	94

*Analyses from Goss & Kay (2009).
†Partial analyses from Kay *et al*. (1994).
Cu and Zn were analyzed at Chilean Geological Survery (SERNAGEOMIN) [see Kay *et al*. (1999) for analytical techniques].

Table 5: Sr, Nd, Pb and O isotopic analyses for Pircas Negras Region samples (~27–28°S latitude)

Sample	Unit	Age	$^{87}Sr/^{86}Sr$	$^{143}Nd/^{144}Nd$	$^{206}Pb/^{204}Pb$	$^{207}Pb/^{204}Pb$	$^{208}Pb/^{204}Pb$	$\delta^{18}O_{ol}$	$\delta^{18}O_{qz}$
CO412	Pircas Negras	~5	0·705767	0·512501	*18·650*	*15·611*	*38·654*		
CC17	Pircas Negras	5·7 ± 0·5	0·705569	0·512513	18·640	15·600	38·578		
AC(PN)409*	Pircas Negras	5·2 ± 0·9	0·705799	0·512489					
AC(PN)406*	Pircas Negras	~8·8	0·706403	0·512478					
CO427	Pircas Negras	~6	0·705560	0·512503	*18·644*	*15·616*	*38·627*		+8·35 ± 0·2
CO179	Pircas Negras	1·9 ± 0·2	0·706255	0·512426	*18·663*	*15·612*	*38·698*		
CO309	Pircas Negras	~5	0·705565	0·512505	*18·631*	*15·611*	*38·603*		
CO310	Pircas Negras	~5	0·705713	0·512477					
CO324	Pircas Negras	~5	0·706193	0·512451	*18·726*	*15·617*	*38·731*	+6·2 ± 0·2	
CO332	Pircas Negras	~5	0·706406	0·512428					
CO507	Pircas Negras	~4			*18·675*	*15·615*	*38·704*		
CO428	Dos Hermanos	~8	0·705738	0·512467					
CC81	Dos Hermanos	7·7 ± 0·4	0·705871	0·512491	18·640	15·610	38·612		
CC271	Pircas Negras	~5·6	0·706415	0·512431	18·680	15·620	38·761		
CC296a	Rodrigo	4·4 ± 0·6	0·706278	0·512396	18·656	15·610	38·709		
CC297	Rodrigo	~4·4	0·706273						
CC01	Valle Ancho	5·8 ± 0·7	0·705667	0·512478				+6·2 ± 0·2	
CC262	Valle Ancho	5·6 ± 0·3	0·705943	0·512493	18·680	15·610	38·619		
CO24	Los Aparejos	9·1 ± 0·6	0·706229	0·512477	*18·688*	*15·613*	*38·588*		
CO446	Escabroso	~21	0·705053	0·512597					
CO335	Escabroso	~21	0·704948	0·512609					
CO292	Escabroso	~21	0·704784	0·512584					
CO264	Escabroso	21·9 ± 0·8	0·704857	0·512625					

Pb analyses in italics were carried out at the University of Florida, others at Cornell University.
*Analyses from Kay *et al.* (1991).

grains in the Valle Ancho lavas, which constitute less than 10% of the phenocrysts, have cores in the range $Fo_{83–73}$ and rims of $Fo_{74–66}$ (Fig. 6c).

Groundmass microlites or microphenocrysts (<0·5 mm) and larger subhedral to anhedral xenocrysts (1–10 mm) are the primary plagioclase grains in the Pircas Negras and Dos Hermanos andesites. The compositions of the analyzed grains are given in Supplementary Data Electronic Appendix 5 and plotted in Fig. 7. Most microlites in the Pircas Negras andesites have compositions of $An_{48–65}$ and show little zoning; a few are less than An_{40}. Microlites from andesite CO412 have the highest average An contents (An_{61}) and those from andesite CO309 the lowest (An_{57}). The microlites in the Dos Hermanos andesites exhibit a wider range ($An_{17–59}$), whereas those in the Valle Ancho basaltic andesite are $An_{46–51}$. A single zoned phenocryst ($An_{46–66}$) in Dos Hermanos andesite CC81 compositionally overlaps the Pircas Negras microlites. The xenocrystic plagioclase grains in the Pircas Negras andesites display extensive resorption, reverse zoning and sieve textures. The compositions of their cores are more albitic ($An_{26–41}$) than the microphenocrysts, whereas the compositions of their rims overlap ($An_{28–49}$). Only in syn-migration Pircas Negras andesite (CO324) do the xenocrysts exceed 5% of the total crystal population.

Calculated temperatures and fO_2

Pre-eruptive crystallization temperatures for Pircas Negras andesites CO412 and CO324 were investigated using coexisting pyroxene (Lindsley, 1983) and magnetite–ilmenite (Andersen & Lindsley, 1988) phase equilibria. The temperatures were calculated using the algorithms in the QUILF95 program (Anderson *et al.*, 1993).

Following Lindsley (1983), coexisting pyroxene temperatures were calculated from Wo–Fs–En end-members in pyroxenes considered to be in equilibrium after correcting for non-quadrilateral components (Fig. 6a; Supplementary Data Electronic Appendices 2, 3 and 9). A preferred temperature range of 1064 ± 72°C to 1074 ± 50°C for andesite CO412 is based on average orthopyroxene (CO412-1; Table 3) and clinopyroxene phenocryst compositions in grains showing similar extents of resorption and

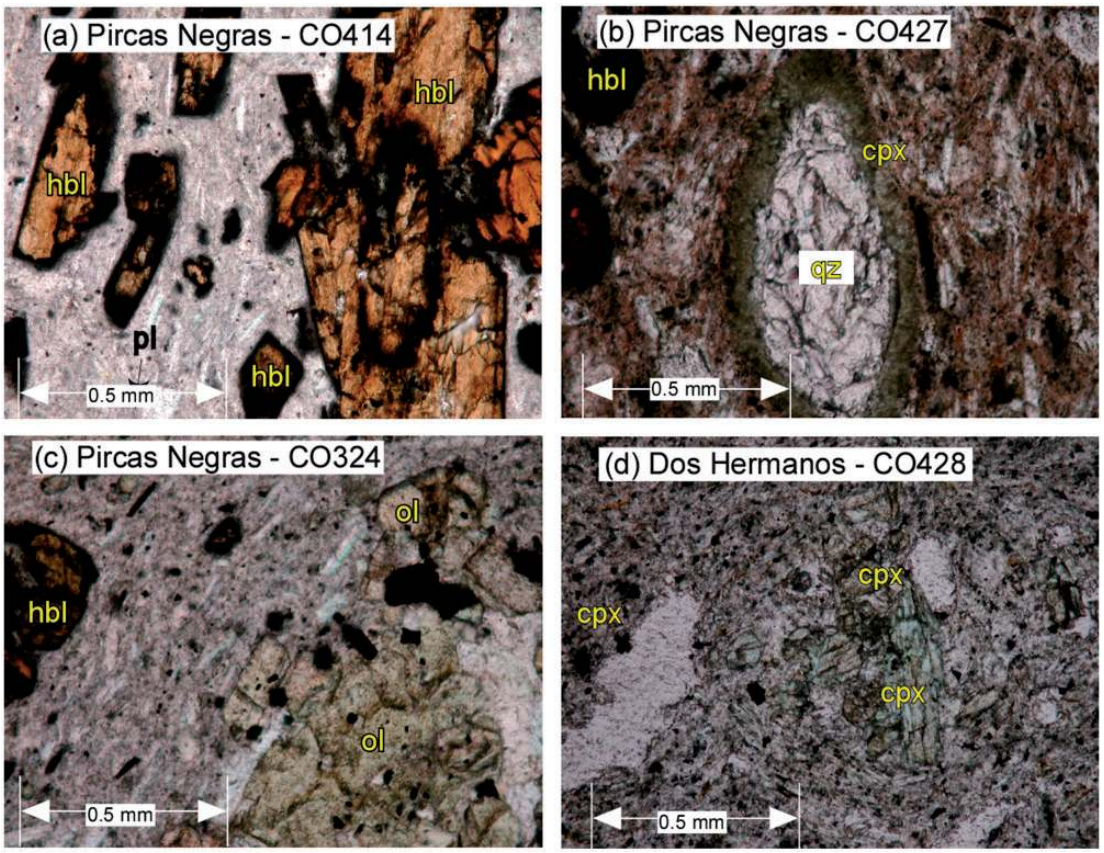

Fig. 4. Photomicrographs: (a) oxidized magnesiohastingitic amphibole (hbl) in ~5·2 Ma Paso Pircas Negros syn-migration andesite CO414; (b) resorbed quartz xenocryst (qz) with clinopyroxene (cpx) reaction corona in ~6·2 Ma Rio Gallina region syn-migration Pircas Negras andesite CO427; (c) glomeroporphyritic olivine (ol) clot in ~5 Ma Rio Veladero region syn-migration Pircas Negras andesite CO324; (d) clinopyroxene in 7·7 Ma Dos Hermanos andesite CO428. Mineral compositions are from Tables 3 and Electronic Appendix Tables 1–6.

disequilibrium with the groundmass. Combining clinopyroxene rim and orthopyroxene compositions results in higher temperatures with larger errors (1072–1082 ± 57–92°C). Calculating a temperature for andesite CO324 is complicated by the bimodal orthopyroxene compositions, reversely zoned clinopyroxene phenocrysts, and petrographic evidence for disequilibrium. Pairing high-Mg orthopyroxene rims on olivine phenocrysts (CO324-2; Table 3) with clinopyroxene phenocrysts gives temperatures of 1067–1069 ± 50°C, which are consistent with those from andesite CO412. Other combinations of orthopyroxene and clinopyroxene cores yield temperatures of 954–977 ± 50–57°C (see Fig. 6a).

In-contact pairs of magnetite and ilmenite grains (Fig. 5; Supplementary Data Electronic Appendices 6 and 10) were used to calculate pre-eruptive fO_2 and temperature using the program of Andersen *et al.* (1993). A single in-contact magnetite–ilmenite pair in andesite CO412 yielded a temperature of 880 ± 23–41 °C at an fO_2 of ~2·5 log units above the quartz–fayalite–magnetite (QFM) buffer. In-contact pairs in andesite CO324 yielded temperatures ranging from 788 ± 10°C to 900 ± 31 °C.

Whole-rock major and trace element variations

The Pircas Negras and Dos Hermanos lavas contain 56–64 wt % SiO_2 with Mg# values of 36–61 (Table 4; Supplementary Data Electronic Appendix 7; Fig. 8a–h), with the most mafic samples (57–59 wt % SiO_2) occurring near Paso Pircas Negras and in the southern Rio Salado region, and the most silicic (62–64 wt % SiO_2) in the northern Rio Salado valley and near the Los Patos stratovolcano (Figs 2b and 3). On the basis of the wt % K_2O–SiO_2 diagram of Le Maitre *et al.* (1989), the Pircas Negras lavas are high- to medium-K andesites and dacites and the Dos Hermanos lavas are high-K andesites (Fig. 8a). On variation diagrams versus wt % SiO_2, the data generally define linear trends in wt % CaO, MgO and total Fe as FeO* (Fig. 8c–e) and wt % TiO_2 (Fig. 8f) from 0·62 to 1·3%. Their wt % Na_2O (3·8–5·5, Fig. 8g) extends to notably high values at variable wt % Al_2O_3 (15–18%, Fig. 8h). Overall, the Dos Hermanos lavas have higher wt % K_2O and Na_2O and lower wt % CaO at the same wt % SiO_2. The ~9 Ma Los Aparejos (~53 wt % SiO_2, Mg# = 66–68) and ~5 Ma Valle Ancho (~57 wt % SiO_2,

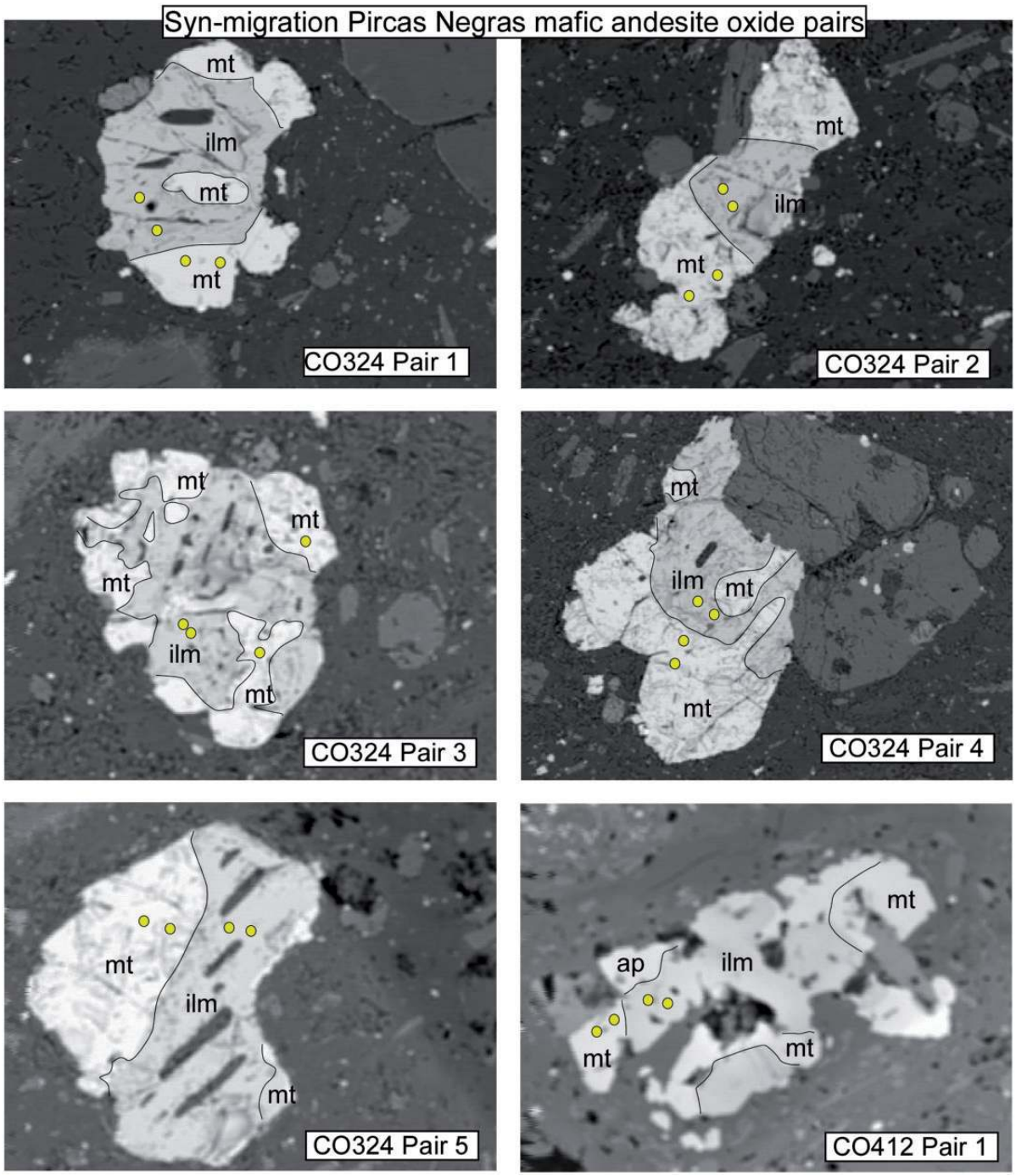

Fig. 5. Electron microprobe backscatter electron images of in-contact magnetite–ilmenite grains in syn-migration Pircas Negras mafic andesites CO324 (59·1% wt % SiO_2) and CO412 (57·4% wt % SiO_2) (see Table 1). Circles indicate analyzed points. Mineral analyses are given in Electronic Appendix 6. Calculated pre-eruptive temperatures are discussed in text and shown in Electronic Appendix 10.

Mg# = 55–58) lavas have lower wt % Na_2O (3·3–3·8) and K_2O (1·5–1·7). In comparison, the older 21–18 Ma Escabroso Formation and 16–13 Ma southern Maricunga Belt lavas are marked by lower wt % K_2O, Na_2O, TiO_2 and MgO at higher wt % Al_2O_3 (Supplementary Data Electronic Appendix 8; Kay *et al.*, 1991, 1994; Mpodozis *et al.*, 1995).

As discussed by Goss & Kay (2009), the Pircas Negras and Dos Hermanos lavas have trace element features that distinguish them from most central Andean andesites.

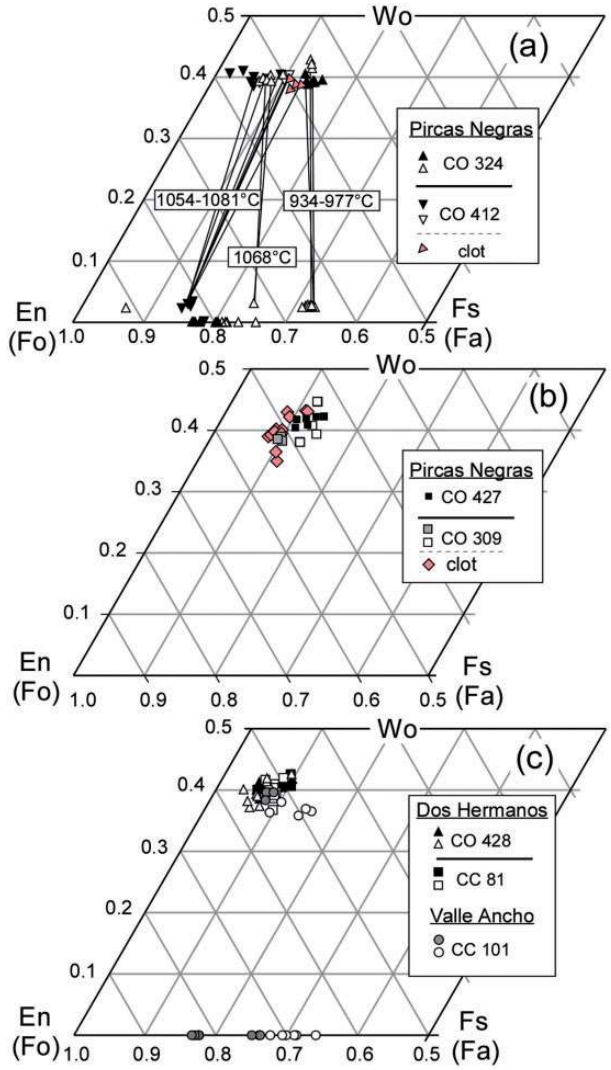

Fig. 6. Compositional variation of pyroxene and olivine (data from Table 3 and Electronic Appendices 2–4). Pyroxene cation totals are corrected for Fe^{2+}/Fe^{3+} using the method of Droop (1987). End-member compositions are En ($MgSiO_3$), Fs ($FeSiO_3$) and Wo ($CaSiO_3$) for pyroxene, and Fo (Mg_2SiO_4) and Fa (Fe_2SiO_4) for olivine (base of diagrams). Filled symbols are cores and clots; open symbols are rims. Analyzed samples: (a) syn-migration Pircas Negras CO324 (~5 Ma Veladero) and CO412 (5·2 Ma Paso Pircas Negras); tie-lines connect pyroxene pairs used in calculating two-pyroxene equilibration temperatures discussed in the text and reported in Electronic Appendix 7; (b) Pircas Negras samples CO427 (~6 Ma La Gallina) and CO309 (~4 Ma Barrancas Blancas); (c) Dos Hermanos samples CO428 and CC81 and Valle Ancho basaltic andesite CC101.

One of these features is their steep REE patterns, which exhibit high degrees of HREE depletion (Figs 9–11). In detail, La/Yb (15–55), La/Sm (4·5–7·5) and Sm/Yb (4·2–8·4) ratios in the Pircas Negras lavas are lower than those in the Dos Hermanos–Redondo lavas (La/Sm = 7–7·5; Sm/Yb = 8–9; Fig. 11a and b). Dy/Yb ratios, which capture the concave-upward curvature of the REE pattern associated with residual amphibole, are generally lower at a given wt % SiO_2 in the amphibole-bearing Pircas Negras (2·2–3·1) than in the amphibole-free Dos Hermanos lavas (2·9–3·1). In comparison, the Valle Ancho basaltic andesites have the lowest La/Sm, Sm/Yb and Dy/Yb (2·18–3·5) ratios (Fig. 11a and b). Eu anomalies are generally small (average Eu/Eu* ~1·0, range 0·88–1·10; Fig. 9a) in the Pircas Negras andesites, whereas those in the Dos Hermanos lavas are slightly positive (1·06–1·11; Fig. 9c).

Other features of the Pircas Negras and Dos Hermanos lavas are their pronounced arc-like large ion lithophile element (LILE) enrichment and high field strength element (HFSE) depletion as seen in mid-ocean ridge basalt (MORB)-normalized trace element patterns (Figs 9 and 10) and plots of La/Ta (>40) versus La/Yb and Ba/Ta (Fig. 11c and d). The Dos Hermanos lavas have the highest LILE concentrations and the largest HFSE depletion (La/Ta >80), and the Valle Ancho basaltic andesites the lowest HFSE depletion (La/Ta = 39–41). The 3–2 Ma Rio Salado andesites show the most LILE enrichment and HFSE depletion (75–80) among the Pircas Negras lavas. All of the lavas have Nb/Ta ratios >16 with the highest ratios (18–20) in the Dos Hermanos andesites (Goss & Kay, 2009). Other common features are positive Pb anomalies (7–17 ppm Pb) in MORB-normalized trace element patterns (Figs 9b, 9 and 10b).

Trace element differences between the ~9–2 Ma lavas and older Maricunga Belt and younger CVZ (e.g. Cerro Peinado, Falso Azufre, San Francisco; Mpodozis *et al.*, 1996; Kay & Mpodozis, 2002) lavas are highlighted in Figs 9, 11 and 12. In comparison, both the 21–18 Ma Escabroso Formation and <3 Ma CVZ andesites have lower Sm/Yb and La/Yb ratios indicating flatter REE patterns, lower HFSE depletion and lower Sr/Yb ratios. Among these, the 21–18 Ma Escabroso Formation andesites have the flattest REE patterns (La/Yb = 8–10; Sm/Yb = 2·2–2·6) and lowest ppm Ni and Cr, and the CVZ lavas the most light REE (LREE) enrichment (La/Sm to 6·5) and highest ppm Cr (30) and Ni (40). The 16–13 Ma Maricunga Belt lavas have La/Yb, Sm/Yb and Sr/Yb ratios and Sr, Ni and Cr contents that overlap the lower ranges in the Pircas Negras and Dos Hermanos lavas. The La/Ta (>42) ratios of the Pircas Negras and Dos Hermanos lavas are uniformly much higher than in the 21–18 Ma or CVZ lavas.

In detail, the pre-, syn- and post-migration groups have distinctive characteristics. The pre-migration (7·7 Ma Dos Hermanos, 8·8 Ma Comecaballos, ~8 Ma Redondo) andesites are characterized by very steep REE patterns (La/Yb = 58–64), and high La/Ta ratios (92–101) that fall off trends for the syn-migration 7–3 Ma lavas (Fig. 11). The steep REE patterns are largely due to very steep HREE patterns (Sm/Yb = 8·0–8·8), and the strong HFSE

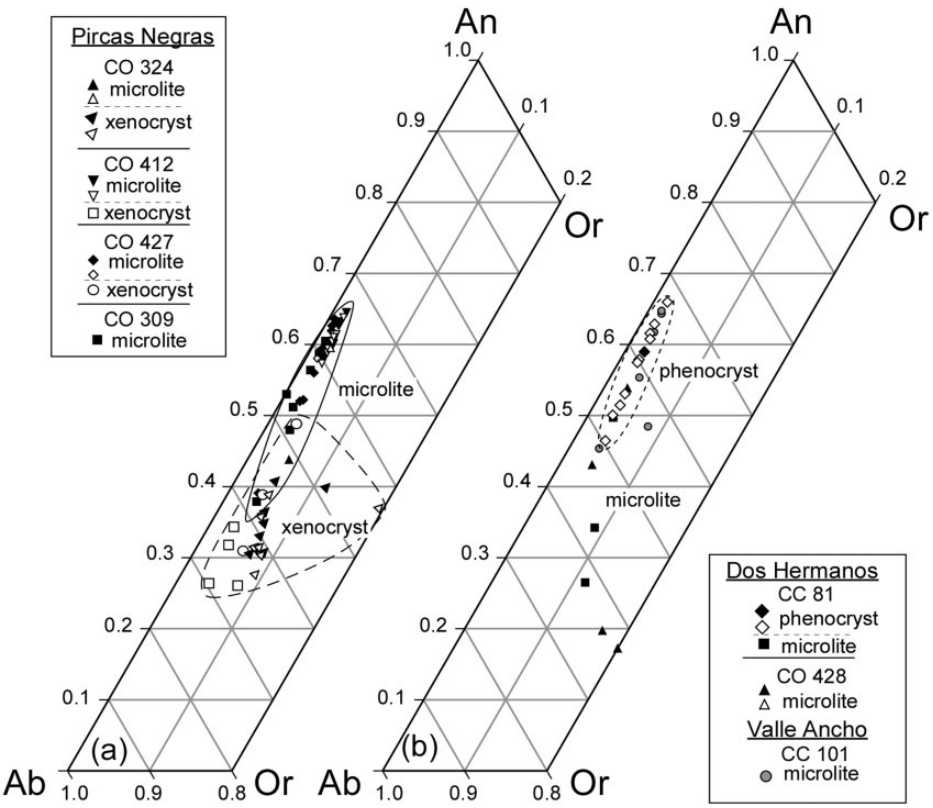

Fig. 7. Triangular plot of Ab ($NaAlSi_3O_8$), An ($CaAl_2Si_2O_8$) and Or ($KAlSi_3O_8$) compositions for plagioclase microlites or microphenocrysts and xenocrysts in Pircas Negras syn-migration andesites, a single phenocryst-like plagioclase and microlites or microphenocrysts in pre-migration Dos Hermanos andesites and microlites or microphenocrysts in the Valle Ancho mafic andesite. Filled symbols are cores; open symbols are rims; xenocrysts are shaded. Data are from Electronic Appendix 5.

depletion (Ba/Ta = 1800–2400) and extreme LREE enrichment are coupled with lower Ba/La ratios (19–24) than in most Pircas Negras andesites (Fig. 11b). The Dos Hermanos andesites are notable for having the highest Sr concentrations (1220–1436 ppm) and Sr/Yb ratios (1216–1302), with those of the Comecaballos lava (800 ppm Sr; Sr/Yb = 1011) also being very high (Fig. 12a and b). Cr is <100 ppm and Ni is <25 ppm in all of these lavas (Fig. 12c and d). In comparison, the more mafic ~9 Ma Los Aparejos lavas have flatter REE patterns (La/Yb = 17–22; Sm/Yb = 3·3–3·8), less HFSE depletion (La/Ta = 55; Ba/Ta = 1126–1285) and lower Sr (720–897 ppm) and higher Cr (632–672 ppm) and Ni (174–228 ppm) concentrations.

The 7–3 Ma syn-migration Pircas Negras andesites show a wide variability in REE patterns (La/Yb = 19–57), degree of HFSE depletion (La/Ta = 36–76) and range of Sr (460–1050 ppm), Cr and Ni concentrations and Sr/Yb ratios. Their REE variability is largely attributable to the HREE, with Sm/Yb ratios ranging from 4 to 8. Cr and Ni concentrations reach 250 ppm and 60 ppm respectively in the 5–3 Ma Paso Pircas Negras and Rio Salado lavas, with the highest values correlating with the lowest Sm/Yb ratios. Similar high Cr and Ni concentrations are absent in the pre- and post-migration lavas, which have higher Sm/Yb ratios. The mafic Valle Ancho lavas are most like the Los Aparejos lavas in showing less LREE enrichment, and higher Cr (195–201 ppm) and Ni (46–59 ppm) concentrations, and in lacking very high Sr (477–593 ppm) concentrations and Sr/Yb ratios (333–426). In contrast, the 3–2 Ma post-migration Pircas Negras lavas have trace element signatures broadly similar to those of the pre-migration andesites. These signatures include higher La/Yb ratios (51–58) at a given wt % SiO_2, higher Sm/Yb (7·8–9·1) and La/Ta (77–81) ratios, and lower maximum Cr (3–28 ppm) and Ni (9–10 ppm) concentrations than the 7–3 Ma syn-migration andesites. Their Sr (824–892 ppm) concentrations and Sr/Yb ratios (913–1040) are like those in the 7–3 Ma lavas.

Nd–Sr–Pb isotopic ratios

A temporal trend to higher $^{87}Sr/^{86}Sr$ and lower $^{143}Nd/^{144}Nd$ ratios in mafic to silicic lavas erupted during and after, compared with before, the eastward displacement of the arc front is superimposed on an enrichment trend with increasing wt % SiO_2 in Fig. 13 (data and references are given in Table 5). In detail, $^{87}Sr/^{86}Sr$ ratios in the Dos Hermanos–Pircas Negras andesites (0·7055–0·7065)

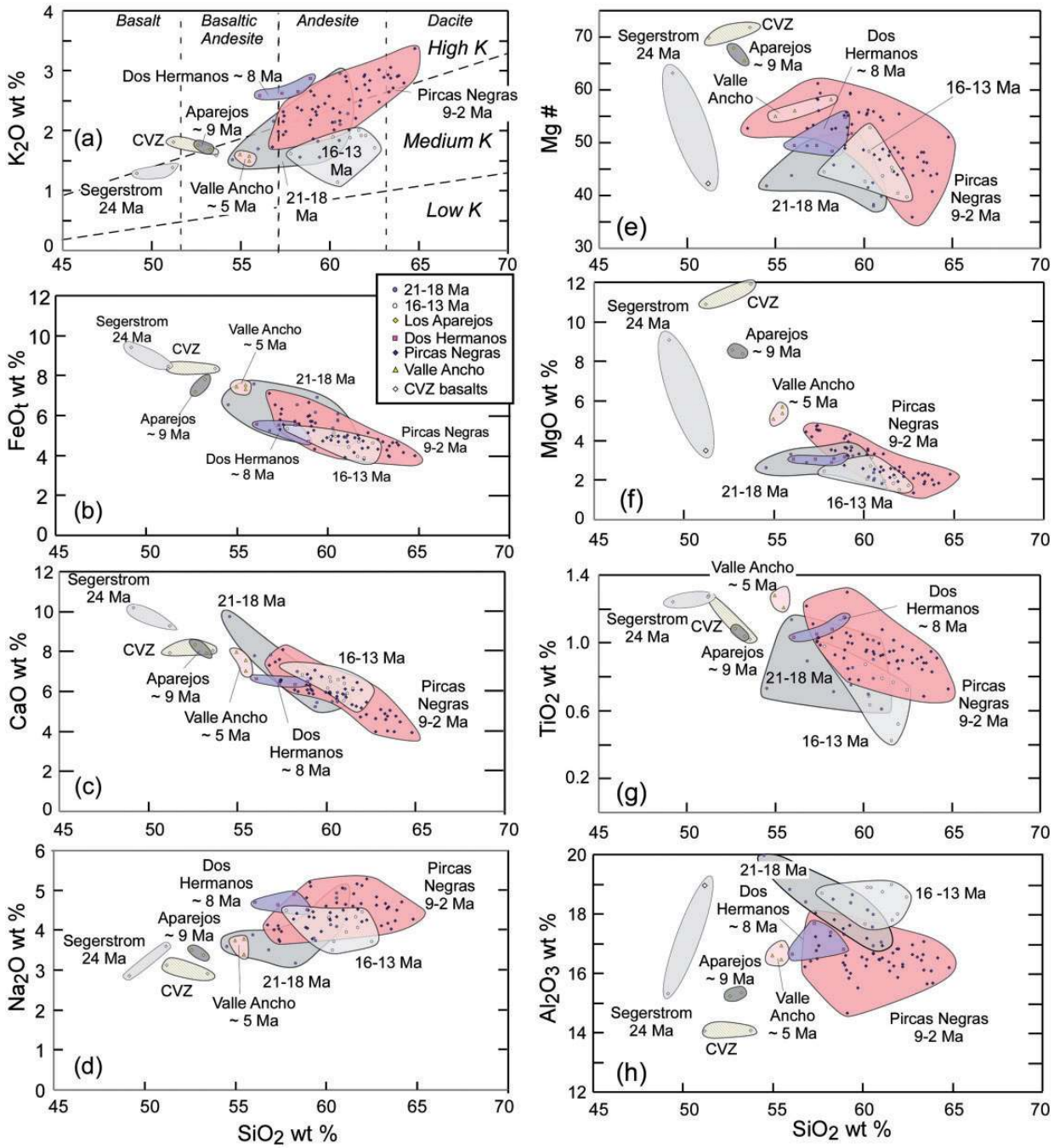

Fig 8. Harker variation diagrams comparing trends for ~24 Ma Segerstrom back-arc basalts, 21–18 Ma and 16–13 Ma Maricunga Belt basaltic andesite lavas; ~9 Ma Los Aparejos basaltic andesite; Dos Hermanos andesites; Pircas Negras andesites to dacites; Valle Ancho basaltic andesites; and southern CVZ Incahuasi and San Francisco mafic volcanic rocks. Low-, medium- and high-K boundaries in (a) are from Le Maitre *et al.* (1989). Data are from Table 4, Electronic Appendices 7 and 8, Kay *et al.* (1991, 1994, and 1999), Mpodozis *et al.* (1995, 1996, 1997), Goss & Kay (2009) and Mpodozis & Kay (2009).

are higher than those in the 21–18 Ma Escabroso (0·7047–0·7051), 16–13 Ma southern Maricunga and 8–7 Ma Jotabeche volcanic rocks (~0·7045–0·7055) at the same wt % SiO_2 (Fig. 13a). The ratios in the 6–3 Ma volcanic rocks near Cerro Bonete and the <3 Ma southern CVZ and Incapillo caldera rocks (Goss *et al.*, 2011) fall on the Pircas Negras trend, as do those of the Valle Ancho lavas (0·7057–0·7059). The $^{87}Sr/^{86}Sr$ of the ~9 Ma Los

Aparejos basaltic andesite (0·7062) is also on the enriched side. The plot of $^{87}Sr/^{86}Sr$ versus ppm Sr (Fig. 13b) shows a similar pattern, with the Dos Hermanos lavas having $^{87}Sr/^{86}Sr$ similar to the Pircas Negras lavas but at significantly higher ppm Sr (1200–1400). The $^{87}Sr/^{86}Sr$ versus $^{143}Nd/^{144}Nd$ plot in Fig. 13c shows a correlative general decrease in $^{143}Nd/^{144}Nd$ in volcanic rocks erupted after frontal arc migration, with $^{143}Nd/^{144}Nd$ compositions in the Dos Hermanos, Pircas Negras, Bonete region and CVZ lavas being higher than those in the 21–18 Ma Escabroso and 16–13 Ma southern Maricunga lavas, and overlapping with those of the 8–7 Ma Jotabeche volcanic rocks. The $^{87}Sr/^{86}Sr$ and $^{143}Nd/^{144}Nd$ ratios of the Valle Ancho and Los Aparejos lavas fall within the field of the Pircas Negras lavas.

The $^{206}Pb/^{204}Pb$ (18·63–18·72), $^{207}Pb/^{204}Pb$ (15·60–15·62) and $^{208}Pb/^{204}Pb$ (38·56–38·76) ratios of the Los Aparejos, Pircas Negras, Dos Hermanos and Valle Ancho lavas (Table 6) generally fall within or near the values of Chilean–Pampean flat-slab arc region and southern CVZ volcanic rocks (Fig. 14) and differ from those of <2 Ma CVZ lavas and Miocene volcanic rocks further east in the

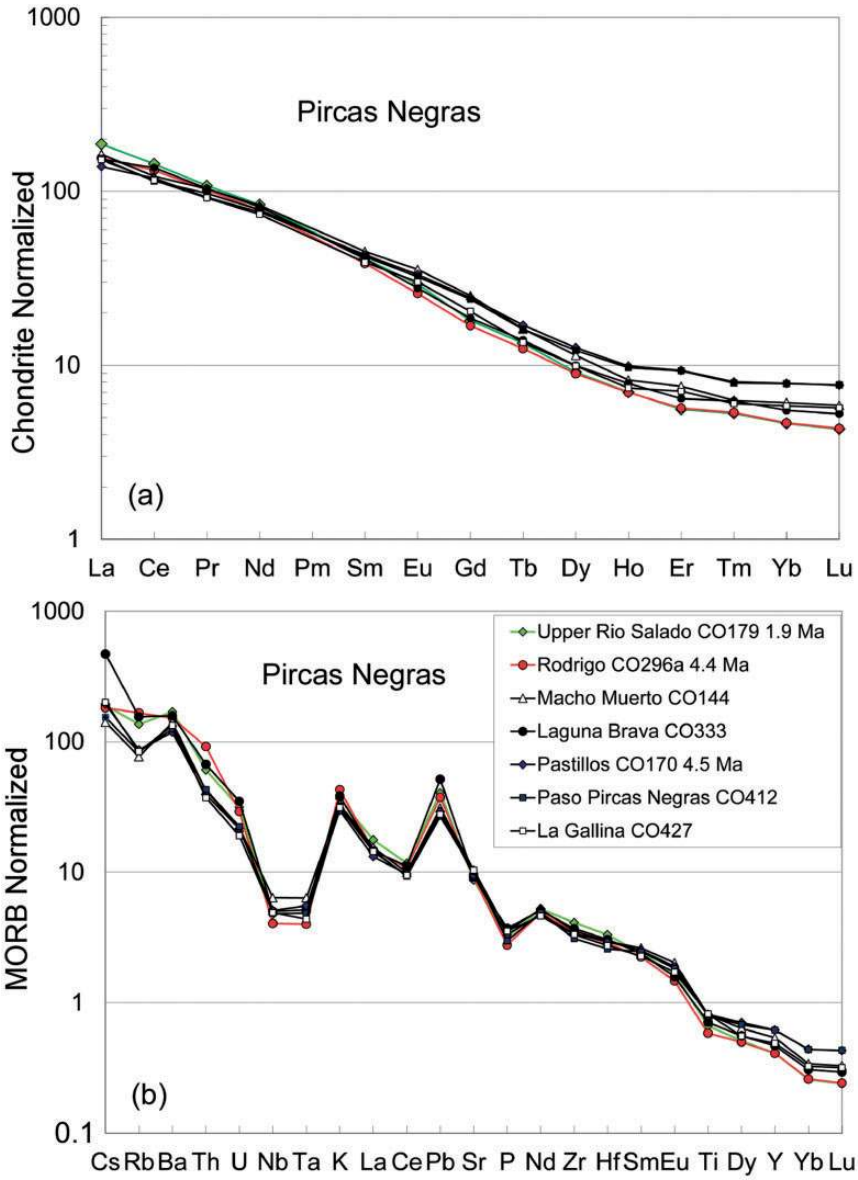

Fig. 9. Cl chondrite-normalized (McDonough & Sun, 1995) REE and MORB-normalized (Sun & McDonough, 1989) extended trace element patterns for representative syn-migration Pircas Negras andesites (a and b) and comparative ~24 Ma Segerstrom basalts, ~9 Ma Los Aparejos basaltic andesites, ~7·7 Ma Dos Hermanos andesites, ~5·5 Ma Valle Ancho basaltic andesites and <2 Ma CVZ Incahuasi and San Francisco mafic lavas (c and d). Data are from Table 4, Kay *et al.* (1999) and Goss & Kay (2009).

(continued)

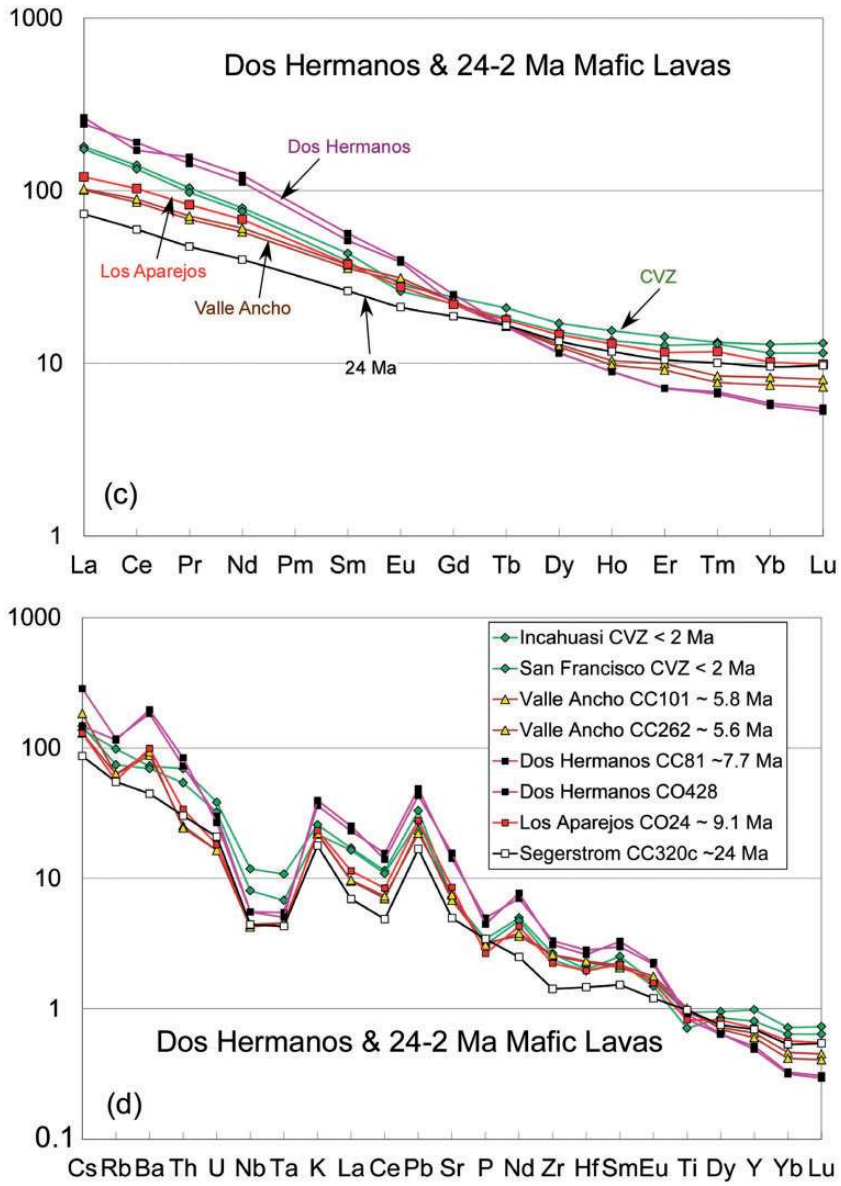

Fig. 9. Continued.

Precordillera and Sierras Pampeanas of the Chilean–Pampean flat-slab.

Oxygen isotope data in Table 5 show that olivine phenocrysts in Valle Ancho basaltic andesite CC101 and syn-migration Pircas Negras andesite CO324 have near mantle $\delta^{18}O$ values of $+6{\cdot}2 \pm 0{\cdot}2‰$ and that a quartz xenocryst in syn-migration Pircas Negras andesite CO427 has a crustal-like $\delta^{18}O$ value of $+8{\cdot}35 \pm 0{\cdot}2‰$.

DISCUSSION

The eruption of the Dos Hermanos and Pircas Negras andesites before, during and after the migration of the frontal arc permits an evaluation of their petrological, geochemical and isotopic characteristics relative to hypotheses for the origin of high-Mg andesites. Importantly, these andesites fall within the realm of magmatic rocks commonly called adakites with regard to their high La/Yb, Sm/Yb and Sr/Yb ratios and Sr concentrations; however, they have Sr and Nd isotopic ratios that are more enriched than those used in most adakite definitions. Below, we refer to them as adakite-like high-Mg andesites and compare them with other andesites to develop a model in which their distinctive characteristics are derived from components associated with fore-arc subduction erosion and evolution in a 65–70 km thick crust.

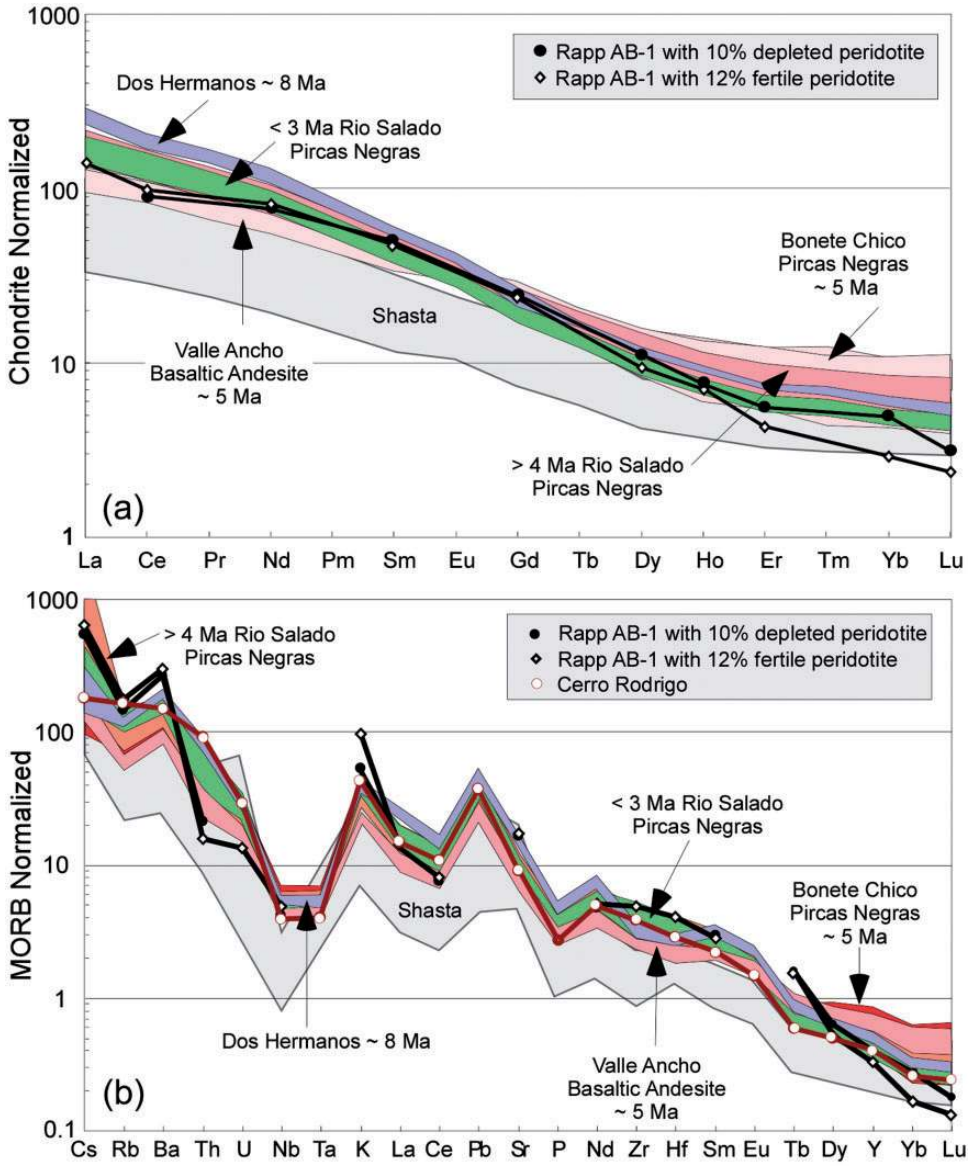

Fig. 10. Chondrite-normalized REE (a) and MORB-normalized trace element (b) diagrams showing fields for pre-migration Dos Hermanos group, syn-migration Pircas Negras and Valle Ancho, and post-migration Pircas Negras volcanic rocks relative to ICP-MS compositions of 3·8 GPa experimental melts of a basaltic amphibolite (AB-1) reacted with depleted (circles) and primitive fertile (diamonds) mantle from Rapp *et al.* (1999). The range for Mt. Shasta andesitic andesites (light gray field) in the Cascades from Grove *et al.* (2002) and the Pircas Negras type Cerro Rodrigo andesite (open circles) are shown for comparison.

Petrogenesis of the Pircas Negras and Dos Hermanos lavas: source and tectonic considerations

Extreme HREE depletion (Sm/Yb = 4–9) like that seen in the adakite-like Dos Hermanos and Pircas Negras high-Mg andesites has been explained by partitioning of HREE into residual garnet (e.g. Gromet & Silver, 1987); their coupled lack of plagioclase phenocrysts, negligible Eu anomalies, and high wt % Na_2O and high ppm Sr concentrations have been attributed to melting in the garnet-in feldspar-out (garnet pyroxenite) stability field at pressures above 1·3 GPa (deeper than 40–45 km). Supporting evidence for these statements comes from experiments showing that amphibole melting reactions above the garnet-in phase boundary at 1·2 GPa (e.g. Wolf & Wyllie, 1994) can produce garnet granulite-like residues (Sen & Dunn, 1994; Rapp & Watson, 1995), that basaltic to andesitic melts in equilibrium with rutile-bearing eclogitic residues can form from 10–50% partial melting of basaltic eclogite at 1250–1335°C and 2–3 GPa (Pertermann &

Hirschmann, 2003), and that ~20–40% vapor-absent partial melting of olivine-normative, tholeiitic amphibolite can produce andesitic magmas in equilibrium with residual eclogite and garnet granulite at 1·2–3·2 GPa (Rapp & Watson, 1995). Other experiments also show that plagioclase is unstable in (1) anhydrous basaltic melts at pressures above 1·2 GPa (e.g. Green & Ringwood, 1968), (2) hydrous gabbroic melts with >3 wt % H_2O at 900–1100°C and 1·5 GPa (Huang & Wyllie, 1986), (3) basaltic andesites with 2·0–5·5 wt % H_2O at 1050°C above 1·3 GPa, (4) andesites with 3·5–4·5 wt % H_2O above 1·0 GPa at 1050°C (Moore & Carmichael, 1998) and (5) high-Mg basaltic andesites with >3 wt % at 1·2 GPa in equilibrium with amphibole and garnet (Müntener *et al.*, 2001).

The question is then the nature of the mafic source that produces the Pircas Negras–Dos Hermanos magmas. Of the possibilities, significant melting of the subducting Nazca plate is discarded as the subducting slab is too old (~50 Ma; Yañez *et al.*, 2001) and cold, and the Pircas Negras–Dos Hermanos andesites do not have MORB-like isotopic compositions (Fig. 13). The remaining possibilities include garnet fractionation from basaltic magmas at high pressure, melting of thickened lower crust and melting of subducted fore-arc eroded components at high pressures.

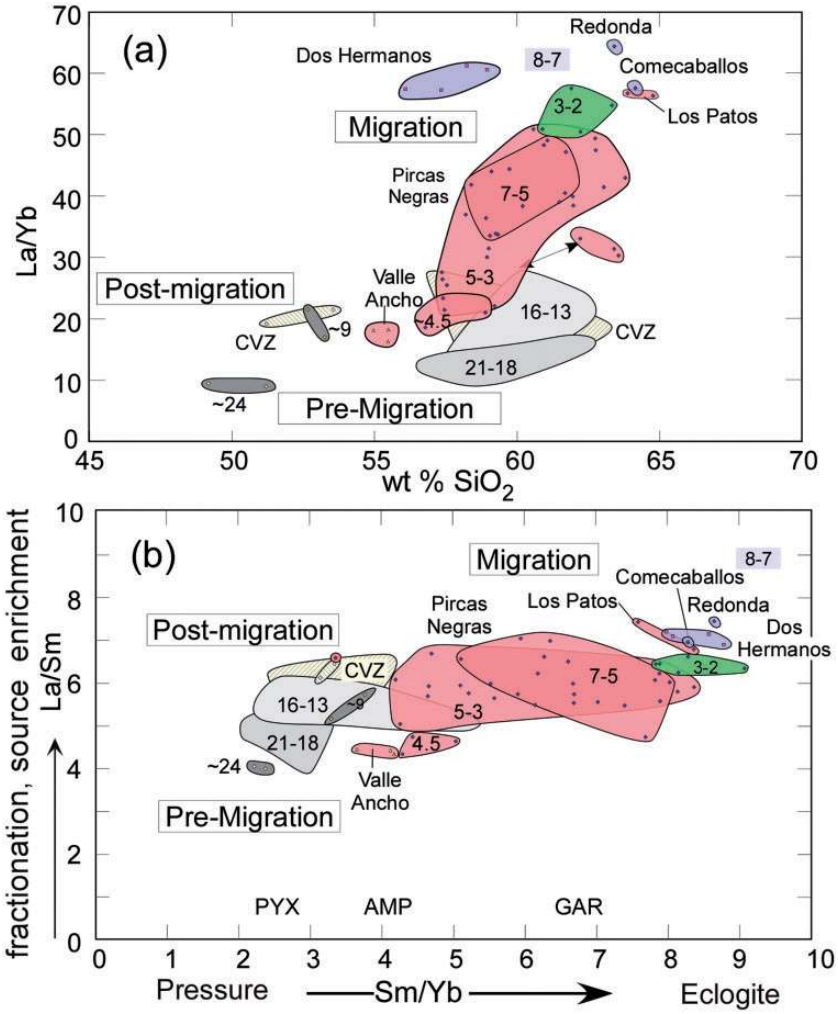

Fig. 11. Variation of selected trace element ratios: (a) La/Yb vs wt % SiO_2, (b) La/Sm vs Sm/Yb, (c) La/Yb vs La/Ta, and (d) Ba/Ta vs La/Ta for ~9–2 Ma Pircas Negras and Dos Hermanos and related volcanic rocks compared with 26–0 Ma lavas from the region between ~27 and 28·5°S. Numbers in fields are ages in Ma. Data for pre-migration ~9–7·5 Ma (Dos Hermanos, Redonda, Comecaballos) lavas, syn-migration Pircas Negras and Valle Ancho lavas (7–3 Ma), and post-migration Pircas Negros lavas (3–2 Ma) are from Table 4, Goss & Kay (2009) and Mpodozis & Kay (2009). Data for 21–18 Ma Escabroso and 16–12 Ma Jotabeche Norte, La Laguna and Cadillal–Yeguas Heladas andesites from the Maricunga Belt are from Table 4, Electronic Appendix 8, Kay *et al.* (1991, 1994, 1999), Mpodozis *et al.* (1995) and Tittler (1995); for ~24 Ma Segerstrom basalts data are from Kay *et al.* (1999); and for CVZ volcanic rocks (Peinado, Falso Azufre, Las Grutas, San Francisco, Incahuasi) data are from Mpodozis *et al.* (1996) and Kay *et al.* (1999, 2013).

(continued)

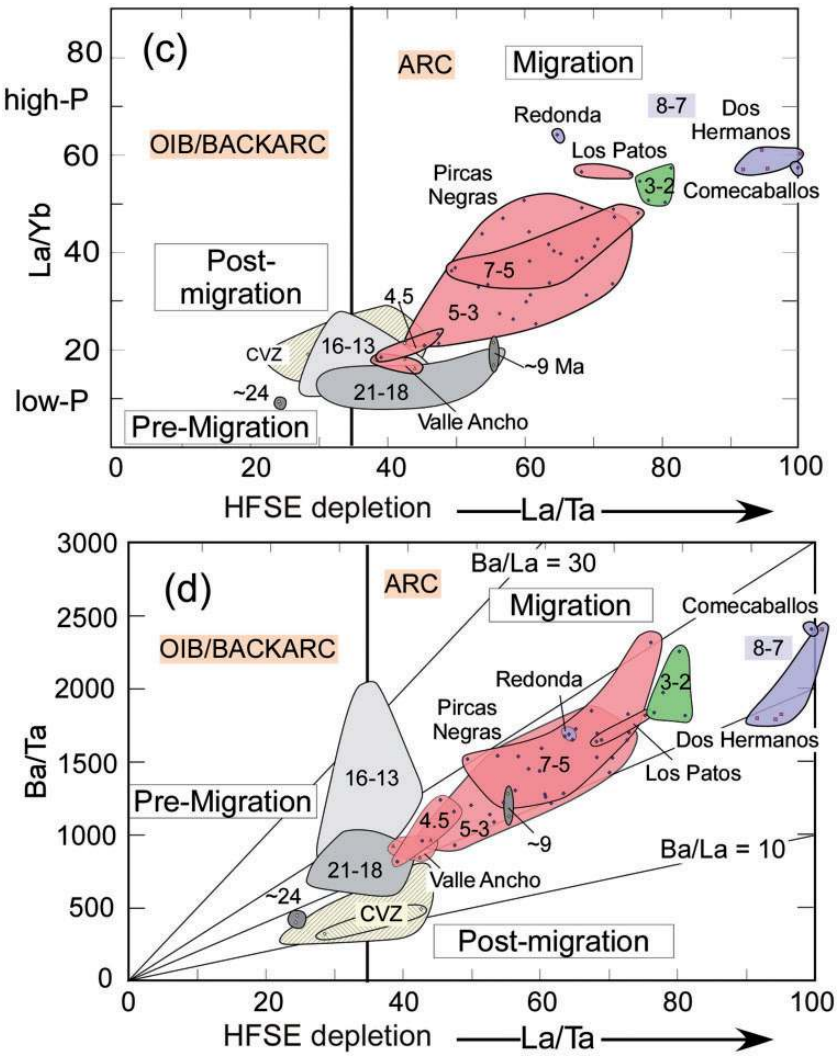

Fig. 11. Continued.

Garnet fractionation

Garnet fractionation from mafic magmas with flat HREE patterns at pressures above 0·8 GPa has been proposed by Macpherson *et al.* (2006) as a mechanism to generate the Philippine arc Surigao high-Mg adakites (Sr/Y = 50–150; Sm/Yb = 4–7). Those workers have suggested that these magmas reflect 30–50% fractionation of an assemblage containing ~12% garnet, based on high-pressure experiments with 5–10 wt % H_2O that yielded 5–15% garnet fractionation from basaltic (Müntener *et al.*, 2001) and andesitic (Ulmer *et al.*, 2003; Alonso-Perez *et al.*, 2004) magmas. Although garnet fractionation could be a factor in the evolution of the Pircas Negras–Dos Hermanos magmas, such a mechanism cannot explain Sm/Yb ratios up to nine as shown by a simple model (Supplementary Data Electronic Appendix 11) starting with a Los Aparejos-type mafic andesite lava, experimental constraints from Müntener *et al.* (2001) and distribution coefficients from Martin (1987). In the model, the Sm/Yb ratio reaches 6·2 at 53% fractionation with ~14% garnet as the melt runs out of MgO (<0·2 wt %) and becomes too K_2O-rich (>3·6 wt %). A similar problem arises starting with compositions like those of the mafic lavas from the southern CVZ Incahuasi and San Francisco volcanoes (Figs 8, 9 and 11–14; Kay *et al.*, 1999). Melting of a depleted mantle-derived magma like that used by Macpherson *et al.* (2006) also fails to explain the isotopic signatures of the Pircas Negras and Dos Hermanos lavas (Figs 13 and 14).

Lower crustal melts

Eclogitic lower crust has frequently been proposed to play a major role in producing Andean adakite-like volcanic rocks (e.g. Kay *et al.*, 1987, 1991; Hildreth & Moorbath, 1988; Petford & Atherton, 1996; Mamani *et al.*, 2010).

Melting models of eclogitic crust involving ponding of mantle-derived magmas in deep crustal 'hot zones' (Annen *et al.*, 2006) conceptually resemble the basaltic melting experiments at 2–2·5 GPa of Rapp & Watson (1995). The 65–70 km thick crust (McGlashan *et al.*, 2008) below the Dos Hermanos–Pircas Negras volcanic fields allows mafic eclogite and garnet-granulite rocks to play a role in generating their adakitic signatures. Kay *et al.* (1991) used this reasoning in modeling the lavas from the Paso Pircas Negras as 10–22% partial melts of basaltic two-pyroxene garnet granulites with the heat derived from arc basaltic magmas ponded in the lower crust. Melting of this crust, which was argued to be have evolved from dehydration of amphibolite residues and to have been thickened by westward crustal flow in response to Miocene crustal shortening, provided an explanation for higher $^{87}Sr/^{86}Sr$ ratios at similar wt % SiO_2 and ppm Sr in the Pircas Negras lavas compared with the older andesites (Fig. 13a and b). The occurrence of quartz and plagioclase xenocrysts has been used as evidence for increased crustal involvement. Similarly, Goss & Kay (2009) used a rutile–garnet-bearing mafic lower crust in modeling the extreme HREE depletion, high ppm Sr, low ppm Cr and Ni, and high Nb/Ta ratios of the Dos Hermanos pre-migration lavas.

Kay *et al.* (1991, 1994, 2013) argued that crustal thickening had taken place in this segment of the Andes by 11–10 Ma, on the basis of the steep REE patterns in the Maricunga Belt volcanic rocks (Fig. 10). Other evidence for crustal thickening and uplift by this time comes from the development of internal drainage in the Puna by the middle Miocene (e.g. Vandervoort *et al.*, 1995; Carrapa *et al.*, 2005), termination of Atacama gravel deposition to the west by 10 Ma (e.g. Nalpas *et al.*, 2008) and very high

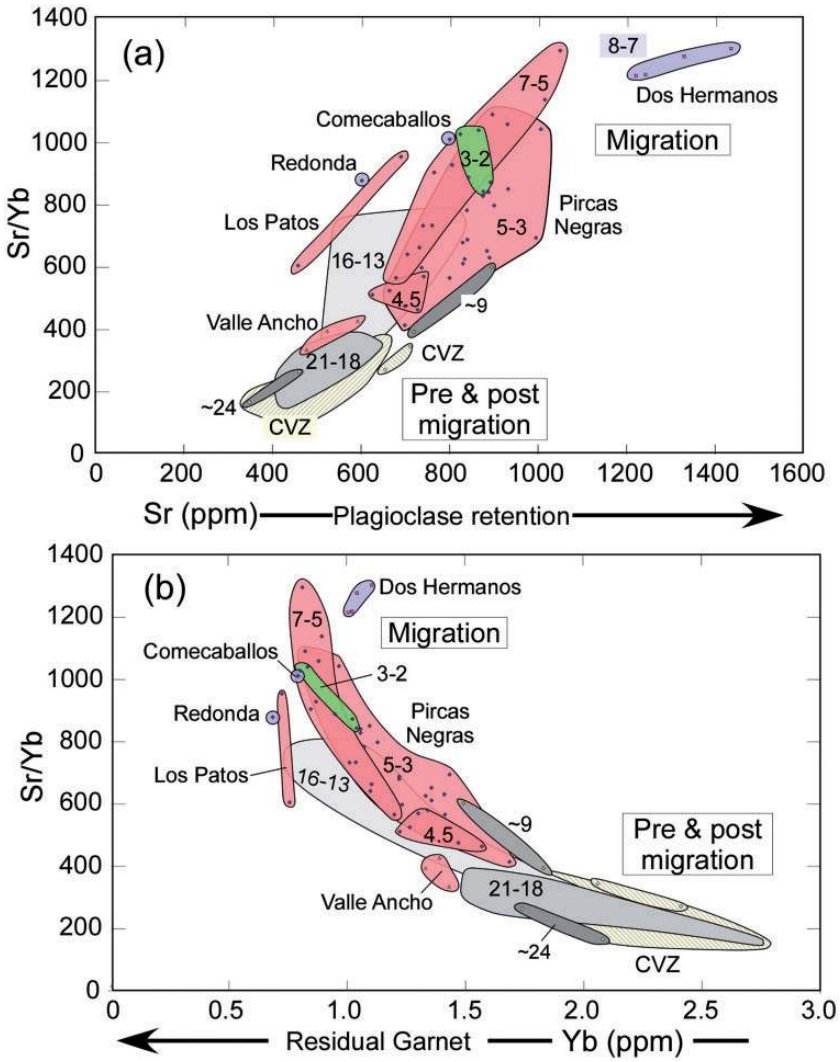

Fig. 12. Variation of Sr/Yb vs ppm Sr (a) and Yb (b), and Sm/Yb vs ppm Cr (c) and Ni (d) for the same samples as in Fig. 11. Cr and Ni for the ~9 Ma Los Aparejos mafic andesites and <2 Ma Incahuasi, and San Francisco CVZ basalts (Kay *et al.*, 1999) plot off scale as indicated.

(continued)

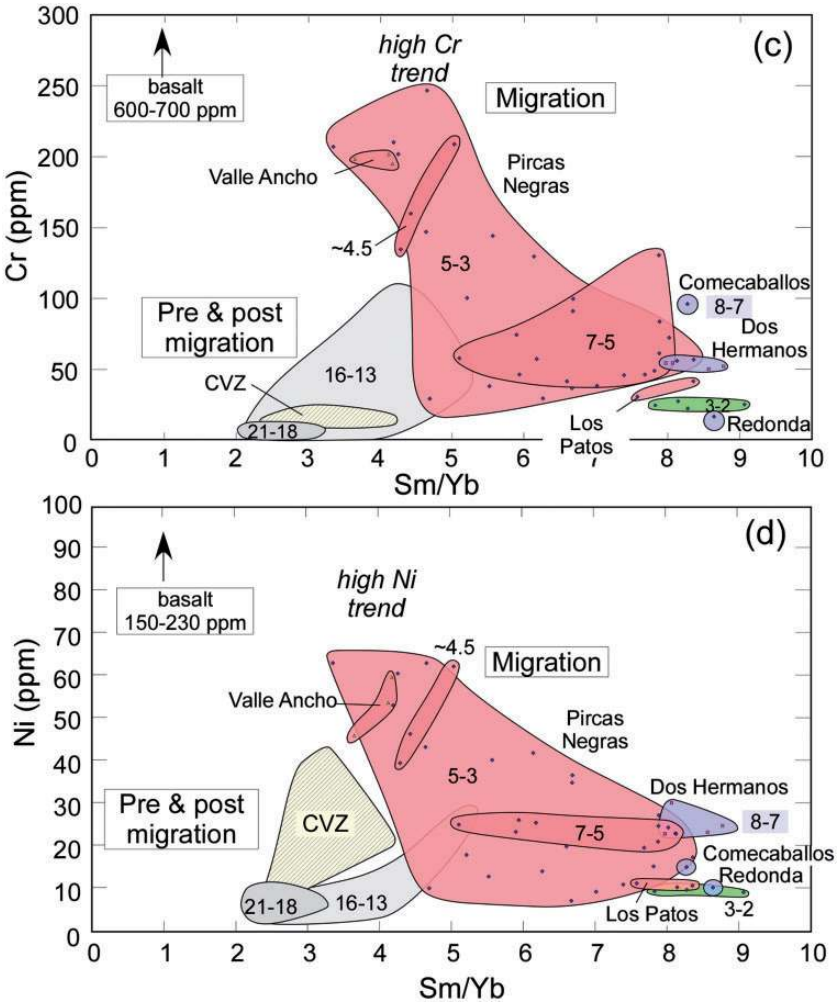

Fig. 12. Continued.

Sm/Yb ratios in 9–8 Ma southern Puna back-arc lavas (e.g. Richards *et al.*, 2006). The lack of high Sm/Yb ratios in southern CVZ lavas erupted through a 65–70 km thick crust can be attributed to a less contractional tectonic regime after 3 Ma leading to little magma storage in the lower crust.

Subduction erosion

The concept of subduction erosion was proposed for the Central Andes by Rutland (1971) and Ziegler *et al.* (1971), who noted that (1) Jurassic arc rocks form most of the modern Coastal Cordillera, (2) Mesozoic accretionary complexes are absent, (3) Paleozoic metamorphic units truncate at the coast at ~34°S and (4) the volcanic arc has periodically stepped eastward since the Mesozoic. They proposed that up to 200 km of the fore-arc has been removed and subducted since the Jurassic. Additional evidence now used for detecting eroding margins includes fore-arc normal faults and subsidence, over-steepened fore-arc prisms, subducted seamount scars and seismic images of detached upper-plate crust at the plate interface (e.g. von Huene *et al.*, 1997, 2004; Ranero & von Huene, 2000; Vannucchi *et al.*, 2001; Laursen *et al.*, 2002). As fore-arc subduction erosion processes are favored at continental arc margins with high convergence rates (>6 cm a^{-1}) and trenches devoid of terrigenous sediments (e.g. von Huene & Scholl, 1991; Clift & Vannucchi, 2004), the transition from a semi-arid to a hyper-arid climate in the Atacama desert by ~16 Ma (Rech *et al.*, 2006) and the development of internal drainage in the Puna by ~15 Ma (Vandervoort *et al.*, 1995) favor such a process on the northern margin of the flat-slab. Fore-arc subduction erosion further provides a way to generate adakitic magmas in arcs with old subducting slabs and where the crust is too thin to stabilize garnet (Kay, 1978, 2006; Goss & Kay, 2006).

Geochemical and tectonic considerations have also been used in calling upon partial melting of crust removed by fore-arc subduction erosion to play a role in the genesis of

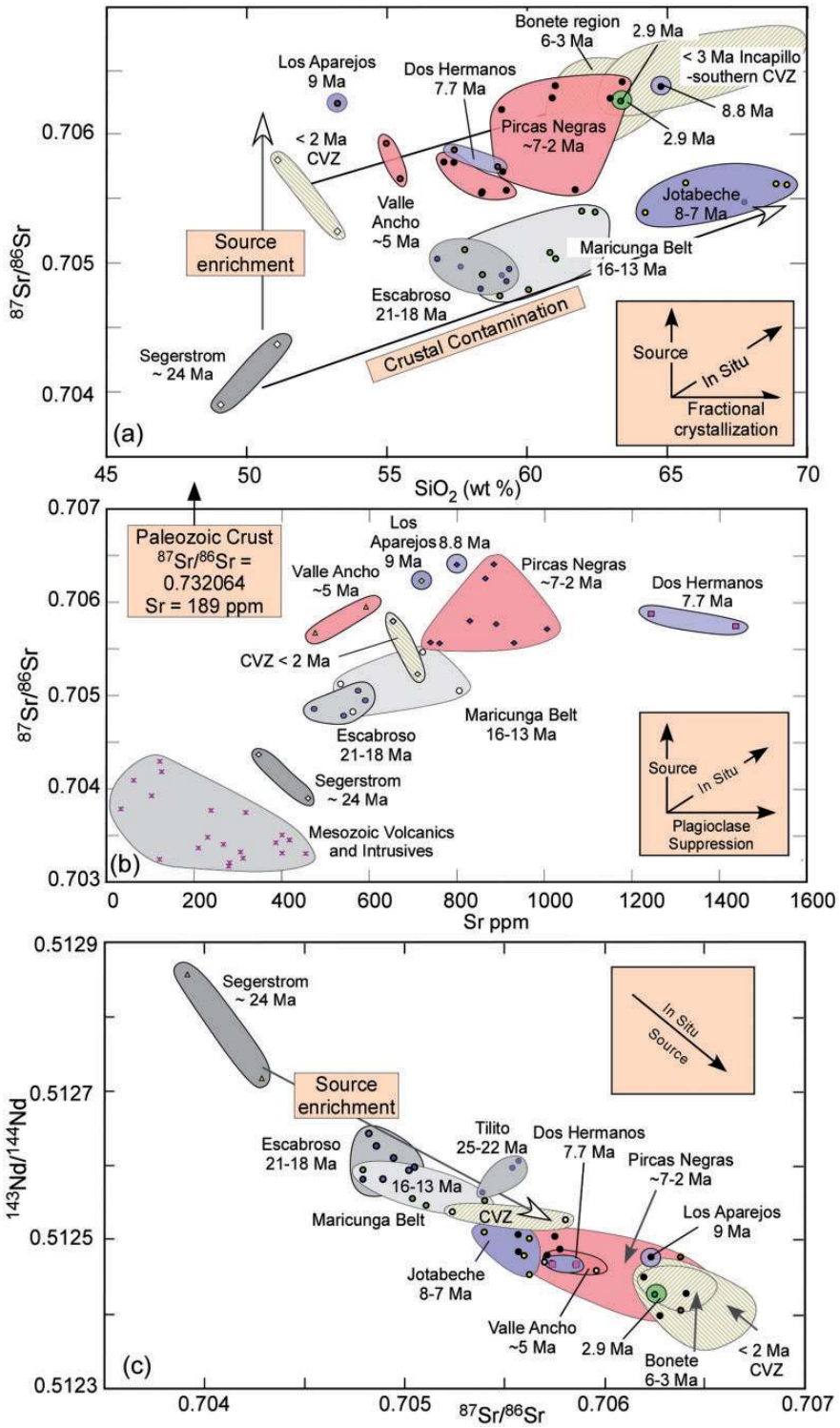

Fig. 13. Variation of $^{87}Sr/^{86}Sr$ ratios vs (a) wt % SiO_2, (b) ppm Sr and (c) $^{143}Nd/^{144}Nd$ for 9–2 Ma Dos Hermanos, Pircas Negras and related volcanic rocks (Table 5) compared with data for ~24 Ma Segerstrom lavas (Kay *et al.*, 1999), 21–18 Ma Escabroso andesites (Table 5), 16–13 Ma Maricunga Belt arc Jotabeche Norte, La Laguna and Cadillal–Yeguas Heladas andesites, and 8–7 Ma Maricunga Belt Jotabeche complex volcanic rocks (Kay *et al.*, 1991, 1994, 1999; McKee *et al.*, 1994), Bonete–Incapillo volcanic rocks (Goss *et al.*, 2009, 2011) and southern CVZ lavas (Mpodozis *et al.*, 1996; Kay *et al.*, 1999).

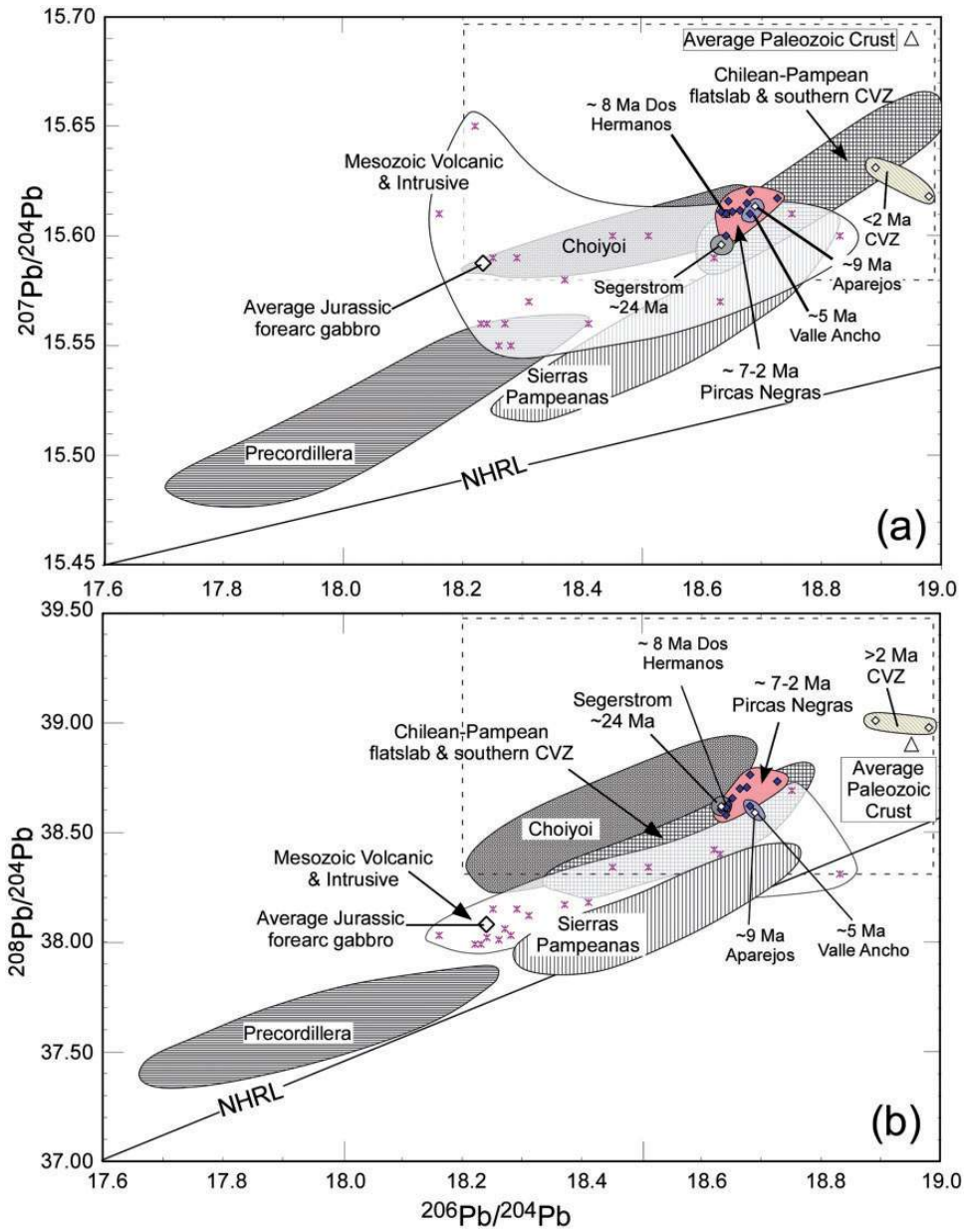

Fig. 14. Variation of $^{206}Pb/^{204}Pb$ vs (a) $^{207}Pb/^{204}Pb$ and (b) $^{208}Pb/^{204}Pb$ for ~9–2 Ma Dos Hermanos, Pircas Negras and related volcanic rocks compared with fields for volcanic rocks from the Chilean–Pampean flat-slab and southern CVZ, Precordillera and Sierras Pampeanas (Kay & Gordillo, 1994; Kay & Abbruzzi, 1996; Kay *et al.*, 1999; and references therein). Crosses in the Mesozoic Volcanic and Intrusive field, large open diamond and large triangle are for present-day ratios in Coastal Cordillera fore-arc rocks (Lucassen & Thirlwall, 1998; Lucassen *et al.*, 2002), average of ratios in Jurassic gabbros of Lucassen *et al.* (2002) and average central Andean Paleozoic crust of Lucassen *et al.* (2001), respectively. Field for Late Paleozoic Choiyoi granite–rhyolite samples is from Moscoso *et al.* (1993). NHRL is the Northern Hemisphere Reference Line from Zindler & Hart (1986). The dashed reactangle is the region shown in Fig. 15.

magmas erupted as the arc front migrated on the margins of the flat-slab region (e.g. Kay & Mpodozis, 2002; Kay *et al.*, 2005; Litvak *et al.*, 2007; Stern *et al.*, 2011). These observations include temporal changes in isotopic compositions and very high Sm/Yb ratios in magmas erupted at times of frontal arc migration (e.g. Kay & Mpodozis, 2002; Kay *et al.*, 2005). These features parallel the high Sm/Yb and Sr/Y ratios seen in the Pircas Negras region during migration of the arc front (Figs 10 and 11), and the change to higher $^{87}Sr/^{86}Sr$ and lower $^{143}Nd/^{144}Nd$ ratios at the same wt % SiO_2 compared with older Maricunga Belt lavas (Fig. 13). Alternative explanations of introducing radiogenic crust into the magma source as the crust thickened by westward (Kay *et al.*, 1991) or along-arc (e.g. Yang *et al.*,

2003) crustal flow provide no explanation for the high Mg# values, high ppm Ni and Cr, or near mantle $\delta^{18}O$ values in olivine in the 5–3 Ma syn-migration Pircas Negras lavas. Given that the only subducted sediment component after the late Miocene in this region is essentially pelagic and that subduction has been a continuous process since long before arc migration at 8–3 Ma, the only ways to introduce radiogenic crust into the mantle source are by fore-arc subduction erosion or delamination (e.g. Kay & Kay, 1993). Fore-arc subduction erosion is also the best way to explain the higher $^{87}Sr/^{86}Sr$ ratios (Fig. 12) at mantle $\delta^{18}O$ values in the <2 Ma CVZ basalts compared with the ~24 Ma Segerstrom basalts (Kay *et al.*, 1999; Kay, 2006).

HFSE depletion, Cr and Ni concentrations and temperature considerations

A role for fore-arc subduction erosion followed by contamination in the overlying thick crust is further supported by HFSE depletion, Cr and Ni concentrations, and thermal considerations in the Pircas Negras andesites.

Origin of HFSE depletion

The marked HFSE depletion (Figs 9, 10 and 12) in the Pircas Negras and Dos Hermanos andesites (La/Ta ~40–100) compared with that in the older Maricunga Belt and younger CVZ andesites (La/Ta ~25–40) requires changing conditions in the magma source that coincide with reducing the asthenospheric wedge volume and increasing fluid pressures as the arc front migrated eastward. In general, marked Ta–Nb depletion relative to the LILE and LREE is attributed to melt equilibration with HFSE-bearing phases in oxidized mafic eclogitic–amphibolitic sources (e.g. Green & Pearson, 1986) and/or to immobility of the HFSE relative to the LILE and LREE in slab-derived fluids (e.g. McCulloch & Gamble, 1991). Goss & Kay (2009) argued that a contrast between the near-chondritic Nb/Ta ratios (~18–20) in the pre-migration Dos Hermanos lavas and the dominantly sub-chondritic ratios (~11–18) observed in the <6 Ma syn-migration Pircas Negras lavas required a role for HFSE-bearing phases, as slab-derived fluids cannot sufficiently fractionate Nb from Ta (e.g. Schmidt *et al.*, 2004). The high La/Ta (90–100) and lower Ba/La (18–25) ratios (Fig. 10c and d) in the pre-migration Dos Hermanos andesites were argued to fit with an amphibole-poor, rutile-bearing eclogitic residue, whereas the lower Nb/Ta ratios (16–18) of the syn-migration Pircas Negras lavas were related to incorporation of anatectic melts of a hydrous amphibole-bearing source. Further, Goss *et al.* (2011) attributed high La/Ta ratios in 5–3 Ma Incapillo rhyodacitic domes to high slab fluid concentrations in magmas generated above the shallowing slab. Support for a similar model for the Pircas Negras lavas comes from their amphibole-rich, feldspar-free phenocryst assemblage and calculated fO_2 of ~1–3 log units above QFM.

Origin of high Mg#, Cr and Ni

Another important issue is the origin of the high Mg# and Cr and Ni contents in the syn-migration 5–3 Ma Pircas Negras andesites (Figs 8b and 12c, d). These relatively high values strongly suggest a more significant sub-arc mantle component in these lavas than do the lower values in the pre- and post-migration lavas. The general correlation of low Cr and Ni contents with high Sm/Yb ratios in the Pircas Negras lavas (Fig. 12c and d) shows that these high Cr and Ni contents are not linked to the same process that produced the HREE depletion. In this way, the 5–3 Ma Pircas Negras lavas are more like high-Mg# (53–56) experimentally produced adakitic melts created by reacting low-Mg adakitic melts with depleted peridotite (Fig. 10), leaving behind a garnet–orthopyroxene-bearing residue, than they are to low-Mg# (37–44) adakites produced at 3·2 GPa by melting a basaltic source (Rapp & Watson, 1995; Rapp *et al.*, 1999). In comparison, the Mg# values of the Pircas Negras lavas are lower than those of western Aleutian (Mg# = 70–72; Yogodzinski *et al.*, 1995) and Setouchi (Mg# = 67–76; Tatsumi & Ishizaka, 1982) andesites modeled as melts of mantle metasomatized by adakitic melts, and their REE patterns are much steeper than those of Mt Shasta high-Mg andesites (Fig. 10) modeled as melts of a hydrated mantle wedge equilibrated with overlying depleted mantle residues (Grove *et al.*, 2002).

Thermal considerations

Thermal conditions for the petrogenesis of the syn-migration Pircas Negras andesites are also in accord with contributions from subducted eroded components. Calculated temperatures for Pircas Negras syn-migration andesites CO412 and CO324 (Table 3, Appendix 7) provide constraints for unraveling their thermal history; coexisting pyroxenes yield temperatures of ~1059–1068°C that are near the andesite liquidus at 5 wt % H_2O (Green, 1982) and just above the upper stability limits of amphibole at ~1050°C (e.g. Davidson *et al.*, 2007). These temperatures agree with isobaric equilibrium crystallization models at 2 units above FMQ from the MELTS program (Ghiorso & Sack, 1995; Asimow & Ghiorso, 1998) that saturate both pyroxenes in compositions such as CO412 and CO324 at 1089–1097°C with 5 wt % H_2O and at 1063–1071°C with 7 wt % H_2O. In contrast, orthopyroxene is not saturated under the same conditions when orthopyroxene-free Pircas Negras compositions (e.g. CO309, CO310) are used. These models permit the highly resorbed Pircas Negras orthopyroxene phenocrysts to be early formed phases that destabilized as magma temperatures and pressures decreased.

Experimental work on the crystallization sequence of a Mt. Shasta basaltic andesite at NNO (the nickel–nickel oxide buffer) and $PH_2O = P$total by Grove *et al.* (2003) shows that pargasitic amphibole (Mg# = 0·80) can be a dominant phenocryst at 1065°C and 0·8 GPa in equilibrium with clinopyroxene, orthopyroxene and an andesite melt (57·2 wt % SiO_2; 17·1 wt % Al_2O_3; 4·9 wt % MgO), whereas above 1077°C olivine and clinopyroxene are the only phenocrysts and below 1054°C amphibole replaces orthopyroxene. The crystallization sequence, pre-eruptive temperature, mineral compositions and modal assemblages in this and other Mt. Shasta experiments permit the Pircas Negras amphiboles to have crystallized from water-rich adakitic melts at pressures greater than 0·8 GPa at ~1060°C. The lack of plagioclase phenocrysts and the glassy textures of the Pircas Negras andesites are consistent with high pre-eruptive water contents.

The calculated pre-eruptive temperatures above are ~50–80°C below those expected to generate hybridized high-Mg# (>55) adakitic melts in equilibrium with eclogite (1100–1150°C; Rapp *et al.*, 2007, 2010). According to Rapp *et al.*, mantle temperatures are generally 100–200°C higher than the adakite solidus (~850–1000°C) and rising low-Mg# primary adakitic melts must entrain thermal energy to prevent complete back-reaction with the mantle. However, the Pircas Negras andesites erupted as the slab shallowed and wedge temperatures may have been cooler owing to the loss of wedge volume. Within a cooler wedge (<1100°C), higher melt:rock ratios (>1:1) are needed to generate 'hybridized' high-Mg andesites that retain adakitic trace element signatures (Kelemen *et al.*, 1998). This observation is consistent with a general lack of orthopyroxene in the Pircas Negras andesites, with the rare resorbed grains being explained as either 'metasomatic' orthopyroxene at low melt:rock ratios (Rapp *et al.*, 1999) or as early liquidus phases that became unstable at lower pressures and temperatures.

The Pircas Negras andesite (CO324) at Veladero is distinctive in showing evidence for a lower temperature history, based on two-pyroxene phenocryst (~950–980°C) and magnetite–ilmenite (~790–900°C) temperatures, followed by secondary injection of hotter magma, based on temperatures from orthopyroxene rims on resorbed olivine coupled with nearby clinopyroxene (~1065°C). This complex evolution fits with evidence for magma mixing from euhedral skeletal relict amphibole replaced by clinopyroxene, reversely zoned plagioclase xenocrysts and An_{60} plagioclase microlites.

A subduction erosion model: isotopic and trace element models

The discussion above shows that many of the features of the syn-migration Pircas Negras lavas are compatible with subduction eroded fore-arc components playing a role in their source. Detecting the presence of this subducted crust depends on knowing the composition of the fore-arc. To this end, the fore-arc in Chile between 30° and 22°S is largely composed of Jurassic basaltic to andesitic arc lavas (La Negra and Punta del Cobre Fms; Pichowiak *et al.*, 1990; Lucassen & Thirlwall, 1998; Lucassen *et al.*, 2002), late Paleozoic and Jurassic plutons, and low-grade Paleozoic turbidite–mélange sediments (Bell, 1987; Dallmeyer *et al.*, 1996; Godoy & Lara, 1998; Mathews *et al.*, 2006). Zircons with ages of ~1760 Ma in these sequences suggest an underlying Proterozoic basement (Gelcich *et al.*, 2005). Geophysical evidence supports a fast ($V_p = 6{\cdot}7$–$7{\cdot}7$ km s^{-1}) and dense (2·9–3·05 g cm^{-3}) fore-arc crust dominantly composed of mafic rocks (>85%) from 21° to 26°S (Wigger *et al.*, 1994; Scheuber & Geise, 1999; Schmitz *et al.*, 1999; Lucassen *et al.*, 2001; Prezzi *et al.*, 2009); a trench-parallel gravity profile indicates that this dense crust extends southward to at least 33°S (Götze *et al.*, 1994; Tassara *et al.*, 2006). Structurally, such a fore-arc will behave as a rigid block analogous to the ophiolitic fore-arc in Central America (e.g. Christeson *et al.*, 1999), where accelerated subduction erosion is argued to have been taking place since the collision of the Cocos Ridge at ~5 Ma (Vannucchi *et al.*, 2003).

Isotopic models

An isotopic test of the hypothesis that subducted mafic Chilean fore-arc crust contaminated the mantle wedge during the migration of the arc front is presented in terms of a two-stage Nd, Sr and Pb simple isotopic mixing model in Fig. 15. The eroded crust is represented by a mixture of mafic and silicic end-members. An averaged composition of Jurassic gabbroic and meta-igneous rocks from the Coastal Cordillera [data from Lucassen *et al.* (2002)] is used as a proxy for the mafic end-member. The average composition of Central Andean Paleozoic rocks (Lucassen *et al.*, 2001), which is similar to average upper crust and Paleozoic crustal compositions employed in fore-arc mixing models by Stern (1991) and Kay *et al.* (2005), is used for the silicic end-member. Pelagic sediments are ignored. The pre-migration mantle composition is based on the isotopic composition of the ~24 Ma Segerstrom basalt ($^{87}Sr/^{86}Sr = 0{\cdot}703309$, $\varepsilon Nd = +6{\cdot}57$, $^{206}Pb/^{204}Pb = 18{\cdot}23$, $^{207}Pb/^{204}Pb = 15{\cdot}59$, $^{208}Pb/^{204}Pb = 38{\cdot}08$; Kay *et al.*, 1999) with Sr (50 ppm) and Nd (3 ppm) concentrations based on Patagonian metasomatized spinel peridotite mantle xenoliths (Gorring & Kay, 2000) and the mantle Pb content (0·175 ppm) from Hofmann (1988).

Mixtures between the mafic and silicic end-members generate bulk fore-arc components with isotopic ratios that plot as the points on the continuous lines in Fig. 15. The best matches for the Pircas Negras lavas have ~80–90% of their Sr and Nd coming from a fore-arc partial melt (54–55% SiO_2) with 80–90% Jurassic gabbro (Fig. 15a), a combination that works well with a fore-arc dominantly composed of mafic rocks. The dashed lines

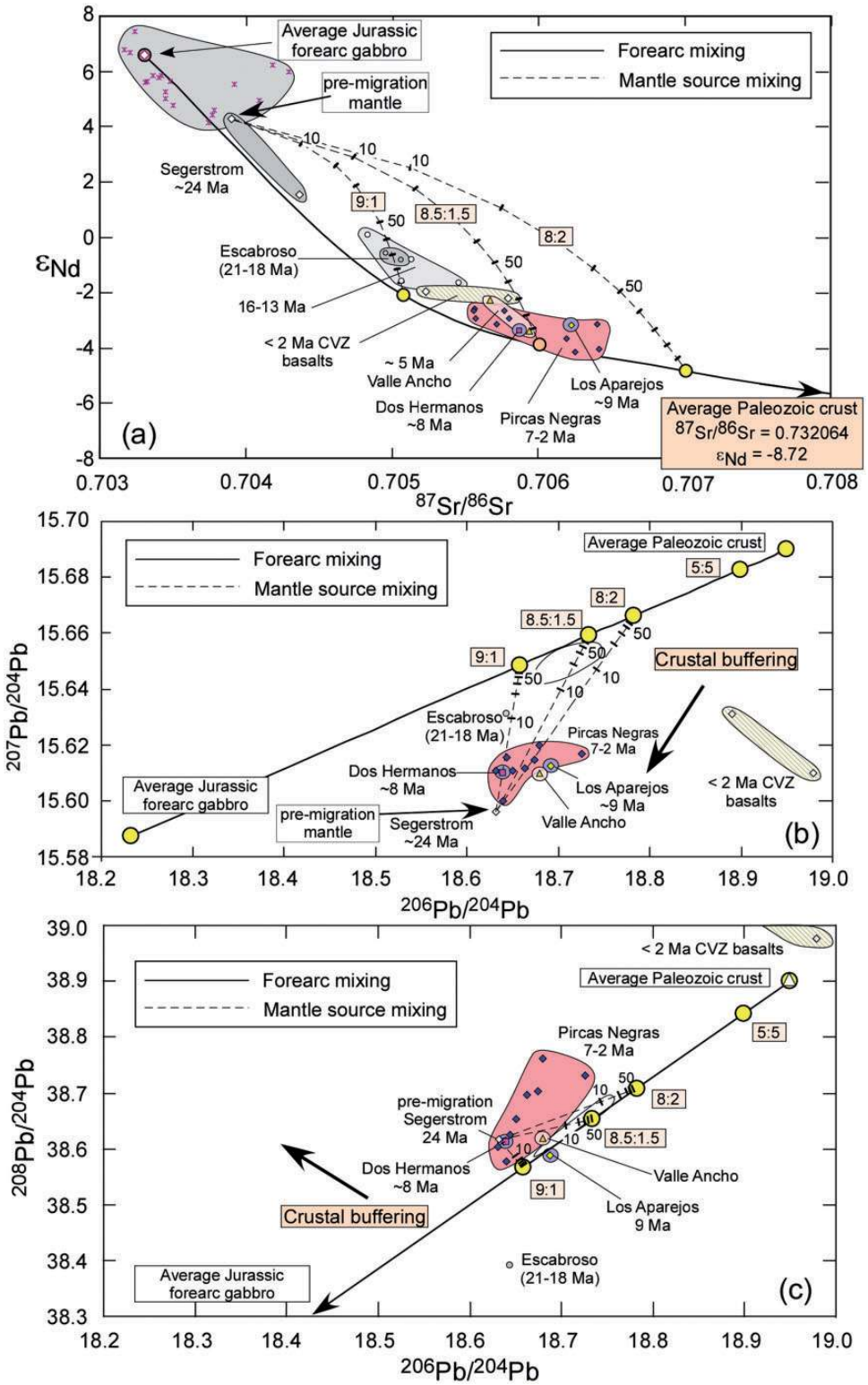

Fig. 15. Isotope variation diagrams showing the two-stage isotopic mixing model for the origin of the Dos Hermanos and Pircas Negras-like high-Mg andesites and related lavas discussed in the text. Fields and data sources for samples are the same as in Figs 11–14. (a) Stage 1: continuous black line is mixing curve for mafic Jurassic gabbro and silicic average Paleozoic crustal fore-arc end-members; large circles represent mixtures with ratios of 9:1, 8·5:1·5 and 8:2. The mafic Jurassic gabbroic end-member is based on averaged analyses from Lucassen *et al.* (2002) and has 52·6 wt % SiO_2, 319 ppm Sr, 2·06 ppm Nd, 1·22 ppm Pb, $^{87}Sr/^{86}Sr = 0{\cdot}703309$, $\varepsilon Nd = +6{\cdot}57$, $^{206}Pb/^{204}Pb = 18{\cdot}23$, $^{207}Pb/^{204}Pb = 15{\cdot}59$

(continued)

show mixing of the mafic and silicic fore-arc melt combinations at ratios of 9:1, 8·5:1·5 and 8:2 with the pre-migration mantle. The resultant hybrid mantle melt has up to 40% of its final Sr and Nd content coming from the pre-migration mantle.

Applying the same model to Pb isotopes (Fig. 15b and c) shows that the Pircas Negras andesites plot at much lower percentages of Pb (<10%) than the fore-arc mixtures. The fact that the model does not work is not surprising, as Pb isotopes in Andean magmas generally correlate with those in the underlying crust (e.g. Aitcheson *et al.*, 1995; Mamani *et al.*, 2008). In this sense, buffering of Pb by the underlying Late Paleozoic granite–rhyolite basement (Fig. 15c; Moscoso *et al.*, 1993) moves ratios of $^{206}Pb/^{204}Pb$ and $^{207}Pb/^{204}Pb$ to lower values and $^{208}Pb/^{204}Pb$ to higher values as required. The CVZ mafic lavas fall off these Pb–Pb mixing lines, suggesting a different crustal contaminant (Kay *et al.*, 2013). Changes in Nd and Sr isotope compositions in the overlying crust are considered secondary, as the $^{87}Sr/^{86}Sr$ (~0·7056) and εNd (~ −3·25) values of the nearby 8–6 Ma Jotabeche ignimbrites (69 wt % SiO_2) overlap those of the Pircas Negras lavas (Fig. 13a and c).

Trace element considerations

Batch melting models of Goss & Kay (2009) show that high-pressure (1·5–3·0 GPa) partial melts of basaltic eclogite can generate the Nb/Ta ratios and REE patterns of the Dos Hermanos and Pircas Negras lavas, starting from an average fore-arc Jurassic basalt composition [data from Lucassen *et al.* (2006)]. The near-chondritic Nb/Ta ratios (21), ~1200 ppm Sr, steep REE patterns (La/Yb = 72) and high Sr/Yb ratios of the Dos Hermanos lavas are best matched by 20–25% partial melts of an eclogite with 53% garnet, 46% clinopyroxene and 1% rutile based on phase proportions in experiments on alkali-rich basalt at 2·2 GPa and 1050°C (Rapp & Watson, 1995). Interactions with the isotopically similar ~8–6 Ma Jotabeche magmas in the mid-crust provide a source for the feldspar and quartz xenocrysts (Kay *et al.*, 1994). Goss & Kay (2009) further modeled the high-Cr and -Ni, amphibole-bearing Pircas Negras lavas with lower La/Ta, Sm/Yb and Nb/Ta ratios as mixtures of 10–40 parts of Dos Hermanos type melts with 60–90 parts of 10–20% partial melts of garnet amphibolite (25% garnet, 25% cpx, 50% amp) or amphibole-bearing eclogite (38% garnet, 37% cpx, 25% amp). The phase proportions for the eclogite and amphibolite come from adding 15% and 40% amphibole respectively to the residue of the 1·6 GPa experiments of Rapp & Watson (1995).

In contrast, Mamani *et al.* (2010) argued that REE patterns like those of the Dos Hermanos and Pircas Negras lavas can be explained by mixing between a <20% partial melt of mafic amphibole-bearing eclogite (10% amp, 40% garnet, 50% cpx), with La/Yb > 450 and Sm/Yb > 24, and a mantle-derived basalt. They argued that unreasonable amounts of melting (>75%) are required to produce these magmas by partial melting alone. In comparison, their models use higher distribution coefficients (Rollinson, 1993), lower initial REE concentrations and less residual amphibole than the models of Goss & Kay (2009), in which the distribution coefficients for garnet and clinopyroxene are from Klemme *et al.* (2002) and Green *et al.* (2000) and those for amphibole are from Brenan *et al.* (1995) and Tiepolo *et al.* (2000).

On the basis of a compilation of Peruvian data, Mamani *et al.* (2010) further argued for a delay between crustal thickening and when steep REE patterns reflecting related high-pressure residues appear in the erupted magmas. The same case might be made for the ~7–2 Ma Pircas Negras lavas, as the presence of thick crust under the Maricunga Belt is reflected by steep REE patterns in the volcanic rocks of the Copiapó center by ~11 Ma (Kay *et al.*, 1994). However, instead of a delay, we propose that the very steep REE patterns in the ~7–2 Ma Pircas Negras lavas and return to shallower patterns in the <2 Ma CVZ lavas reflect flooding of the mantle wedge by mafic fore-arc crust fragments during a period of accelerated fore-arc crustal erosion that took place from ~7 to 3 Ma.

In an earlier study, Haschke *et al.* (2002) explained temporal trends in increasing La/Yb and $^{87}Sr/^{86}Sr$ and decreasing $^{143}Nd/^{144}Nd$ in eastward steps of the Jurassic to Miocene arc fronts between 20° and 26°S as being due to alternating crustal thickening and thinning. Mathews & Cornejo (2004) used a similar explanation for changes in REE slopes in successive arc fronts at 26–27°S. Both used data from the Maricunga Belt (e.g. Kay *et al.*, 1994), which show that the steepest REE slopes and most enriched isotopic ratios appear in the late Miocene. In a discussion of the Haschke *et al.* (2002) model, Mamani *et al.* (2010) argued that the fluctuating REE patterns reflect magma evolution at distinct crustal levels; they emphasized that

Fig. 15. Continued
and $^{208}Pb/^{204}Pb = 38·08$. The silicic end-member is the average central Andean Paleozoic upper crust from Lucassen *et al.* (2001) and has 68·3 wt % SiO_2, 189 ppm Sr, 24·3 ppm Nd, 16 ppm Pb, $^{87}Sr/^{86}Sr = 0·732064$, εNd = −8·72, $^{206}Pb/^{204}Pb = 18·95$, $^{207}Pb/^{204}Pb = 15·69$ and $^{208}Pb/^{204}Pb = 38·90$. (b) Stage 2: dashed lines show contamination models for pre-migration mantle represented by mixing of ~24 Ma Segerstrom basalt (Kay *et al.*, 1999) with the fore-arc mixtures from Stage One. Dashes represent 10% mixing intervals. Empty outlined fields in (b) and (c) are isotopic ranges for Pb mixtures given the same proportions as those for Nd and Sr. As discussed in the text, buffering of Pb concentrations by the *in situ* late Paleozoic Choiyoi crustal basement is suggested to be responsible for the deviation from the model. Dark arrows point toward the isotopic field for Choiyoi granites and rhyolites (see Fig. 14).

although migration of the frontal arc has occurred repeatedly in the Mesozoic and Tertiary, the most significant isotopic enrichment is associated with extreme crustal thickening in the last 30–20 Myr. Although this is the case, Mamani *et al.* offered no explanation of why the steepest REE patterns occur at times of arc migration, why the most enriched isotopic trends correlate with the steepest REE patterns, why high Cr and Ni contents occur in high-Mg# andesites, or why elsewhere along the Pacific margin steep REE patterns occur in arc lavas erupted through thin crust over old subducting slabs (e.g. Aleutians; Kay, 2006; see also Goss & Kay, 2006).

On a regional scale, Rogers & Hawkesworth (1989) proposed that eastward isotopic enrichment patterns in Andean Mesozoic to Neogene mafic lavas reflect contamination of mantle-derived magmas by a progressively more enriched lithosphere to the east. Stern (1991) used the same data to argue for mantle source enrichment by subducted sediments and fore-arc crust, and Kay *et al.* (1999) used Neogene mantle source enrichment to explain isotopic enrichment in <2 Ma CVZ compared with ~24 Ma Segerstrom basalts. Mamani *et al.* (2010) allowed a small amount of subducted crust (~1%) and fluid from the subducted slab in the mantle source, but pointed to Rb/Cs ratios increasing in concert with isotopic ratios as the crust thickens to support contamination within the continental crust. However, the observation that Rb/Cs ratios in Pircas Negras lavas are high in even the most Mg-, Cr- and Ni-rich lavas, and do not increase with wt % SiO_2, supports crustal contamination in the mantle source as well as the crust.

Thus, contamination of the mantle wedge with dominantly mafic crust removed by fore-arc subduction erosion can help to explain both the spatial and temporal geochemical variations in the Pircas Negras lavas between 27°S and 28°S. The transient increase in Sm/Yb during the peak of frontal arc migration is consistent with an ephemeral high-pressure mafic crustal source flooding the sub-arc mantle. Partial melts of eclogitized fore-arc crust in the mantle wedge reacting with peridotite provide an explanation for elevated Cr and Ni contents in the high-Mg# 5–3 Ma Pircas Negras andesites.

Subduction erosion rates, fluxes, arc migration and melting dynamics

A mass-balance model for fore-arc subduction erosion and migration of the arc front for the Pircas Negras region is shown in the trench-normal pre-, syn- and post-migration cross-sections in Fig. 16a–c. The Wadati–Benioff shape is based on a profile near 28°S from Pardo *et al.* (2002) and the Benioff zone contours of Mulcahy (2012). The modern crustal thickness is from McGlashan *et al.* (2008). In accord with frontal arc displacement owing to fore-arc subduction erosion, the eastward motion of the arc front is equated with fore-arc subduction erosion. Given ~50 km of arc displacement from 8 to 3 Ma and the observation that the modern arc–trench gap is ~300 km along most of the Andean margin, the trench is placed ~50 km west of its present position at 8 Ma. A geometric restoration of this profile requires a loss of ~992 km^3 of fore-arc per kilometer of arc length, which is equivalent to a rate of ~198 $km^3\,Myr^{-1}km^{-1}$ from 8 to 3 Ma.

This estimated fore-arc subduction erosion rate can be compared with estimates of long- and short-term rates for the Chilean margin. Long-term estimates since the Jurassic range from 35 to 50 $km^3\,Myr^{-1}km^{-1}$ with accommodations for episodic accelerations owing to changes in convergence parameters or subduction of bathymetric features (von Huene & Scholl, 1991; Scheuber, 1994). Short-term estimates range from 72 to 135 $km^3\,Myr^{-1}km^{-1}$ (von Huene *et al.*, 1999; von Huene & Ranero, 2003; Clift & Vannucchi, 2004) with Laursen *et al.* (2002) arguing for an average rate of 3–4 km Myr^{-1} over the last 10 Myr near the Juan Fernandez Ridge at 34°S (Fig. 1). Clift & Hartley (2007) proposed an average rate of 13 $km^3\,Myr^{-1}km^{-1}$ over the last 20 Myr for the Chile–Peru margin based on sea-level depth to basement reconstructions and an estimated 35 km of trench retreat near 23–24°S (von Huene & Ranero, 2003). This rate is consistent with the relatively stationary arc front north of 26°S, but not with the rate inferred here from the 8–3 Ma migration of the arc front at 27–28°S or the nearly equivalent rate near 34°S (Kay *et al.*, 2005). A higher rate at this time around the Chilean–Pampean flat-slab is in accord with the marine sediment studies of Encinas & Finger (2007) and their proposal for a slowdown in sedimentation rate at ~4–2 Ma, which is in good agreement with stabilization of the southern CVZ arc front at this time.

A logical explanation for an accelerated fore-arc subduction erosion rate on the northern margin of the flat-slab region is the passage of the bend in the Juan Fernandez Ridge on the subducting Nazca plate, as the angle of impingement changed from highly oblique to essentially trench normal at ~10 Ma near 30–32°S (Yañez *et al.*, 2001). The revisions to the shape of the Wadati–Benioff zone in the studies by Mulcahy *et al.* (2010) and Mulcahy (2012) show that the subducting slab curves eastward (Fig. 1) under the area of the Pircas Negras region near the Incapillo caldera, where the last Pleistocene arc activity occurred at the southern end of the CVZ at ~0·5 Ma (Goss *et al.*, 2009). This timing also fits well with maximum flattening of the flat-slab after 10 Ma and particularly from ~8 to 3 Ma (e.g. Kay & Abbruzzi, 1996; Kay & Mpodozis, 2002).

A final consideration is the mantle wedge temperature needed to produce the melting of the subducted eroded crust to create the Pircas Negras magmas. Various mechanisms have been proposed to induce fluid-saturated conductive heating of fore-arc crust as it is transported through

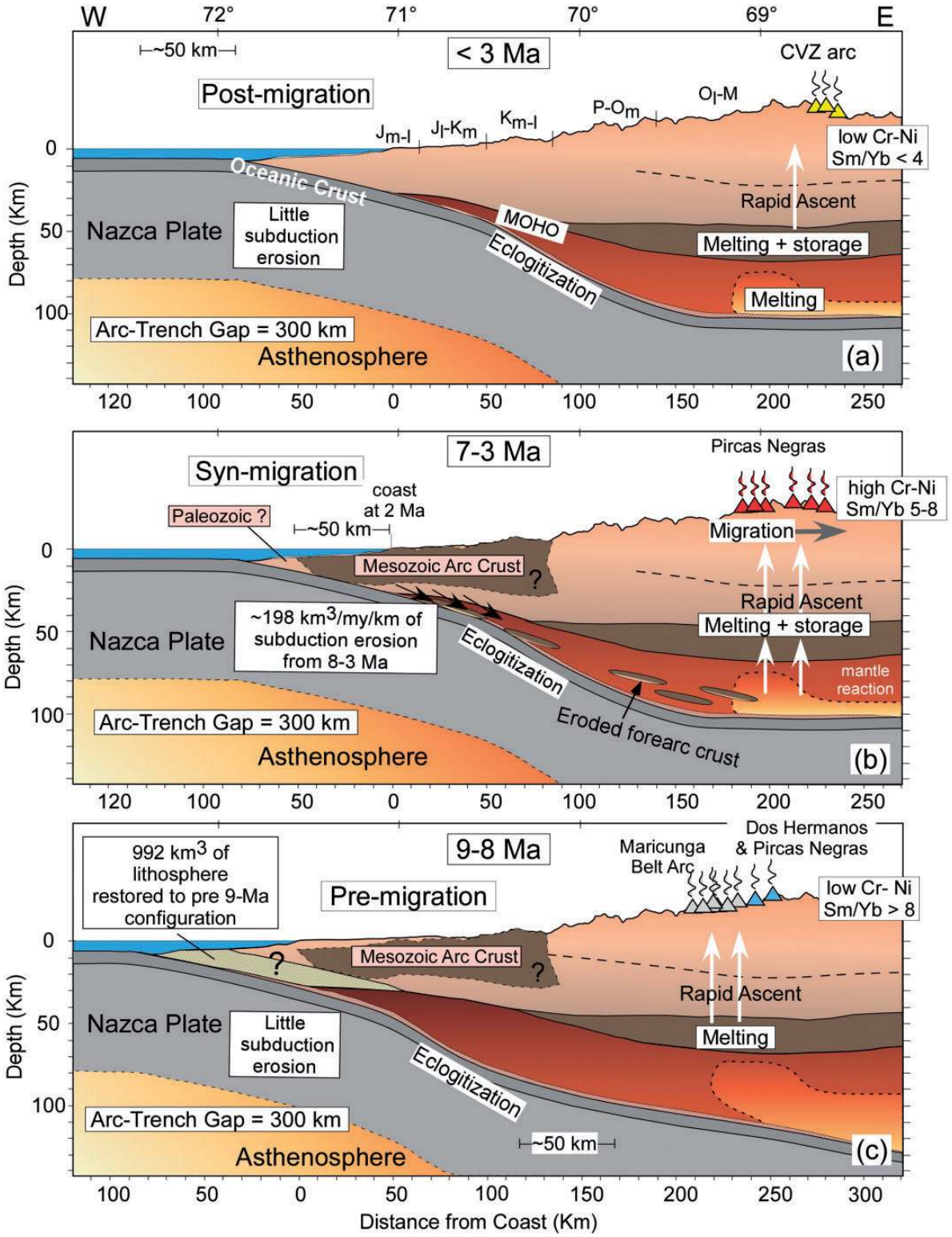

Fig. 16. Schematic near-trench to back-arc cross-section at about 28·5–27°S showing major tectonomagmatic features and processes before, during and after late Miocene to Pliocene arc front migration. Sections assume a nearly constant 300 km arc–trench gap. Volcanic centers in each period are shown schematically by triangles. (a) Modern tectonic setting, with the topography exaggerated 10 times. The crust below ~45 km depth is shaded to emphasize the stability field of eclogite in mafic compositions. The shape of the subducted Nazca plate is based on the configuration in transect S1 of Pardo *et al.* (2002) and is consistent with the Wadati–Benioff zone contours shown in Fig. 1. The crustal

(continued)

the subduction channel into the mantle wedge. At 3 GPa, the melting point of mafic eclogite is ~740°C (Hacker *et al.*, 2003), which is significantly lower than that of the mantle, but higher than isoviscous modeled slab–mantle interface temperatures at 100 km (Peacock *et al.*, 1994). As pointed out by Kelemen *et al.* (2003), eroded basal fore-arc crust should melt before the slab as initial temperatures at the base of the eroded crust are higher than at the top of the slab. Those researchers demonstrated that small density differences (50–150 kg m^{-3}) at low strain rates (~10–14) in a 1 km thick lens of eclogitized crust could induce diapirs to rise into the overlying mantle peridotite. A mixture of eclogitic fore-arc crust composed of 15% silicic (3·1 g cm^{-3}; Richardson & England, 1979) and 85% mafic (3·4 g cm^{-3}) crust would be neutrally buoyant in a peridotitic mantle (3·35 g cm^{-3}). Mantle corner flow and rising slab-derived fluids would help to sweep eroded fore-arc crust into hotter regions of the wedge where fluid-saturated melting would occur.

CONCLUSIONS

The ~7·7 Ma Dos Hermanos and 7–2 Ma Pircas Negras adakitic andesites are a chemically and petrographically distinct suite of lavas that erupted as the Andean arc front was displaced ~40–50 km eastward on the northern margin of the shallowing Chilean–Pampean flat-slab at 27–28·5°S as the aseismic Juan Fernandez Ridge on the subducting Nazca plate was entering the trench. The distinctive features of these lavas are compatible with fore-arc crust removed by fore-arc subduction erosion being incorporated into their mantle source area, with the resulting magmas then passing through an ~65–70 km thick overlying crust in which interaction with that crust occurred. Important observations are as follows.

(1) The Dos Hermanos and Pircas Negras lavas occur in an ~50 km wide east–west band located between the arc front of the ~26–6 Ma Maricunga Belt arc to the west and the <3 Ma CVZ arc front to the east.

(2) Most of the Pircas Negras lavas (Mg# 36–61) are glassy andesites containing amphibole, sparse clinopyroxene and rare resorbed orthopyroxene phenocrysts, olivine clusters, and plagioclase and quartz xenocrysts with clinopyroxene reaction rims, whereas the Dos Hermanos lavas (Mg# = 48–55) contain clinopyroxene as their only phenocryst. All are adakitic-like lavas with pronounced HREE depletion (Sm/Yb = 4–8) and high Sr/Y ratios that require equilibration with a plagioclase-free, garnet-bearing residue, and all have marked HFSE depletions, indicating interaction with slab components. These features are much more extreme than in pre-migration 26–10 Ma Maricunga Belt and post-migration <3 Ma CVZ arc andesites.

(3) The high Cr and Ni contents, resorbed orthopyroxene phenocrysts and calculated pre-eruption temperatures (>1060°C) in some 5–3 Ma high-Mg# Pircas Negras high-Mg andesites are consistent with an origin like that of adakitic andesites produced by experimentally reacting basalt with peridotite at pressures above 1·2 GPa (e.g. Rapp & Watson, 1995; Rapp *et al.*, 2007).

(4) Higher $^{87}Sr/^{86}Sr$ and lower $^{143}Nd/^{144}Nd$ ratios in the Pircas Negras lavas than in older Maricunga Belt lavas at the same wt % SiO_2 are best explained by mantle source contamination by radiogenic fore-arc crust introduced into the sub-arc mantle by fore-arc subduction erosion. A major role for subducted terrigenous sediments can be excluded as these sediments generally ceased to enter the trench by 9 Ma and the pelagic sediment contribution was constant from the west. A correlation of increasing $^{87}Sr/^{86}Sr$ and decreasing $^{143}Nd/^{144}Nd$ ratios from an enriched base level with increasing $\delta^{18}O$ in the same samples reflects subsequent contamination in the thick crust.

(5) Isotopic modeling shows that many of the key features of the Pircas Negras andesites are consistent with reacting adakitic melts of Chilean margin subducted fore-arc crust, whose composition is constrained by outcrop and geophysical data, with mantle peridotite. To match the Pircas Negras andesites, these adakite-like melts need to be mixtures of 80–90% Jurassic gabbro and 10–20% radiogenic Paleozoic crust that acquire an additional 10–40% of their Nd and Sr (ppm) from the surrounding mantle peridotite. The

Fig. 16. Continued
thickness is based on McGlashan *et al.* (2008) and Bianchi *et al.* (2013). The extent of dense mafic Mesozoic arc crust shown in (b) and (c) is inferred from surface mapping (SERNAGEOMIN, 2003) and regional geophysical studies of the northern Chilean fore-arc (Wigger *et al.*, 1994; Schmitz *et al.*, 1999; Lucassen *et al.*, 2001; Tassara *et al.*, 2006; Prezzi *et al.*, 2009). (b) Tectonic setting during arc migration, with the horizontal arrow indicating the ~50 km of frontal arc migration from the ~26–6 Ma Maricunga Belt to the <3 Ma CVZ arc front (e.g. Bonete Chico, Pissis, Veladero). Slivers of fore-arc material composed of 80–90% mafic Mesozoic crust and 10–20% Paleozoic crust are shown being removed from the base of the overriding crust at the time of arc migration. The removed fore-arc crust is then transported into the sub-arc mantle wedge, where flux melting and reaction with mantle peridotite generates the 7–3 Ma syn-migration high-Mg adakite-like Pircas Negras andesites. Rapid eruption to the surface is preceded by storage and assimilation in the lower crust. (c) The restored pre-arc migration cross section at 9–7 Ma with the paleo-coastline and trench located some 50 km to the west of the modern arc front. The wedge near the coast shows the 992 km^3 of material needed to restore the fore-arc to its position before removal by fore-arc subduction erosion between 8 and 3 Ma (rate of ~198 km^3 Myr^{-1}km^{-1}). The positions of the Middle to Late Jurassic (J_{m-l}); Late Jurassic to Middle Cretaceous (J_l–K_m), Middle to Late Cretaceous (K_{m-l}), Paleocene to middle Oligocene (P–O_m) and Late Oligocene to Miocene (O_l–M, Maricunga Belt) volcanic rocks in section (a) show the pre-Miocene migration of the arc based on the geological map of Chile (SERNAGEOMIN, 2003).

same modeling shows that Pb isotopic ratios are more controlled by the crust, through which the magmas rise and which contains a large Late Paleozoic granite–rhyolite component.

(6) The ~40–50 km eastward displacement of the arc front coincides with a period of rapid fore-arc subduction erosion during which fore-arc crust flooded the sub-arc mantle wedge. This led to high-pressure melting in the subduction channel and mantle wedge, generating adakitic melts that reacted with the surrounding peridotite. The resulting hydrous magmas crystallized pargasitic amphibole near the base of the >60 km thick crust before rapidly ascending to the surface and erupting as the Pircas Negras andesites. Given a constant arc–trench gap for the last 25 Myr, a schematic cross-section based on geophysical constraints requires ~198 $km^3 Myr^{-1} km^{-1}$ of crustal material to be removed by fore-arc subduction erosion from the fore-arc on the northern margin of the Chilean–Pampean flat-slab between 8 and 3 Ma.

(7) In summary, the features of the Dos Hermanos and Pircas Negras lavas can be explained by migration of the arc front during a period of accelerated fore-arc subduction erosion as rapid shallowing of the Nazca plate produced the present-day flat-slab region to the south. The extreme HREE depletion and low Mg, Cr and Ni concentrations of the 9–7 Ma Dos Hermanos, Comecaballos and Redondo lavas erupted during the last stages of the evolution of the Maricunga Belt arc can be largely linked to partial melting of eclogitic crust produced in association with ponded mantle-derived arc magmas such as the ~9 Ma back-arc Los Aparejos lavas. The switch from oblique to near trench-normal subduction of the Juan Fernandez Ridge (Yañez *et al.*, 2001) produced a period of instability, in which the arc front was displaced eastwards from the Maricunga Belt to the CVZ arc. The ~7–3 Ma syn-migration Pircas Negras adakite-like andesites, which erupted at this time, contain partial melt components from the dominantly mafic fore-arc crust that reacted with the overlying mantle wedge to generate magmas with elevated Cr, Ni and Mg# values that contain corroded orthopyroxene. Subsequent storage at lower levels of the thick crust suppressed plagioclase and facilitated amphibole crystallization and crustal assimilation. Quartz and plagioclase xenocrysts were incorporated from locally pooled silicic magmas in the mid-crust and the basement during final ascent. The last Pircas Negras lavas erupted at 3–2 Ma as the CVZ arc stabilized have a dominantly lower-crustal eclogitic contaminant.

Fore-arc subduction erosion has been shown to be a potentially important process in shaping arc magmas, particularly during periods of arc instability when fore-arc crust floods the mantle wedge. The signature of this fore-arc crust is detectable in the arc lavas at this time and is potentially a transiently important component in arc magmas. The fore-arc component not involved in producing these magmas is a potentially important factor in enriching the back-arc mantle.

ACKNOWLEDGEMENTS

We particularly thank Robert Kay for invaluable discussions and assistance with the INAA data; the Chilean SERNAGEOMIN for K/Ar ages and some chemical analyses; Moyra Gardeweg, Paula Cornejo, Andrew Tittler, Beatriz Coira, Daniel Rubiolo, Pablo Caffé and Gabriela Depine for invaluable contributions in the field; Gerhard Wörner and the group at the Universität Göttingen for oxygen isotopic data; George Kamenov at the University of Florida for MC-ICP-MS Pb isotopic data; and Jorge Lemp and Antonio Diaz for professional driving skills that made the sampling possible.

FUNDING

Financial support came from a FONDECYT grant (1950025) and the SERNAGEOMIN in Chile, US National Science Foundation EAR Grants (0126000 and 0538112) and a NASA Earth Systems Science Graduate Research Fellowship to A.R.G.

SUPPLEMENTARY DATA

Supplementary data for this paper are available at *Journal of Petrology* online.

REFERENCES

Aitcheson, S. J., Harmon, R. S., Moorbath, S., Schneider, A., Soler, P., Soria, E. E., Steele, G., Swainbank, I. & Wörner, G. (1995). Pb isotopes define basement domains of the Altiplano, Central Andes. *Geology* **23**, 555–558.

Alonso-Perez, R., Ulmer, P., Muentener, O. & Thompson, A. B. (2004). Role of garnet fractionation in H_2O-undersaturated andesite liquids at high pressure. *Lithos* **73**, S1–S2.

Andersen, D. & Lindsley, D. H. (1988). Internally consistent solution models for Fe–Mg–Mn–Ti oxides: Fe–Ti oxides. *American Mineralogist* **73**, 714–726.

Andersen, D., Lindsley, D. H. & Davidson, P. (1993). QUILF: A Pascal program to assess equilibria among the Fe–Mg–Mn–Ti oxides, pyroxenes, olivine, and quartz. *Computers and Geosciences* **19**, 1333–1350.

Annen, C., Blundy, J. D. & Sparks, R. S. J. (2006). The genesis of intermediate and silicic magmas in deep crustal hot zones. *Journal of Petrology* **47**, 505–539.

Asimow, P. D. & Ghiorso, M. S. (1998). Algorithmic modifications extending MELTS to calculate subsolidus phase relations. *American Mineralogist* **83**, 1127–1131.

Bell, C. M. (1987). The Late Paleozoic Evolution of the Gondwanaland Continental Margin in Northern Chile. In: Mckenzie, G. D. (ed.)

Gondwana Six: Structure, Tectonics, and Geophysics. American Geophysical Union.

Bianchi, M., Heit, B., Jakovlev, A., Yuan, X., Kay, S., Alonso, R., Sandvol, E. & Kind, R. (2013). Teleseismic tomography of the southern Puna plateau in Argentina and adjacent regions. *Tectonophysics* **586**, 65–83.

Brenan, J. M., Shaw, H. F., Ryerson, F. J. & Phinney, D. L. (1995). Experimental determination of trace-element partitioning between pargasite and a synthetic hydrous andesitic melt. *Earth and Planetary Science Letters* **135**, 1–11.

Cahill, T. A. & Isacks, B. L. (1992). Seismicity and shape of the subducted Nazca Plate. *Journal of Geophysical Research* **97**, 17503–17529.

Carrapa, B., Adelmann, D., Hilley, G. E., Mortimer, E., Sobel, E. R. & Strecker, M. R. (2005). Oligocene range uplift and development of plateau morphology in the southern Central Andes. *Tectonics* **24**, 1–19.

Christeson, G. L., McIntosh, K. D., Shipley, T. H., Flueh, E. R. & Goedde, H. (1999). Structure of the Costa Rica convergent margin, offshore Nicoya Peninsula. *Journal of Geophysical Research—Solid Earth* **104**, 25443–25468.

Clift, P. & Hartley, A. (2007). Slow rates of subduction erosion and coastal underplating along the Andean margin of Chile and Peru. *Geology* **35**, 503–506.

Clift, P. & Vannucchi, P. (2004). Controls on tectonic accretion versus erosion in subduction zones. Implications for the origin and recycling of the continental crust. *Reviews of Geophysics* **42**, doi:10.1029/2003RG000127.

Dallmeyer, R. D., Brown, M., Grocott, J., Taylor, G. K. & Treloar, P. J. (1996). Mesozoic magmatic and tectonic events within the Andean plate boundary zone, 26°–27°30'S, North Chile: Constraints from mineral ages. *Journal of Geology* **104**, 19–40.

DeMets, C., Gordon, R. G., Argus, D. F. & Stein, S. (1990). Current plate motions. *Geophysical Journal International* **101**, 425–478.

Droop, G. T. R. (1987). A general equation for estimating Fe^{3+} concentrations in ferromagnesian silicates and oxides from microprobe analyses using stoichiometric criteria. *Mineralogical Magazine* **51**, 431–435.

Encinas, A. & Finger, K. (2007). Slow rates of subduction erosion and coastal underplating along the Andean margin of Chile and Peru: Comment. *Geology* **35**, doi:10.1130/G24305C.1.

Gelcich, S., Spooner, E. T. C. & Davis, D. W. (2005). Tracking the basement of the early Andean magmatism. U–Pb ages of zircon xenocrysts of the La Negra Formation in the Coastal Cordillera near Chañaral (~26°S), Northern Chile. In: *6th International Symposium on Andean Geodynamics*, *Barcelona*, 308–311.

Ghiorso, M. S. & Sack, R. O. (1995). Chemical mass transfer in magmatic processes IV: A revised and internally consistent thermodynamic model for the interpolation and extrapolation of liquid–solid equilibria in magmatic systems at elevated temperatures and pressures. *Contributions to Mineralogy and Petrology* **119**, 197–212.

Godoy, E. & Lara, L. 1998. Carta Geológica de Chile, Hojas Chanñaral y Diego del Almagro, No. 5–6, escala 1:100,000. Servicio Nacional de Geología y Minería, Santiago de Chile.

Gorring, M. L. & Kay, S. M. (2000). Carbonatite metasomatized peridotite xenoliths from southern Patagonia: Implications for lithospheric processes and Neogene plateau magmatism. *Contributions to Mineralogy and Petrology* **140**, 55–72.

Goss, A. R. & Kay, S. M. (2006). Steep REE patterns and enriched Pb isotopes in southern Central American arc magmas: Evidence for fore-arc subduction erosion? *Geochemistry, Geophysics, Geosystems* **7**, doi:10.1029/2005GC001163.

Goss, A. R. & Kay, S. M. (2009). Extreme high field strength element (HFSE) depletion and near-chondritic Nb/Ta ratios in Central Andean adakite-like lavas (~27°S, ~68°W). *Earth and Planetary Science Letters* **270**, 97–109.

Goss, A. R., Kay, S. M., Mpodozis, C. & Singer, B. S. (2009). The Incapillo Caldera and dome complex (~28°S): A stranded magma chamber over a dying Andean arc. *Journal of Volcanology and Geothermal Research* **184**, 384–404.

Goss, A. R., Kay, S. M. & Mpodozis, C. (2011). The geochemistry of a dying continental arc: the Incapillo Caldera and Dome Complex of the southernmost Central Andean Volcanic Zone (~28 S). *Contributions to Mineralogy and Petrology* **161**, 101–128.

Götze, H.-J., Lahmeyer, B., Schmidt, S. & Strunk, S. (1994). The lithospheric structure of the Central Andes (20°–26°S) as inferred from interpretation of regional gravity. In: Reutter, K. J., Scheuber, E. & Wigger, P. J. (eds) *Tectonics of the Southern Central Andes: Structure and Evolution of an Active Continental Margin*. Springer, pp. 1349–1343.

Green, T. H. (1982). Anatexis of mafic crust and high pressure crystallization of andesite. In: Thorpe, R. S. (ed.) *Andesites: Orogenic Andesites and Related Rocks*. John Wiley, pp. 465–487.

Green, T. H. & Pearson, N. J. (1986). Ti-rich accessory phase saturation in hydrous mafic–felsic compositions at high *PT*. *Chemical Geology* **54**, 185–201.

Green, T. H. & Ringwood, A. E. (1968). Genesis of the calc-alkaline igneous rock suite. *Contributions to Mineralogy and Petrology* **18**, 105–162.

Green, T. H., Blundy, J. D., Adam, J. & Yaxley, G. M. (2000). SIMS determination of trace element partition coefficients between garnet, clinopyroxene and hydrous basaltic liquids at 2–7·5 GPa and 1080–1200°C. *Lithos* **53**, 165–187.

Gromet, L. P. & Silver, L. T. (1987). REE variations across the Peninsular Ranges batholith: Implications for batholithic petrogenesis and crustal growth in magmatic arcs. *Journal of Petrology* **28**, 75–125.

Grove, T. L., Parman, S. W., Bowring, S. A., Price, R. C. & Baker, M. B. (2002). The role of an H_2O-rich fluid component in the generation of primitive basaltic andesites and andesites from the Mt. Shasta region, N. California. *Contributions to Mineralogy and Petrology* **142**, 375–396.

Grove, T. L., Elkins-Tanton, L. T., Parman, S. W., Chatterjee, N., Muentener, O. & Gaetani, G. A. (2003). Fractional crystallization and mantle-melting control on calc-alkaline differentiation trends. *Contributions to Mineralogy and Petrology* **145**, 515–533.

Hacker, B. R., Abers, G. A. & Peacock, S. M. (2003). Subduction factory: 1, Theoretical mineralogy, densities, seismic wave speeds, and H2O contents. *Journal of Geophysical Research* **108**, doi:10.1029/2001JB001127.

Haschke, M. R., Siebel, W., Günther, A. & Scheuber, E. (2002). Repeated crustal thickening and recycling during the Andean orogeny in north Chile (21°–26°S). *Journal of Geophysical Research* **107**, 1–18.

Hildreth, W. & Moorbath, S. (1988). Crustal contributions to arc magmatism in the Andes of central Chile. *Contributions to Mineralogy and Petrology* **98**, 455–489.

Hofmann, A. W. (1988). Chemical differentiation of the Earth: The relationship between mantle, continental crust, and oceanic crust. *Earth and Planetary Science Letters* **90**, 297–314.

Huang, W.-L. & Wyllie, P. J. (1986). Phase relationships of gabbro–tonalite–granite–water at 15 kb with applications to differentiation and anatexis. *American Mineralogist* **71**, 301–316.

Jarosewich, E., Nelen, J. A. & Norberg, J. A. (1980). Reference samples for electron microprobe analysis. *Geostandards Newsletter* **4**, 43–47.

Kay, R. W. (1978). Aleutian magnesian andesites; melts from subducted Pacific Ocean crust. *Journal of Volcanology and Geothermal Research* **4**, 117–132.

Kay, R. W. (2006). Subduction erosion and recycled crust at convergent margins: The Adak adakite example. *Geological Society of America, Abstracts, Special Meeting* **2**, 93.

Kay, R. W. & Kay, S. M. (1993). Delamination and delamination magmatism. *Tectonophysics* **219**, 177–189.

Kay, S. M. & Abbruzzi, J. M. (1996). Magmatic evidence for Neogene lithospheric evolution of the central Andean 'flat-slab' between 30°S and 32°S. *Tectonophysics* **259**, 15–28.

Kay, S. M. & Coira, B. (2009). Shallowing and steepening subduction zones, continental lithosphere loss, magmatism and crustal flow under the Central Andean Altiplano–Puna plateau. In: Kay, S. M., Ramos, V. A. & Dickinson, W. M. (eds) *Backbone of the Americas: Shallow Subduction, Plateau and Ridge and Terrane Collisions. Geological Society of America, Memoir* **204**, 229–260.

Kay, S. M. & Gordillo, C. E. (1994). Pocho volcanic rocks and the melting of depleted continental lithosphere above a shallowly dipping subduction zone in the Central Andes. *Contributions to Mineralogy and Petrology* **117**, 25–44.

Kay, S. M. & Mpodozis, C. (2002). Magmatism as a probe to the Neogene shallowing of the Nazca plate beneath the modern Chilean flat-slab. *Journal of South American Earth Sciences* **15**, 39–57.

Kay, S. M., Maksaev, V., Moscoso, R., Mpodozis, C. & Nasi, C. (1987). Probing the evolving Andean lithosphere: mid–late Tertiary magmatism in Chile (29°–30°30') over the modern zone of subhorizontal subduction. *Journal of Geophysical Research* **92**, 6173–6189.

Kay, S. M., Mpodozis, C., Ramos, V. A. & Munizaga, F. (1991). Magma source variations for mid–late Tertiary magmatic rocks associated with a shallowing subduction zone and a thickening crust in the Central Andes (28 to 33°S). In: Harmon, R. S. & Rapela, C. W. (eds) *Andean Magmatism and its Tectonic Setting. Geological Society of America, Special Papers* **265**, 113–137.

Kay, S. M., Mpodozis, C., Tittler, A. & Cornejo, P. (1994). Tertiary magmatic evolution of the Maricunga mineral belt in Chile. *International Geology Review* **36**, 1079–1112.

Kay, S. M., Mpodozis, C. & Coira, B. (1999). Neogene magmatism, tectonism, and mineral deposits of the Central Andes (22° to 33°S latitude). In: Skinner, B. J. (ed.) *Geology and Ore Deposits of the Central Andes. Society of Economic Geology, Special Publication* **7**, 27–59.

Kay, S. M., Godoy, E. & Kurtz, A. (2005). Episodic arc migration, crustal thickening, subduction erosion, and magmatism in the south–central Andes. *Geological Society of America Bulletin* **117**, 67–88.

Kay, S. M., Coira, B. L. & Mpodozis, C. (2008). Field trip guide to the Neogene to Recent Evolution of the Puna plateau and the Southern Central Volcanic Zone. In: Kay, S. M. & Ramos, V. A. (eds) *Field Trip Guides to the Backbone of the Americas in the Southern and Central Andes. Geological Society of America, Field Guide Series* **13**, 117–181.

Kay, S. M., Coira, B., Wörner, G., Kay, R. W. & Singer, B. S. (2011). Geochemical, isotopic and single crystal $^{40}Ar/^{39}Ar$ age constraints on the evolution of the Cerro Galán ignimbrites. *Bulletin of Volcanology* **73**, 1487–1511.

Kay, S. M., Mpodozis, C. & Gardeweg, M. (2013). Magma sources and tectonic setting of Central Andean andesites (25·5°–28°S) related to crustal thickening, fore-arc subduction erosion and delamination. In: Gomez-Tuena, A. *et al.* (eds) *Orogenic Andesites and Crustal Growth. Geological Society, London, Special Publications* **385**, doi: 10.1144/SP385.11.

Kelemen, P. B., Hart, S. R. & Bernstein, S. (1998). Silica enrichment in the continental upper mantle via melt/rock reaction. *Earth and Planetary Science Letters* **164**, 387–406.

Kelemen, P. B., Hanghøj, K. & Green, A. R. (2003). One view of the geochemistry of subduction-related magmatic arcs, with emphasis on primitive andesite and the lower crust. In: Holland, H. D. & Turekian, K. K. (eds) *Treatise on Geochemistry 3.* Elsevier, pp. 593–659.

Klemme, S., Blundy, J. D. & Wood, B. J. (2002). Experimental constraints on major and trace element partitioning during partial melting of eclogite. *Geochimica et Cosmochimica Acta* **66**, 3109–3123.

Laursen, J., Scholl, D. W. & von Huene, R. (2002). Neotectonic deformation of the central Chile margin: Deep-water fore-arc basin formation in response to hot spot ridge and seamount subduction. *Tectonics* **21**, 1–27.

Leake, B. E., Woolley, A. R., Arps, C. E. S., Birch, W. D., Gilbert, M. C., Grice, J. D., Hawthorne, F. C., Kato, A., Kisch, H. J., Krivovichev, V. G., Linthout, K., Laird, J., Mandarino, J. A., Maresch, W. V., Nickel, E. H., Rock, N. M. S., Schumacher, J. C., Smith, D. C., Stephenson, N. C. N., Ungaretti, L., Whittaker, E. J. W. & Guo, Y. (1997). Nomenclature of amphiboles; report of the Subcommittee on Amphiboles of the International Mineralogical Association, Commission on New Minerals and Mineral Names. *American Mineralogist* **82**, 1019–1037.

Le Maitre, R. W., Bateman, R., Dudek, A., Keller, J., Lameyre, J., La Bas, M. J., Sabine, P. A., Schmid, R., Sorensen, H., Streckeisen, A., Woolley, A. R. & Zanettin, B. (1989). *A Classification of Igneous Rocks and Glossary of Terms*. Blackwell.

Lindsley, D. H. (1983). Pyroxene thermometry. *American Mineralogist* **68**, 477–493.

Litvak, V., Poma, E. & Kay, S. M. (2007). Paleogene and Neogene magmatism in the Valle del Cura region: New perspective on the evolution of the Pampean flat slab, San Juan province, Argentina. *Journal of South American Earth Sciences* **24**, 117–137.

Lucassen, F. & Thirlwall, M. F. (1998). Sm–Nd ages of mafic rocks from the Coastal Cordillera at 24°S, northern Chile. *Geologische Rundschau* **86**, 767–774.

Lucassen, F., Becchio, R., Harmon, R., Kasemann, S., Franz, G., Trumbull, R., Wilke, H. G., Romer, R. L. & Dulski, P. (2001). Composition and density model of the continental crust at an active continental margin: Central Andes between 21° and 27°S. *Tectonophysics* **341**, 195–223.

Lucassen, F., Escayola, M., Romer, R. L., Viramonte, J., Koch, K. & Franz, G. (2002). Isotopic composition of late Mesozoic basic and ultrabasic rocks from the Andes (23–32°S); implications for the Andean mantle. *Contributions to Mineralogy and Petrology* **143**, 336–349.

Lucassen, F., Kramer, W., Bartsch, V., Wilke, H., Franze, G., Romer, R. & Dulski, P. (2006). Nd, Pb, and Sr isotope composition of juvenile magmatism in the Mesozoic large magmatic province of northern Chile (18–27°S): Indications for a uniform subarc mantle. *Contributions to Mineralogy and Petrology* **152**, 571–589.

Macpherson, C., Dreher, S. T. & Thirlwall, M. F. (2006). Adakites without slab melting: high pressure differentiation of island arc magma, Mindanao, the Philippines. *Earth and Planetary Science Letters* **243**, 581–593.

Mamani, M., Tassara, A. & Wörner, G. (2008). Composition and structural control of crustal domains in the Central Andes. *Geochemistry, Geophysics, Geosystems* **9**, doi:10.1029/2007GC001925.

Mamani, M., Wörner, G. & Sempere, T. (2010). Geochemical variations in igneous rocks of the Central Andean orocline (13°S to 18°S): Tracing crustal thickening and magma generation through time and space. *Geological Society of America Bulletin* **122**, 162–182.

Martin, H. (1987). Petrogenesis of Archaean trondhjemites, tonalites and granodiorites from eastern Finland: major and trace element geochemistry. *Journal of Petrology* **28**, 921–953.

Martina, F., Viramonte, G. J., Astini, R. A., Pimentel, M. & Dantas, E. (2009). Evidence of Early Carboniferous pre-Choiyoi volcanism in western Gondwana: First isotopic, geochemical, and

U–Pb SHRIMP data. In: *XXI Colloquium on Latin American Earth Sciences, Göttingen, Germany.*

Matthews, S. & Cornejo, P. (2004). Middle to late Eocene high-sulphidation Cu–Au vein mineralization at Guanaco Mine and Cerro Inesperado, II Region, Chile. In: *International Association Volcanology and Chemistry of Earth's Interior General Assembly*, Pucón, Chile.

Matthews, S., P. Cornejo, and R. Riquelme (2006). Hoja Inca de Oro, Carta Geol. Chile, 1:100,000 scale, Serv. Nac. Geol. y Min., Santiago.

McCulloch, M. T. & Gamble, J. A. (1991). Geochemical and geodynamical constraints on subduction zone magmatism. *Earth and Planetary Science Letters* **102**, 358–374.

McDonough, W. F. & Sun, S. S. (1995). The composition of the Earth. *Chemical Geology* **120**, 223–253.

McGlashan, N., Brown, L. D. & Kay, S. M. (2008). Crustal thickness in the central Andes from teleseismically recorded depth phase precursors. *Geophysical Journal International* **175**, 1013–1022.

McKee, E., Robinson, A. C., Rybuta, J. J., Cuitiño, L. & Moscoso, R. (1994). Age and Sr-isotopic composition of volcanic rocks in the Maricunga Belt, Chile: Implications for magma sources. *Journal of South American Earth Sciences* **7**, 167–177.

Moore, G. & Carmichael, I.S. E. (1998). The hydrous phase equilibria (to 3 kbar) of an andesite and basaltic andesite from western Mexico: Constraints on water content and conditions of phenocryst growth. *Contributions to Mineralogy and Petrology* **130**, 304–319.

Moscoso, R., Maksaev, V., Cuituno, L., Diaz, F., Koeper, R., Tosdal, R., Cunningham, C., McKee, E. & Rytuba, J. (1993). El Complejo Cerros Bravos, región de Maricunga, Chile: geología, alteración hidrotermal y mineralización, Investigación de metales preciosos en los Andes Central. Projecto BID/PC 88-02-32-spi63-8. Bolivia Servicio Geológico, BID (Banco Interamericano de Desarrollo).

Mpodozis, C. & Kay, S. M. (1992). Late Paleozoic to Triassic evolution of the Gondwana margin: Evidence from Chilean Frontal Cordilleran batholiths (28°S to 31°S). *Geological Society of America Bulletin* **104**, 999–1014.

Mpodozis, C. & Kay, S. M. (2009). Evolution of less than 10 Ma Valle Ancho region lavas, southern end of the Central Andean Volcanic Zone (~27·5°S). In: *XII Congreso Geológico Chileno Actas, Santiago*, S7–019.

Mpodozis, C., Cornejo, P., Kay, S. & Tittler, A. (1995). La Franja de Maricunga: síntesis de la evolución del frente volcánico oligoceno-mioceno de la zona sur de los Andes Centrales. *Revista Geológica de Chile* **22**, 273–313.

Mpodozis, C., Kay, S. M., Gardeweg, M. P. & Coira, B. (1996). Geología de la región de Ojos del Salado (Andes centrales, 27°S): Implicancias de la migración hacia el este del frente volcánico Cenozoico superior. In: *13° Congreso Geológico Argentino Actas, Buenos Aires*, pp. 539–548.

Mpodozis, C., Kay, S. M., Gardeweg, M. & Coira, B. (1997). Geología de la región de Valle–Ancho–Laguna Verde (Catamarca, Argentina): Una ventana al basamento del extremo sur de la zona volcánica de los Andes Centrales. In: *8° Congreso Geológico Chileno Actas, Antofagasta, Chile*, pp. 1689–1693.

Mulcahy, P. (2012). The southern Puna seismic experiment: seismicity and the morphology of the subduction zone, MS thesis, Cornell University, 84 pp.

Mulcahy, P., Chen, C., Kay, S. M., Brown, L. D., Alvarado, P. M., Sandvol, E. A., Heit, B. & Yuan, X. (2010). The SOUTHERN PUNA seismic experiment: shape of the subducting Nazca Plate, areas of concentrated mantle and crustal earthquakes, and crustal focal mechanisms. *EOS Transactions American Geophysical Union, Fall Meeting Supplement* **91(53)**, Abstract T11A-2050.

Müntener, O., Kelemen, P. B. & Grove, T. L. (2001). The role of H_2O during crystallization of primitive arc magmas under uppermost mantle conditions and genesis of igneous pyroxenites: an experimental study. *Contributions to Mineralogy and Petrology* **141**, 643–658.

Nalpas, T., Dabard, M.-P., Ruffet, G., Vernon, A., Mpodozis, C., Loi, A. & Hérail, G. (2008). Sedimentation and preservation of the Miocene Atacama gravels in the Pedernales–Chañaral Area, Northern Chile: Climatic or tectonic control? *Tectonophysics* **459**, 161–173.

Pardo, M., Comte, D. & Monfret, T. (2002). Seismotectonic and stress distribution in the central Chile subduction zone. *Journal of South American Earth Sciences* **15**, 11–22.

Pardo-Casas, F. & Molnar, P. (1987). Relative motion of the Nazca (Farallon) and South American plates since Late Cretaceous time. *Tectonics* **6**, 233–248.

Peacock, S. M., Rushmer, T. & Thompson, G. (1994). Partial melting of subducting oceanic crust. *Earth and Planetary Science Letters* **121**, 227–244.

Pertermann, M. & Hirschmann, M. M. (2003). Anhydrous partial melting experiments on MORB-like eclogite: Phase relations, phase compositions and mineral–melt partitioning of major elements at 2–3 GPa. *Journal of Petrology* **44**, 2173–2201.

Petford, N. & Atherton, M. P. (1996). Na-rich partial melts from newly underplated basaltic crust: the Cordillera Blanca batholith, Peru. *Journal of Petrology* **37**, 1491–1521.

Pichowiak, S., Buchelt, M. & Damm, K. W. (1990). Magmatic activity and tectonic setting of the early stages of the Andean cycle in northern Chile. In: Kay, S. M. & Rapela, C. W. (eds) *Plutonism from Antarctica to Alaska. Geological Society of America, Special Papers* **241**, 127–144.

Prezzi, C. B., Götze, H.-J. & Schmidt, S. (2009). 3D density model of the Central Andes. *Physics of the Earth and Planetary Interiors* **177**, 217–234.

Ranero, C. R. & von Huene, R. (2000). Subduction erosion along the Middle America convergent margin. *Nature* **404**, 748–755.

Rapp, R. P. & Watson, E. B. (1995). Dehydration melting of a metabasalt at 8–32 kbar: Implications for continental growth and crust–mantle recycling. *Journal of Petrology* **36**, 891–931.

Rapp, R. P., Laporte, D. & Martin, H. (2007). Primary high magnesian andesites from adakite-metasomatized peridotite: Insights from melting–hybridization–assimilation experiments at 1·5–4·0 GPa. In: *State of the Arc. Extended Abstracts. Puyehue, Chile*, pp. 194–197.

Rapp, R. P., Shimizu, N., Norman, M. D. & Applegate, G. S. (1999). Reaction between slab-derived melts and peridotite in the mantle wedge: Experimental constraints at 3·8 GPa. *Chemical Geology* **160**, 335–356.

Rapp, R. P., Norman, M. D., Laporte, D., Yaxley, G. M., Martin, H. & Foley, S. F. (2010). Continent formation in the Archean and chemical evolution of the cratonic lithosphere: melt–rock reaction experiments at 3–4 GPa and petrogenesis of Archean Mg-diorites (sanukitoids). *Journal of Petrology* **51**, 1237–1266.

Rech, J. A., Currie, B. S., Michalski, G. & Cowan, A. M. (2006). Neogene climate change and uplift in the Atacama Desert, Chile. *Geology* **34**, 761–764.

Richards, J. P., Ulrich, T. & Kerrick, R. (2006). The late Miocene Quaternary Antofalla volcanic complex, southern Puna, NW Argentina: Protracted history, diverse petrology and economic potential. *Journal of Volcanology and Geothermal Research* **152**, 197–239.

Richardson, S. W. & England, P. C. (1979). Metamorphic consequences of crustal eclogite production in overthrust orogenic zones. *Earth and Planetary Science Letters* **42**, 183–190.

Rogers, G. & Hawkesworth, C. J. (1989). A geochemical traverse across the north Chilean Andes: Evidence for crustal generation from the mantle wedge. *Earth and Planetary Science Letters* **91**, 271–285.

Rollinson, H. (1993). *Using Geochemical Data: Evaluation, Presentation, Interpretation*. Longman, 352 p.

Rubiolo, D., Zappettini, E., Lizuain, A. & Hickson, C. (2002). Regional aspects of the southern end of the central volcanic zone (between 27° and 28°S), Argentina. In: *5th International Symposium on Andean Geodynamics, Toulouse, France*. IRD – Institut de recherché pour le développement, pp. 557–560.

Rudnick, R. L. & Fountain, D. M. (1995). Nature and composition of the continental crust: A lower crustal perspective. *Reviews of Geophysics* **33**, 267–309.

Rutland, R. W. R. (1971). Andean orogeny and ocean floor spreading. *Nature* **233**, 252–255.

Scheuber, E. (1994). Tektonische Entwicklumg des nordchilenischen aktiven Kontinentalrandes: Der Einfluß von Plattenkonvergenz und Rheologie. *Geotektonische Forchungen* **81**, 1–131.

Scheuber, E. & Geise, P. (1999). Architecture of the Central Andes—compilation of geoscientific data along a transect at 21°S. *Journal of South American Earth Sciences* **12**, 103–107.

Schmidt, M. W., Dardon, A., Chazot, G. & Vannucci, R. (2004). The dependence of Nb and Ta rutile–melt partitioning on melt composition and Nb–Ta fractionation during subduction processes. *Earth and Planetary Science Letters* **226**, 415–432.

Schmitz, M., Lessel, K., Giese, P., Wigger, P., Araneda, M., Bribach, J., Graeber, F., Grunewald, S., Haberland, C., Lueth, S., Roewer, P., Ryberg, T. & Schulze, A. (1999). The crustal structure beneath the Central Andean fore-arc and magmatic arc as derived from seismic studies; the PISCO 94 experiment in northern Chile (21°–23°S). *Journal of South American Earth Sciences* **12**, 237–260.

Sen, C. & Dunn, T. (1994). Dehydration melting of a basaltic composition amphibolite at 1·5 and 2·0 GPa: Implications for the origin of adakites. *Contributions to Mineralogy and Petrology* **117**, 394–409.

SERNAGEOMIN. (2003). *Mapa Geológico de Chile. Publicación Geológica Digital 4*. Servicio Nacional de Geología y Minería.

Somoza, R. (1998). Updated Nazca (Farallon)–South America relative motions during the last 40 my: Implications for mountain building in the Central Andean region. *Journal of South American Earth Sciences* **11**, 211–215.

Stern, C. R. (1991). Role of subduction erosion in the generation of Andean magmas. *Geology* **19**, 78–81.

Stern, C. R. (2011). Subduction erosion: Rates, mechanisms, and its role in arc magmatism and the evolution of the continental crust and mantle. *Gondwana Research* **20**, 284–308.

Stern, C. R., Floody, R. & Espineira, D. (2011). Olivine–hornblende–lamprophyre dikes from Quebrada los Sapos, El Teniente, Central Chile (34°S): implications for the temporal geochemical evolution of the Andean subarc mantle. *Andean Geology* **38**, 1–22.

Sun, S. S. & McDonough, W. F. (1989). Chemical and isotopic systematics of oceanic basalts: implications for mantle composition and processes. In: Saunders, A. D. & Norry, M. J. (eds) *Magmatism in the Ocean Basins. Geological Society, London, Special Publications* **42**, 313–345.

Tassara, A., Gotze, H. J., Schmidt, S. & Hackney, R. (2006). Three-dimensional density model of the Nazca plate and the Andean continental margin. *Journal of Geophysical Research* **111**, B09404, doi:10.1029/2005JB003976.

Tatsumi, Y. & Ishizaka, K. (1982). Origin of high-magnesian andesites in the Setouchi volcanic belt, Southwest Japan: I, Petrographically and chemical characteristics. *Earth and Planetary Science Letters* **60**, 293–404.

Tiepolo, M., Vannucci, R., Oberti, R., Foley, S., Bottazzi, P. & Zanetti, A. (2000). Nb and Ta incorporation and fractionation in titanian pargasite and kaersutite: crystal chemical constraints and implications for natural systems. *Earth and Planetary Science Letters* **176**, 185–201.

Tittler, A. (1995). The chemistry of Miocene Andean volcanic rocks from the 'flat-slab' to Central Volcanic Zone transition, Chile, 26° to 28°S, MS thesis, Cornell University, Ithaca, NY, 142 pp.

Ulmer, P., Müntener, O. & Alonzo-Pérez, R. (2003). Potential role of garnet fractionation in H_2O-undersaturated andesite liquids at high pressure: An experimental study and a comparison with the Kohistan arc. *Geophysical Research Abstracts* **5**, 08308.

Vandervoort, D. S., Jordan, T. E., Zeitler, P. K. & Alonso, R. N. (1995). Chronology of internal drainage development and uplift, southern Puna plateau, Argentine central Andes. *Geology* **23**, 145–148.

Vannucchi, P., Scholl, D. W., Meschede, M. & McDougall-Reid, K. (2001). Tectonic erosion and consequent collapse of the Pacific margin of Costa Rica: Combined implications from ODP Leg 170, seismic offshore data, and regional geology of the Nicoya Peninsula. *Tectonics* **20**, 649–668.

Vannucchi, P., Ranero, C. R., Galeotti, S., Straub, S. M., Scholl, D. W. & McDougall-Ried, K. (2003). Fast rates of subduction erosion along the Costa Rica Pacific margin: Implications for nonsteady rates of crustal recycling at subduction zones. *Journal of Geophysical Research* **108**, doi:10.1029/2002JB002207.

Vila, T. & Sillitoe, R. H. (1991). Gold-rich porphyry systems in the Maricunga belt, northern Chile. *Economic Geology* **86**, 1238–1260.

von Huene, R. & Ranero, C. R. (2003). Subduction erosion and basal friction along the sediment-starved convergent margin off Antofagasta, Chile. *Journal of Geophysical Research* **108**, doi:10.1029/2001JB001569.

von Huene, R. & Scholl, D. W. (1991). Observations at convergent margins concerning sediment subduction, subduction erosion, and the growth of continental crust. *Reviews of Geophysics* **29**, 279–316.

von Huene, R., Corvalan, J., Flueh, E. R. *et al.* (1997). Tectonic control of the subducting Juan Fernandez Ridge on the Andean margin near Valparaiso, Chile. *Tectonics* **16**, 474–488.

von Huene, R., Weinrebe, W. & Heeren, F. (1999). Subduction erosion along the North Chile margin. *Geodynamics* **27**, 345–358.

von Huene, R., Ranero, C. R. & Vannucchi, P. (2004). Generic model of subduction erosion. *Geology* **32**, 913–916.

Wigger, P. J., Schmitz, M., Araneda, M., Asch, G., Baldzuhn, S., Giese, P., Heinsohn, W.-D., Martinez, E., Ricaldi, E., Roewer, P. & Viramonte, J. (1994). Variation in the crustal structure of the southern Central Andes deduced from seismic refraction investigations. In: Reutter, K. J., Scheuber, E. & Wigger, P. J. (eds) *Tectonics of the Southern Central Andes; Structure and Evolution of an Active Continental Margin*. Springer, pp. 23–48.

Wolf, M. B. & Wyllie, P. J. (1994). Dehydration-melting of amphibolite at 10 kbar: The effects of temperature and time. *Contributions to Mineralogy and Petrology* **115**, 369–383.

Yañez, G. A., Ranero, C., von Huene, R. & Díaz, J. (2001). Magnetic anomaly interpretation across the southern Central Andes (32°–34°S): The role of the Juan Fernandez Ridge in the late Tertiary evolution of the margin. *Journal of Geophysical Research* **106**, 6325–6345.

Yang, Y., Liu, M. & Stein, S. (2003). A 3-D geodynamic model of lateral crustal flow during Andean mountain building. *Geophysical Research Letters* **30**, 2093.

Yogodzinski, G. M., Kay, R. W., Volynets, O. N., Koloskov, A. V. & Kay, S. M. (1995). Magnesian andesite in the western Aleutian Komandorsky region: Implications for slab melting and processes in the mantle wedge. *Geological Society of America Bulletin* **107**, 505–519.

Ziegler, A. M., Barrett, S. F. & Scotese, C. R. (1971). Paleoclimate, sedimentation and continental accretion. *Philosophical Transactions of the Royal Society of London, Series A* **301**, 253–264.

Zindler, A. & Hart, S. (1986). Chemical geodynamics. *Annual Review of Earth and Planetary Sciences* **14**, 493–571.